Aalto University
School of Engineering

Aalto University, P.O. BOX 11000, 00076 AALTO
www.aalto.fi

AALTO UNIVERSITY
School of Engineering
Department of Engineering Design and Production

Niklas Kretzschmar

Economic validation of metal powder bed based AM processes

A Master's Thesis
Espoo, 7th of May, 2015

Supervisor Professor Jouni Partanen
Instructor Inigo Flores, MSc

Aalto University
School of Engineering

Aalto University, P.O. BOX 11000, 00076 AALTO
www.aalto.fi

Abstract of master's thesis

Author	Niklas Kretzschmar
Title of thesis	Economic validation of metal powder bed based AM processes
Degree programme	MSc Mechanical Engineering and Management (Technical University Munich)
Major/minor	Production Engineering — **Code** /
Thesis supervisor	Professor Jouni Partanen
Thesis advisor(s)	Doctoral candidate Inigo Flores
Date	07.05.2015 — **Number of pages** 98 — **Language** English

Abstract

This master thesis focused on current metal-based Additive Manufacturing (AM) systems in terms of cost and feasibility by developing a metal-based AM decision support tool. In addition, the main differences between laser-beam (DMLM) and electron-beam (EBM) based systems have been investigated.

Initially, main principles in AM and powder bed fusion (PBF) are presented. Moreover, DMLM and EBM based systems are compared in terms of performance characteristics, such as build size, beam power as well as beam spot size. Subsequently, existing AM classification schemes are shown and resulting research gaps are outlined. Secondly, a cost and time decision support system based on ”MathWorks Matlab” has been developed to provide a comparison of two metal-based AM machines simultaneously. In total, 9 different machines (i.e. EOS, SLM and Arcam), 3 different material types (i.e. aluminum, tool steel and titanium alloys) and 3 different accuracy levels (i.e. high, low, and skin-core) can be chosen as input parameters. Therefore, build volume rates of machines in the range of 50 to 3000 W were calculated and implemented into the model. As an output of the model, the decision maker receives information, such as cost per part, total cost comparison and a build time evaluation for the selected machines, materials and accuracy level. This information allows to select which machine the best choice is for the user’s specific interests.

To conclude, several experiments including a sensitivity analysis for mass and building height, followed by a skin-core analysis (novel AM production method), an exemplary comparison of DMLM and EBM machines and a random test on all implemented machines and five exemplary parts showing differences in volume and size were performed. Moreover, the Design of Experiments is finished with a Taguchi L-18 orthogonal array test, leading to main effects and influences on several parameters on costs and build time.

Keywords Additive Manufacturing, Powder bed fusion, Direct Metal Laser Melting, Electron Beam Melting, Decision Making Tool, “Mathworks Matlab” simulation tool

ECONOMIC VALIDATION OF METAL POWDER BED BASED AM PROCESSES

Preface

This master thesis was written at Aalto University (Finland) in the Digital Manufacturing Department from January 2015 to May 2015 and was handed in at the Technical University Munich (Germany) based on the Erasmus SMP exchange program.

Special thanks go to my supervisor Prof. Jouni Partanen and my instructor, doctoral candidate MSc. Inigo Flores, both from Aalto University. Additional thanks to doctoral candidate, MSc. Max Lutter-Günther from the Technical University Munich, who supported me during this time as my instructor from my home university.

Espoo, 7.5.2015

_____

Nomenclature

List of abbreviations

AM	Additive Manufacturing
CAD	Computer Aided Design
CM	Conventional Manufacturing
DED	Directed Energy Deposition
DMLM	Direct Metal Laser Melting
DMLS	Direct Metal Laser Sintering
DoE	Design of Experiments
EBM	Electron Beam Melting
FDM	Fused Deposition Modeling
LM	Laser Melting
LS	Laser Sintering
PBF	Powder Bed Fusion
RM	Rapid Manufacturing
RP	Rapid Prototyping
SEM	Scanning Electron Microscope
SLA	Stereolithography
SLM	Selective Laser Melting
SLS	Selective Laser Sintering

List of figures

List of tables

1 Introduction

In this initial chapter an introduction of the initial position, focus definition of the thesis as well as the structure and proceeding is presented. It aims to provide easy access into this topic for the reader and outlines the major goals to be achieved.

1.1 Initial position

According to the renowned British business magazine "The Economist" Additive Manufacturing (AM) could cause "a third industrial revolution". They were reporting that subsequent to the development of steam engines and the insertion of electricity, layer-by-layer deposition will replace conventional manufacturing methods (The Economist, 2012).

As a consequence, the traditional way of producing goods will change. From a production of goods in big volumes by manufacturing companies, which can be called Factory 1.0, to a Factory 2.0. Therefore, design and production of goods is strongly linked to changing demands of the consumers and flexibility of production systems (National Academy of Engineering of the National Academies, 2012, p.5).

Even though these statements are meant to be an outlook into the future, they will not necessarily be fulfilled in short term. Literature shows a significant potential for the technology together with its technological development. The market for materials, systems and services in AM is supposed to quadruple within the following 10 years. In the year 2012 it provided a turnover of EUR 1.7 bn and it is estimated to rise with exponentially to EUR 7.7 bn by the year 2023 (Roland Berger Strategy Consultants, 2013, pp.5–21).

Next to a steady growth of sales and earnings for AM companies, also the technology itself is improving. From the stage of Rapid Prototyping (RP), Rapid Manufacturing (RM) is used more often and implemented in a wide variety of product development process and manufacturing. For this reason, firms like the American industrial conglomerate "General Electric (GE)" plan to build up the world's first AM plant producing metal-based jet engine nozzles in volume production (General Electric, 2014).

The untapped potential resulting from this technology is positioned in metal applications. Therefore, first 3D metal powder printers were launched by the company EOS in the year 2001 (Madeley and Chaphalkar, 2013, p.4). Due to a continuous increase in the built rate, process reliability and improvements concerning technical parameters, such as the surface quality, 3D metal printing technologies are becoming more competitive versus conventional production processes. These economic advantages occur in particular when geometry complexity is high and production volumes are low (Ruffo et al., 2006, p.1418; Holmström et al., 2010, p.688).

The implementation of AM methods is increasing rapidly in various fields, such as aerospace and medical industries. Additionally, this technology becomes more likely to be implemented into automotive industries, enabling to build large and complex components without tooling (Concept Laser, 2015, pp.1–2).

1.2 Focus definition

This master thesis is mainly focused on cost and suitability of metal powder-based AM technologies. First of all, a definition of unique terms regarding Additive Manufacturing is presented. Consequently, several economical and technological dimensions are defined, such as input parameters, cost functions and command variables.

On the basis of the software program "MathWorks Matlab", a classification scheme is established which is implementing input parameters from a user. With this information, MathWorks Matlab is providing cost and suitability conclusions using logical algorithms and hidden cost functions.

Figure 1.1 shows a model of the used classification scheme including input parameters, an adjusting lever and output parameters. Input parameters, such as machine type and material, are implemented by the user.

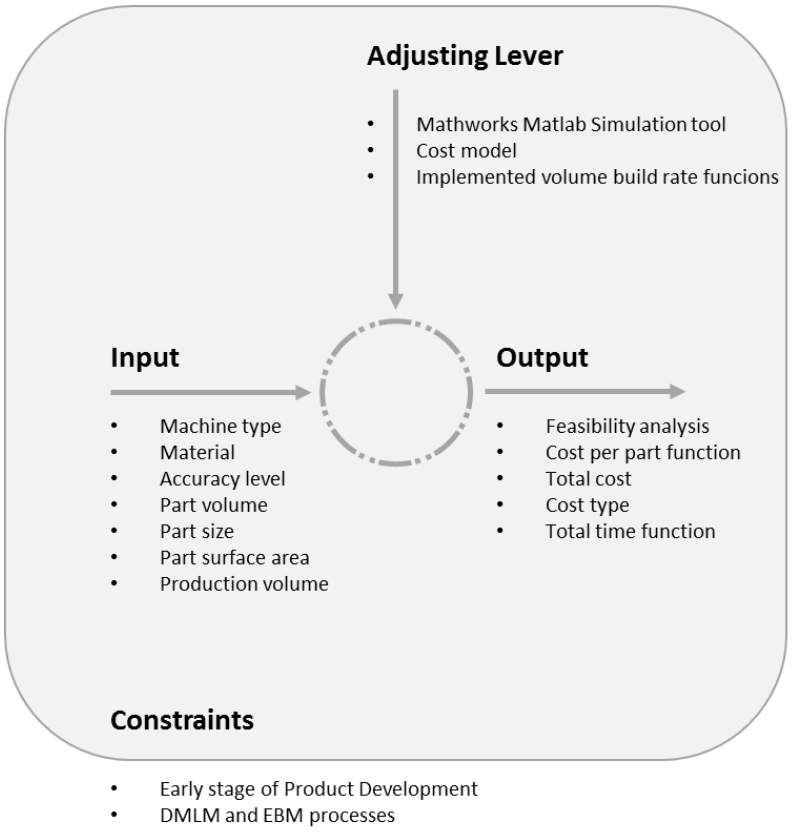

Figure 1.1: Classification scheme

This information is transferred to a simulation tool based on “Mathworks Matlab”, which acts as an adjusting lever implementing a cost model with several hidden volume build rate functions. As an output, first of all input parameters are evaluated in terms of feasibility. Secondly, cost functions such as cost per part and total time functions are generated and conclusions can be drawn. The listed parameters and the model itself are described more precisely in chapter 4 and 5 leading to clear definitions regarding this objective.

1.3 Structure and proceeding

The first chapter “Introduction” provides quick access for the reader to understand the focus and the main goal of this thesis. In the second chapter, metal- and powder bed based Additive Manufacturing (AM) are introduced. Additionally, the term AM is defined precisely and main processes in laser beam-based as well as electron beam-based Powder Bed Fusion (PBF) are outlined.

Subsequently, chapter 3 describes classification schemes to support the evaluation of manufacturing processes in AM. Based on this knowledge, research gaps are exposed and an overview of the research design methodology is shown in a process diagram. This figure divides the research design into three main parts, the input data and context (chapter 4), a simulation tool based on “MathWorks Matlab” (chapter 5) and a Design of Experiments (chapter 6). Chapter 4 includes input data for the simulation tool, such as machine prices, material costs and build volume rates for Maraging Steel 1.2709, aluminum alloy AlSi10Mg and titanium alloy Ti6Al4V. Moreover, the context of EBM and DMLM machines is described, which is elementary to understand results of the simulation tool.

Chapter 5 outlines the structure of the simulation tool, which is divided into material costs, expenses on machine and expenses on workforce. Furthermore, the Graphical User Interface (GUI) is shown and consequently output figures are described. Chapter 6, the Design of Experiments, comprises a sensitivity analysis between mass and building height, a skin-core analysis to evaluate different manufacturing methods, a comparison between laser beam-based and electron beam-based systems as well as random and Taguchi testing on five exemplary parts. Consequently, a result validation has been carried out and conclusions were drawn. In Chapter 7, a final discussion on the research questions, limitations, contributions and future research has been portrayed.

2 Basics of metal- and powder bed based Additive Manufacturing (AM)

In this chapter the term Additive Manufacturing is explained and its benefits are shown by providing numerous aspects of it. Based on this term, a common understanding for Powder Bed Fusion (PBF) is presented for the reader. This master thesis will focus only on laser beam-based and electron beam-based technologies, a final differentiation of terms is supposed to gain understandable and explicit definitions.

2.1 Additive Manufacturing

Recently, back in year 2009, a final definition of the term Additive Manufacturing was given by the ASTM International F42 Committee on Additive Manufacturing Technologies. AM is defined as a:

> *"process of joining materials to make objects from 3D model data, usually layer upon layer, as opposed to subtractive manufacturing methodologies."*
> (National Academy of Engineering of the National Academies, 2012, p.6)

As mentioned in this definition, AM describes a generative process, which creates 3D components generally through continuous layer-by-layer deposition. Examples for AM technologies "include stereolithography, fused deposition modeling, 3D printing, selective laser melting, laser engineered net shape processes, ultrasonic consolidation, and selective laser sintering (National Academy of Engineering of the National Academies, 2012, p.3)". The first step is to draw a 3D model with a Computer Aided Design (CAD) software. Subsequently, the CAD-file is transformed into the Surface Tessellation Language (STL) file, which divides the surface into numerous triangles. The 3D printing system slices the model into a large number of thin digital layers. These layers determine the generative deposition for 3D printers to enable layer-by-layer proceedings. After the STL-file is transferred to the 3D printing machine and the setup of this machine is executed, the building process can be started and the component is generated from the bottom to the top. Concluding, post-processing is essential in many cases and results in an increased total process time. AM is frequently combined with the terms Rapid Prototyping (RP) and Rapid Manufacturing (RM). The difference between these two terms can be found in its output rates and purposes. Whereas RP is meant to create prototype models rapidly for the visualization of components, RM is used for the production of small batch sizes of end-user industrial components with high complexity (Gibson et al., 2010, pp.1–5).

Major benefits and impacts of AM can be observed in several domains. According to Garrett (2013), these domains can be classified into the supply chain, customization, design and sustainability of products. The effect of AM on the supply chain includes beneficial impacts both on the agile/ lean supply chain management and the reduction of the inventory size. It enables mass customization and allows more complex geometries and lighter products to be built. Moreover, AM provides positive effects on the environmental, social and economic sustainability (Garrett, 2013, pp.1–6). Further advantages can be named, such as the elimination of the tooling process, a lower amount of assembly parts and a reduction in production steps. As a result, components can be printed directly without the need of process planning.

Next to the advantages, numerous disadvantages occur in low build rates based on technological barriers, high manufacturing costs due to metal powder costs and slow build rates. Additionally, the need of post-processing which arises from insufficient surface qualities, accuracies and component anisotropy as well as its limitation in the component size resulting from the dimensions of the chamber are the main disadvantages of AM processes. The two most relevant technologies in AM for metal-based production are the powder bed fusion (PBF) technology with the highest relevance and the directed energy deposition (DED). PBF describes a melting process of metal particles in a powder bed, whereas DED uses the thermal energy to depose fused metal parts on given surfaces. Because PBF is characterized as the most convenient manufacturing process for prototyping and direct part production, the focus will be positioned on it in this thesis (Roland Berger Strategy Consultants, 2013, pp.14–18).

2.2 Powder Bed Fusion

The first PBF technology was developed by the University of Texas (USA) resulting in Selective Laser Sintering (SLS). One or more thermal sources can partially or fully melt both polymer and metal powders to unite particles. During the cooling phase the powder material changes into a solid phase and components are developed through this layer-by-layer deposition process. Due to limitations in temperature levels generated by ancient laser beams, high melting particles could only be connected through low melting particles acting as a glue (Gibson et al., 2010, pp.103–109). To avoid misunderstandings concerning terms of sintering and melting, chapter 2.3 provides a clear distinction of terms necessary for powder bed based AM. Because of higher build rates and more appropriate isotropy properties full melting technologies are more relevant for current metal-based 3D printers (Kruth et al., 2007, p.745). They can be distinguished into laser beam-based and electron beam-based technologies, dependent on their inserted type of energy source.

2.2.1 Laser beam-based PBF

Mechanism

The platform of SLS/SLM machines consists of two feed cartridges, in which the unused metal powder is located. Between the cartridges a build platform is positioned to form the powder bed. On the top, a laser beam is directed to 2-axis mirrors, which deflects its massless photons on the powder bed and selectively melts the powder through energy transfer. Current SLS/SLM machines insert YB-fiber lasers with up to 1000 W and have replaced CO_2 lasers in previous direct metal printing machines with lower power levels (Kruth et al., 2007, p.732). A multi-beam technology was developed to use up to 4 laser beams at the same time to increase the build time and reduce manufacturing costs (SLM Solutions, 2014, p.4). Subsequent to the melted particles solidifying, the build platform is lowered and the feed cartridges are lifted. Thus, metal powder is set free and positioned as a new layer on the powder bed by using a counter-rotating powder revealer. This process is consecutively repeated until the final layer of the component is melted. Finally, the enclosing powder of the component can be removed and potential post-processing starts.

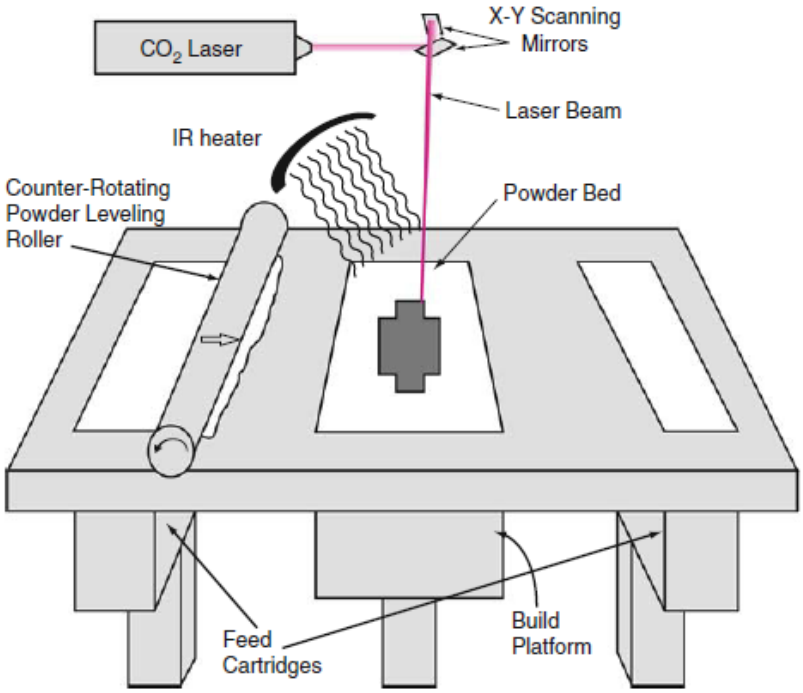

Figure 2.1: Mechanism of Laser beam-based powder bed systems (Gibson et al., 2010, p.104)

Best in class (build size, productivity)

The biggest laser melting machine so far belongs to the company "Concept Laser" (X line 1000R) with powder bed dimensions of 630 x 400 x 500 mm (x,y,z). Stainless steel, pure titanium, aluminum-, nickel- and titanium alloy powders are processed by a 1 kW fiber laser (Concept Laser, 2015). The fastest 3D metal printer is offered by SLM Solutions and is named

SLM 500 HL. Up to 4 lasers and scanners are working at the same time with either 4x400W or 2x (400W+1000W) fiber lasers. The powder bed dimensions are 500x280x320 cm^3 and a build rate with up to 105 ccm/h is achieved under perfect conditions (SLM Solutions, 2014). Build rates of 70 ccm/h for the SLM 500 HL are realized in another source, unfortunately without mentioning material properties and process parameters (Wohlers, 2013, p.91).

Advantages and disadvantages

Advantages of laser-beam based PBF can be seen in good surface finish qualities, high feature resolution and the ability to produce relatively big components. Further, a wide range of different materials and multi laser developments seem to be interesting for a big ratio of manufacturing companies. On the other hand, disadvantages like high residual stresses can lead to micro cracks in produced parts. Furthermore, mechanical properties (ultimate tensile strength and ductility, yield strength) provide improvement potential in general (Manfredi et al., 2014, p.11).

2.2.2 Electron beam-based PBF

Mechanism

In figure 2.2 the mechanism of an Electron beam-based powder bed system is presented. A tungsten filament is heated up and is setting free electrons, which are accelerated up to 75 % of the speed of light. A focusing coil and a deflection coil guarantee the induction of heat arising from converted energy of the electrons. The deflection is executed through electromagnetic lenses.

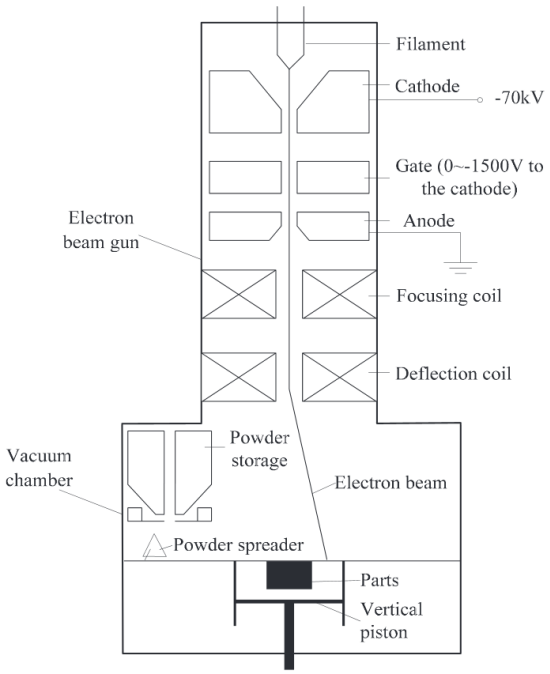

Figure 2.2: Mechanism of Electron beam-based powder bed systems (Ge et al., 2014, p.1194)

To avoid oxidation in the produced part, the melting procedure has to take place in vacuum surroundings. About 85 % of power is transferred from kinetic energy into heat energy in solid state processes, whereas up to 95 % of it is converted in liquid state processes. Remaining power portions are deflected in various forms of energy, such as x-rays, heat radiation, backscattered-, thermionic- and secondary electrons (Encyclopedia of Tribology, 2013, pp.923–924). A powder storage supplies the system with new powder, which is transported to the powder bed by a powder spreader. Similarly to laser-beam based PBF, the processed part is lowered to spread new powder on the powder bed and melt a consecutive layer out of metal particles. If the production of the component is completed, unused powder will be removed and post processing can be started.

Best in class (build size, productivity)

The Arcam Q20 enables maximum build sizes of 350 mm in diameter and 380 mm in height. With a maximum beam power of 3000 W and a minimum beam diameter of 180 µm, a build speed of up to 80 ccm/h can be achieved, process and material parameters were not mentioned in the published file (Arcam AB, 2013, p.4).

Advantages and disadvantages

In a study published by the Encyclopedia of Tribology (2013), main advantages can be seen in the deflectability through magnetic fields and the formability by the focusing coil allowing numerous beam deflection patterns. Furthermore, high efficiency levels (95% in liquid state processes), good beam stability and beam profiles are major advantages of the electron beam technology (Encyclopedia of Tribology, 2013, pp. 924).

Wohlers (2013) claims that the electron beam can be split up into up to 100 separate beams. Hence, the build rate is increased and reaches its maximum of 55 to 80 ccm/h under perfect conditions with Ti-6Al-4V alloys. These AM systems gain from high power and consequently fast build rates. The level of power implemented in current EBM machines is reaching up to 3000 W (Arcam AB, 2013, p.4). Additionally, low thermal stresses and thermal gradients appear with EBM. The customers of Arcam machines are mainly related to orthopedic and aerospace industries, as well as research institutes. The biggest disadvantage in EBM is described by a poor surface finish and lower accuracies compared to most laser-based PBF systems, caused by insufficient minimum beam diameters, process instabilities and a lack of knowledge in beam-surface interactions (Wohlers, 2013, pp.72–73). Moreover, a wide range of materials is not given, EBM is mainly used for titanium components.

2.3 Differentiation of terms

As shown by ASTM International (2012), standard terminologies in AM exist for the terms "laser sintering", "selective laser sintering (SLS)" and "direct metal laser sintering/ melting (DLMS/ DMLM)".

Table 2.1: Standard Terminology for AM Technologies (ASTM, 2012, pp.1–3)

Laser sintering (LS)	"a powder bed fusion process used to produce objects from powder materials using one or more lasers to selectively fuse or melt the particles at the surface, layer by layer, in an enclosed chamber. DISCUSSION—Most LS machines partially or fully melt the materials they process. The word "sintering" is a historical term and a misnomer, as the process typically involves full or partial melting, as opposed to traditional powdered metal sintering using a mold and heat and/or pressure."
Selective laser sintering (SLS)	"denotes the LS process and machines from 3D Systems Corporation"
Direct metal laser sintering (DMLS) **Direct metal laser melting (DMLM)**	"a powder bed fusion process used to make metal parts directly from metal powders without intermediate "green" or "brown" parts; term denotes metal-based laser sintering systems from EOS GmbH – Electro Optical Systems. **Synonym: direct metal laser melting**"

Table 2.2: Further Terminology for Additive Manufacturing Technologies (Wohlers, 2013, p.60)

Selective laser melting (SLM)	The term "Selective Laser Melting" is licensed by the German Additive Manufacturing company SLM Solutions and based on its mechanism it is similar to all other listed terms in Table 2.1 (Deutsches Patent- und Markenamt).
Laser melting (LM)	Related to the British company Renishaw
LaserCUSING	Registered by the German company Concept Laser GmbH
Electron beam melting (EBM)	Used by the Swedish company Arcam AB

As mentioned in Table 2.1, the term "sintering" is confusing because of its historical background bringing high melting particles and low melting particles together. However, terms like SLS and DMLS are well established and popular in literature (Wohlers, 2013, p.60).

Basically each company and research department uses its own term for direct metal fabrication processes. In contrast to the assumption that the company 3D Systems is using the term "Selective laser sintering" for both plastic and metal parts, a closer look at their webpages points out differences. When they talk about SLS, plastic is the processed material. For metal parts 3D Systems uses the term "Direct Metal Printing (DMP)" (3D Systems, 2015).

According to Wohlers (2013), almost 200 metal AM systems were sold in the year 2012 and EOS GmbH had the biggest ratio of vended machines. When 74 companies were asked in an industry survey, which technology they would like to install in their own company, the majority voted for the powder bed fusion technology from EOS (Wohlers, 2013, pp.133–144).

For these reasons, the term "Direct Metal Laser Melting (DMLM)" is being used in this master thesis and is standing for direct metal part fabrication by fully melting selective parts of the powder bed. Even though EOS mostly calls their own metal printing process sintering, melting is describing more precisely this technology and avoids misunderstandings.

For powder bed fusion processes with electron beams the term EBM is used in this thesis, because Arcam AB is the only company implementing electron beams for direct metal layer-by-layer deposition.

In chapter 2, the definition of relevant terms and an introduction to AM was given. Its potential, general mechanism and benefits as well as disadvantages were outlined. Focusing on powder bed fusion processes as one of most relevant techniques in AM for industrial companies, a distinction between laser beam-based and electron beam-based PBF was established. Powder bed-based techniques were characterized by terms of mechanisms, best-in-class machines and advantages but also disadvantages. Finally, a differentiation of terms in PBF was provided, calling direct metal part fabrication by fully melting selective parts of the powder bed Direct Metal Laser Melting (DMLM).

3 Classification schemes to support evaluation of manufacturing processes in AM

3.1 State of the art

Classification schemes in AM were created to support the selection process between different machines and/or AM processes. Typical criteria for AM process selection can be listed in cost, time, quality, accuracy, wall thickness, material properties and price of the AM system (Byun and Lee, 2005, p.1339). Moreover, most decision making tools include stereolithography (SLA), selective laser sintering (SLS) and fused deposition modeling (FDM) (A. Lifton et al., 2014, p.404).

In table 3.1, an overview of existing classification schemes between the years 2005 and 2010 is presented.

Table 3.1: Summary of AM decision-making tools (Ghazy, 2012, p.32)

Year	System	Developers	RP	RM	RT	Process Selection	Material Selection	Machine Selection
2005	RP Selector	IVF (Sweden)	✔	✔	✔	✔	✔	✔
2005	RM Selector	Georgia Institute of Technology	✔	✔		✔		✔
2005	IRPDMS	Mahesh et al.	✔	✔		✔		✔
2007	RT databases	Pal & Ravi			✔	✔		
2007	Computer Aided RT Selection	Hanumaiah et al.			✔	✔		
2008	RM Selector	Smith & Rennie	✔	✔			✔	✔
2010	RMADS	Munguia et al.	✔	✔		✔	✔	
2010	KARMA	FP7 Project	✔	✔		✔	✔	✔

Two of the listed systems, the RP Selector from IVF in Sweden and the KARMA system of FP7 Project cover a wider range of functionalities. They include machine selection, material selection, process selection, rapid prototyping and rapid manufacturing. Additionally, the RP Selector from 2005 allows rapid tooling.

3.2 AM decision support system based on “Math Works Matlab”

Ghazy (2012) developed an AM decision support system based on MathWorks Matlab. It includes a graphical user interface (GUI) and asks for the length, width and height of the part, the production volume, its surface finish, accuracy levels and minimum wall thickness. Subsequently, a list with possible manufacturing processes is given as an output. Additionally, an implementation of material properties and a ranking of criteria by the user of the tool leads to more precise results. Finally, a total ranking of different AM processes is shown, which supports the user in choosing the most suitable process (Ghazy, 2012, pp.20–55).

3.3 Resulting research gaps

Nevertheless, during the formal benchmark of this master thesis a decision support tool mainly focusing on metal-based AM has not been found. Most AM decision-making tools are based on specialized plastic-based evaluation models, while metal-based AM processes are included rarely or not at all. Additionally, due to a rapid development in DMLM and EBM machines, current improved machine systems are not included in latest decision support systems dealing with metal-based AM systems. Especially machines with laser-beams over 200 W can be rarely found in existing decision support systems.

Moreover, the differences in cost and time between electron beam-based and laser beam-based systems are not fully investigated, the waste and powder recycling process is typically not added and new build up technologies such as the skin-core method do not play a role in existing decision support models.

These findings lead to several research questions (RQ) defined below:

RQ1: How can several current metal-based Additive Manufacturing machines up to 3000 W be compared and evaluated with each other in terms of cost and feasibility?

RQ2: What are the main differences between laser-beam and electron-beam based systems?

RQ3: What are the most influential input variables to evaluate the performance of AM systems?

3.4 Research Design methodology diagram

Figure 3.1 shows the Research Design methodology diagram behind the created selection support system based on MathWorks Matlab. It consists of three major phases, the input data and context (chapter 4), the simulation tool (chapter 5) and the DoE (chapter 6). The outlined model includes Rapid Manufacturing, a process selection between DMLM and EBM, a selection of current machines with beam powers between 50 and 3000 W as well as material and accuracy selection. It adds newest build strategies (skin-core) and respects powder recycling processes. As a result, two different or equal printers can be compared with each other simultaneously, presenting cost per part, total cost, total time and cost type values.

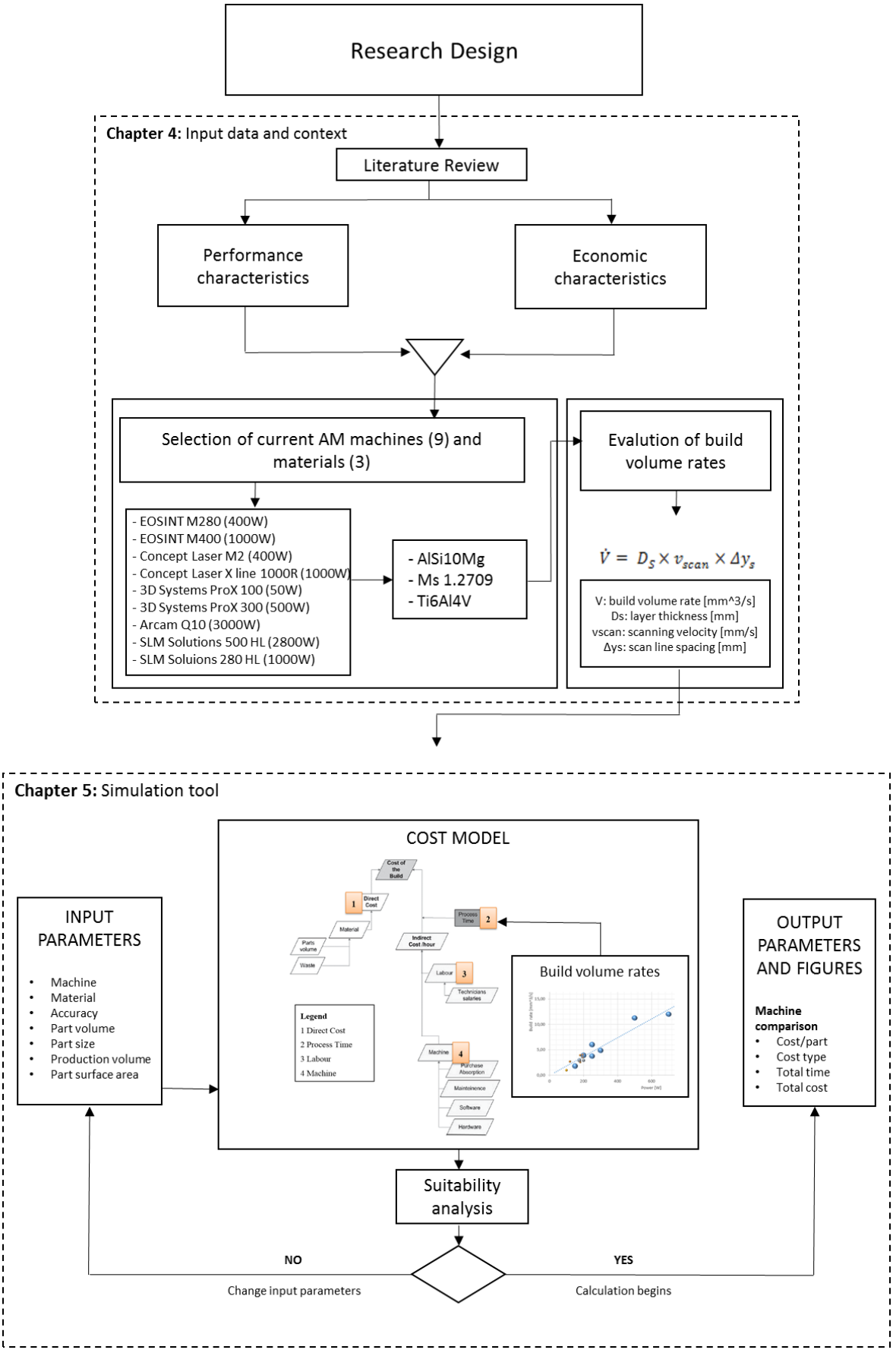
Research Design
Chapter 4: Input data and context
Literature Review
Performance characteristics
Economic characteristics
Selection of current AM machines (9) and materials (3)
- EOSINT M280 (400W)
- EOSINT M400 (1000W)
- Concept Laser M2 (400W)
- Concept Laser X line 1000R (1000W)
- 3D Systems ProX 100 (50W)
- 3D Systems ProX 300 (500W)
- Arcam Q10 (3000W)
- SLM Solutions 500 HL (2800W)
- SLM Soluions 280 HL (1000W)
- AlSi10Mg
- Ms 1.2709
- Ti6Al4V
Evalution of build volume rates
$\dot{V} = D_S \times v_{scan} \times \Delta y_s$
V: build volume rate [mm^3/s]
Ds: layer thickness [mm]
vscan: scanning velocity [mm/s]
Δys: scan line spacing [mm]
Chapter 5: Simulation tool
INPUT PARAMETERS
Machine
Material
Accuracy
Part volume
Part size
Production volume
Part surface area
COST MODEL
Legend
1 Direct Cost
2 Process Time
3 Labour
4 Machine
Build volume rates
OUTPUT PARAMETERS AND FIGURES
Machine comparison
Cost/part
Cost type
Total time
Total cost
Suitability analysis
NO
Change input parameters
YES
Calculation begins

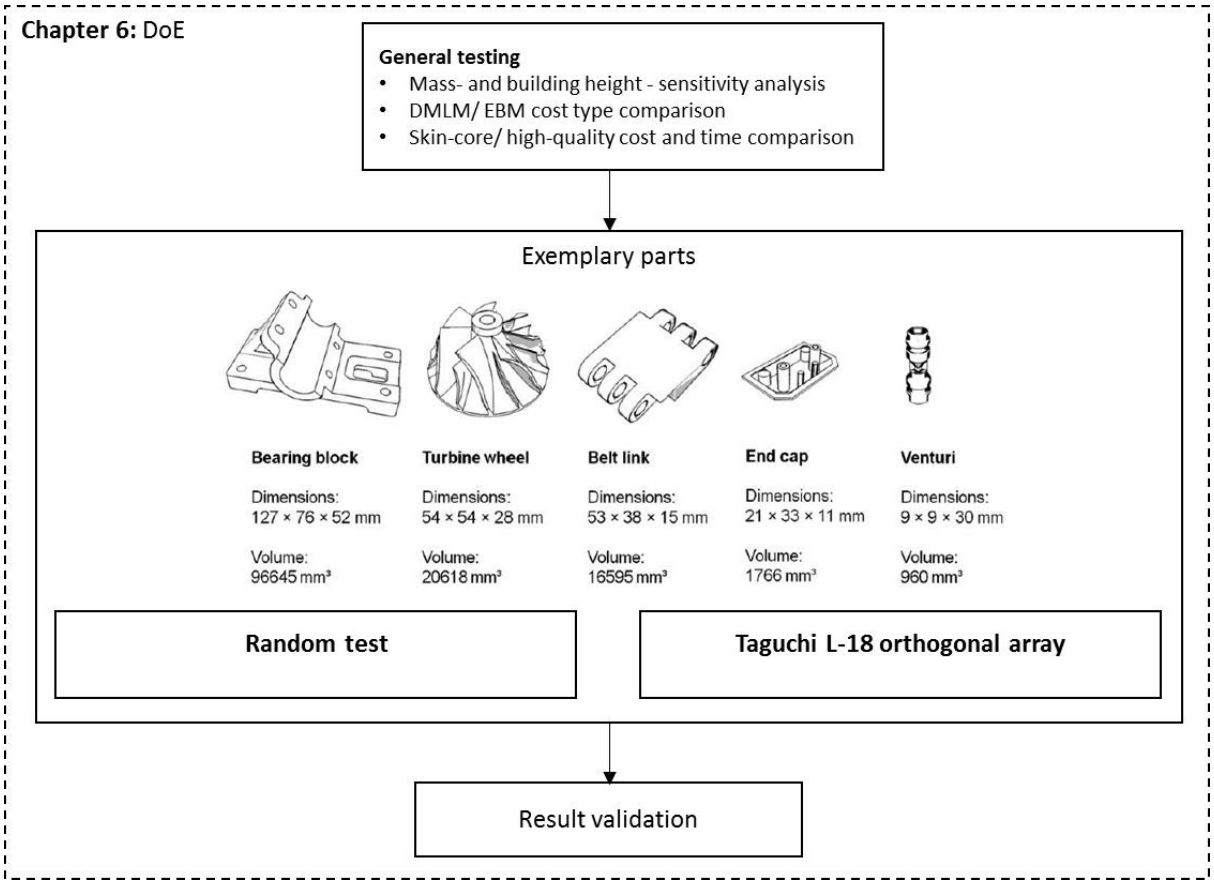

Figure 3.1: Research Design

The methodology of the "Research Design" consists of three different segments. First, the input data and context defines relevant machines and materials by including performance and economic characteristics. Subsequently, build volume rates are calculated by implementing layer thickness, scan speeds and scan line distances into a given formula. The main source for this data was transferred from porosity/ scan-speed figures by setting a maximum porosity level of 2 % respectively 0.5 % and deriving build volume rate functions out of it.

In a second step, a Matlab Simulation program was created to evaluate costs per part, different cost types, total time and total costs of two machines at the same time. The core element can be seen in the cost model with build volume rates running in the background. A suitability analysis guarantees that the input parameters fulfill the machine properties of selected systems.

The DoE segment includes a generalized mass- and building height- sensitivity analysis by varying mass respectively the building height. Moreover, 5 exemplary parts with different dimensions, volumes and surface areas, are tested in a random test and a Taguchi L-18 orthogonal array. Finally, results are validated and presented.

4 Input data and context for the planning of a Simulation tool for metal-based AM

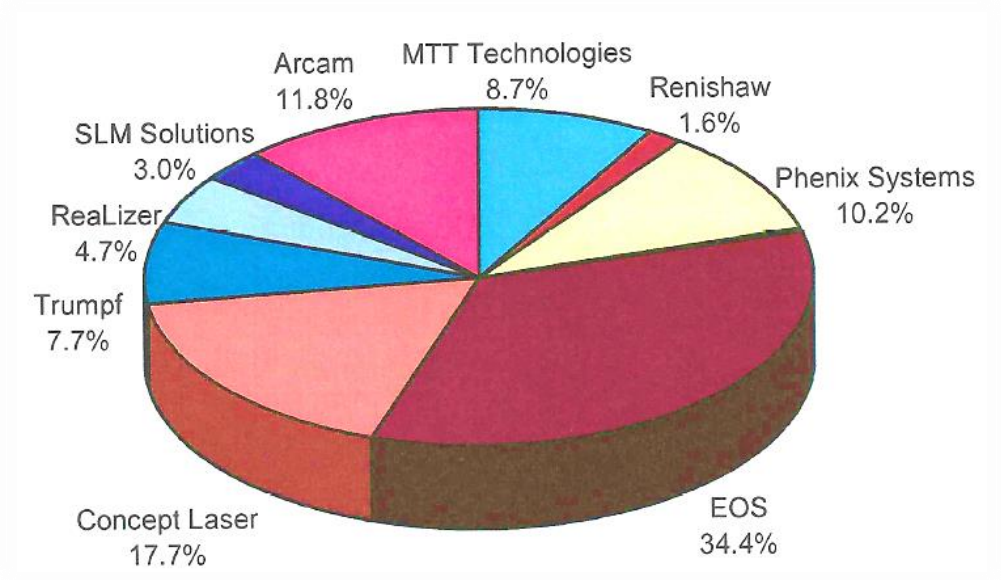

Figure 4.1: Cumulative market shares of metal-based machines sold in 2012 (Wohlers, 2013, p.159)

In order to analyze DMLM and EBM it is important to examine market shares, the development of technical parameters and differences of these two divergent metal-based AM systems. To collect information about the leading companies in metal-based AM a market analysis is presented, which determines the two most successful companies in metal-based AM. Based on this information, their technology parameters will be compared and differences will be explained.

In total, 1029 metal-based additive manufacturing machines were sold until end of 2012. The leading company during this period was EOS with a market share of 34.4 %, which leads to a number of 354 machines. The second place is represented by the company Concept Laser (17.7 %) with 182 machines being sold until 2012. Arcam on the third place with a market share of 11.8% was vending 121 machines (Wohlers, 2013, p.159). The difference between these three companies can be observed in their technology. Whereas EOS and Concept Laser are using DMLM, Arcam is known to be the only EBM company. Additionally, it has to be mentioned that the company Trumpf produces AM machines based on the direct energy deposition process. Furthermore, MTT Technologies was renamed into SLM Solutions. For this reason, the cumulative market shares of MTT Technologies and SLM Solutions can be summed up, which results in a market share of 11.7 % representing 120 sold machines until 2012. First, most current DMLM and EBM machines will be compared. Subsequently, a comparison of DMLM and EBM systems will be elaborated with the focus on market leading metal-based companies.

4.1 Direct Metal Laser Melting (DMLM) machines

This chapter shows an up-to-date list of DMLM machines of market leading companies. In addition, main parameters like the beam power [W], the layer thickness range [µm], the maximum build volume [ccm] and the minimum beam spot size [µm] will be reported.

Table 4.1: EOSINT M270 parameters (A1)

EOSINT M270	
Beam power [W]	200
Layer thickness range [µm]	20 - 100
Max. Build volume [ccm]	13437,5
Beam spot size range [µm]	100 - 500

Table 4.2: SLM 500HL parameters (A2)

SLM 500HL	
Beam power [W]	2800
Layer thickness range [µm]	20 – 200
Max. Build volume [ccm]	45500
Beam spot size range [µm]	150 - 700

All relevant machine parameters can be found in the appendix. An overview showing additional machines is portrayed in Table 4.3.

Table 4.3: In this study implemented DMLM machines

EOSINT M280 (400W)	3D Systems ProX 300 (500W)
EOSINT M400 (1000W)	SLM Solutions 500 HL (2800W)
Concept Laser M2 (400W)	SLM Solutions 280 HL (1000W)
Concept Laser X line 1000R (1000W)	3D Systems ProX 100 (50W)

In total, a selection of 8 different DMLM machines will be included to a simulation tool based on MathWorks Matlab with power ranges between 50 to 2800 W and significant distinctions in the maximum build volume.

4.2 Electron Beam Melting (EBM) machines

Analogous to chapter 4.1, in which DMLM systems were presented, chapter 4.2 focuses on EBM machines. Two machines, the Arcam Q20 and the Arcam Q10 are outlined in detail, further machine parameters are described in the appendix.

Table 4.4: Arcam Q20 parameters (A7)

Arcam Q20	
Beam power [W]	3000
Layer thickness range [µm]	?
Max. Build volume [ccm]	9139,8
Beam spot size range [µm]	180 – 1000

Table 4.5: Arcam Q10 parameters (A16)

Arcam Q10	
Beam power [W]	3000
Layer thickness range [µm]	?
Max. Build volume [ccm]	7200
Beam spot size range [µm]	100 – 1000

Table 4.6: In this study implemented EBM machines

Arcam Q10 (3000W)

Next to the described DMLM machines, an EBM Arcam Q10 will be part of this study. This one was chosen because it belongs to one of the newest models and has a square build platform, while the Q20 is equipped with a round build platform. As a consequence, the evaluation of the batch size (production volume during one build-up procedure) can be standardized and does not have to be adjusted for round platforms.

4.3 Comparison of DMLM and EBM machines

A comparison between DMLM and EBM machines is provided in order to have a better understanding of the differences of each system. Consequently, performance and economic characteristics are shown and analyzed.

4.3.1 Performance characteristics

In this historical comparison of technology parameters, meaningful and easy-accessible parameters were summarized by filtrating information from specific technical data sheets (A3 to A5). The starting point of this survey is positioned at the first DMLM system being sold in 1995 by EOS. The following timeline shows the year of introduction and the name of the system. In figure 4.2, the first row is represented by EOS machines, the second one by Arcam and the third one by Concept Laser systems.

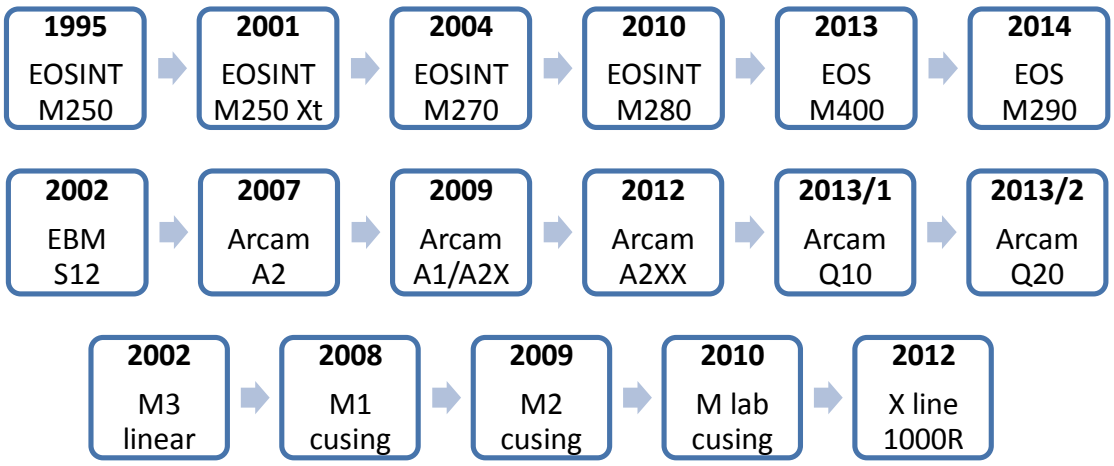

Figure 4.2: Timelines of EOS, Arcam and Concept Laser DMLM/ EBM systems from 1995 to 2014

According to figure 4.2, EOS was introducing their first DMLM system much earlier than their biggest rival Concept Laser. In 2002, Concept Laser and Arcam were placing the “M3 linear” and the “EBM S12” on commercial markets. Furthermore, it can be observed that many new system models were established in recent years. From 2009 to 2014 this number is already amounting ten, showing strong demand from customers and strategies of diversification by system suppliers. Further, significant improvements of technology parameters can be measured, such as build size, maximum beam power and the minimum beam size.

Build size

Build sizes are determining the maximum space-capacity of 3D printers. Bigger sizes allow higher batch sizes respective equal component sizes. This results in higher productivity rates and lower costs, if equal build rates for different build sizes are assumed. In the chart of figure 4.3, the development of maximum build sizes until 2014 is described. Arcam introduced two EBM systems (Q10/Q20) in the same year, this explains a distinction into Arcam1 (Q10) and Arcam2 (Q20).

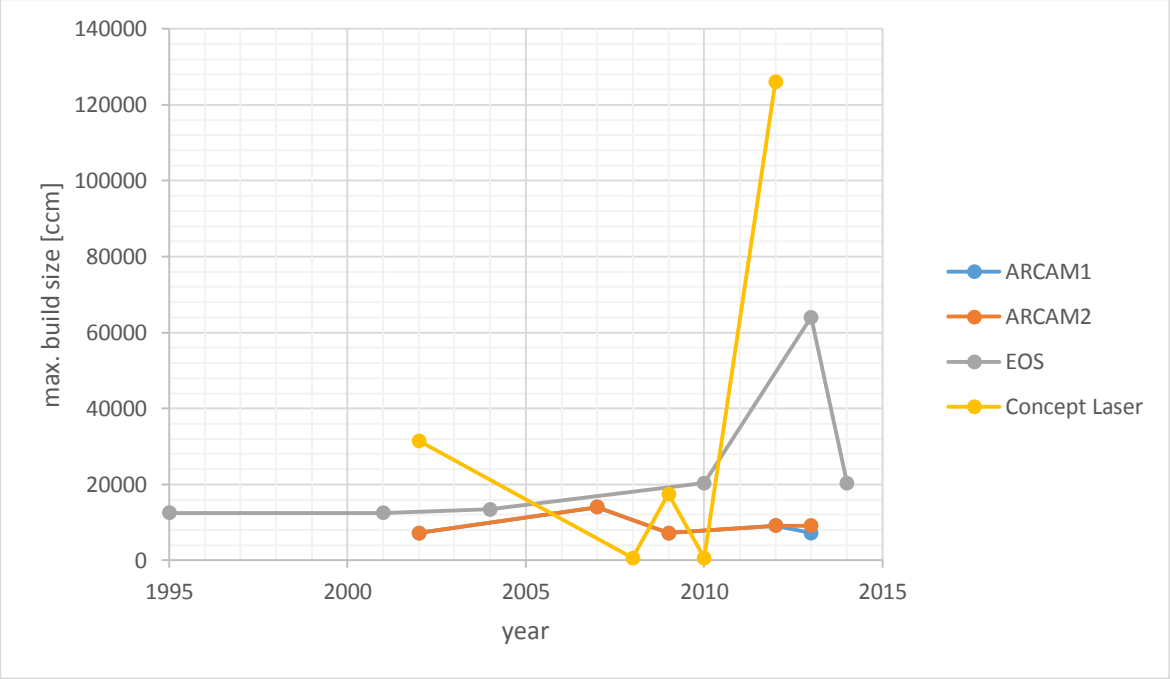

Figure 4.3: Development of the build size from 1995 to 2014

Build size values can be received by multiplying length, width and height. DMLM systems represent higher maximum build sizes in general. It seems that Arcam tried to compete in build sizes until the year 2007, but then focused on smaller ones for e.g. medical implants. Whereas EOS never produced DMLM systems with build sizes under 10000 ccm, Concept Laser published their models “M1 cusing” and “M lab cusing” with 648 ccm for small part production, including jewelry into the AM portfolio.

Comparing the biggest DMLM system (X line 1000R), which was designed for the Daimler AG to produce whole engine blocks, with the biggest EBM system (M250 Xt), a build size ratio of 9 can be calculated. This number shows the enormous difference in build sizes between EBM and DMLM systems.

$$build\ size\ ratio = \frac{126000\ ccm}{14000\ ccm} = 9$$

Beam Power

Figure 4.4 represents the maximum beam power between EBM and DMLM systems. A big gap between these systems can be observed.

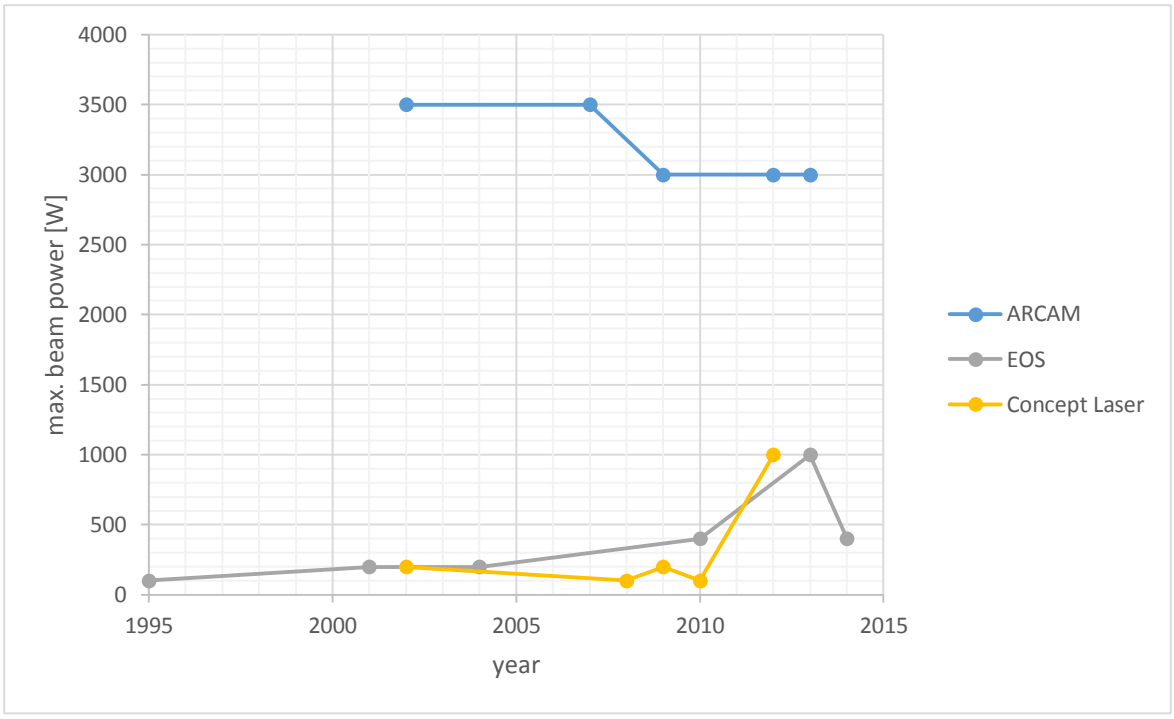

Figure 4.4: Development of maximum beam powers from 1995 to 2014

Whereas Arcam started with maximum beam powers of 3500 W, EOS was implementing 200 W lasers into their newest model in 2001. EOS constantly increased its maximum beam power, in contrast to Concept Laser, which were using relatively low beam powers between 100 W to 200 W until 2010. It has to be mentioned that SLM Solutions established a DMLM system with a max. beam power of 2800 W in total, arising from a new multibeam technology (SLM Solutions, 2014). Therefore, four separate laser sources are implemented into the current system.

Higher beam powers are leading to shorter particle melting periods. Consequently, build times can be increased and higher competitive standards compared to conventional manufacturing can be achieved. Additionally, high beam powers on small beam spot sizes guarantee high intensity levels. This leads to higher penetration depths in the powder bed and can affect several layers at once, which consequently leads to lower accuracy levels. Beside intensity levels, penetration time of photons (DMLM) or electrons (EBM) has a significant influence on the penetration depth.

Beam spot size

Figure 4.5 describes the minimum sport sizes in EBM and DMLM systems during the last 20 years.

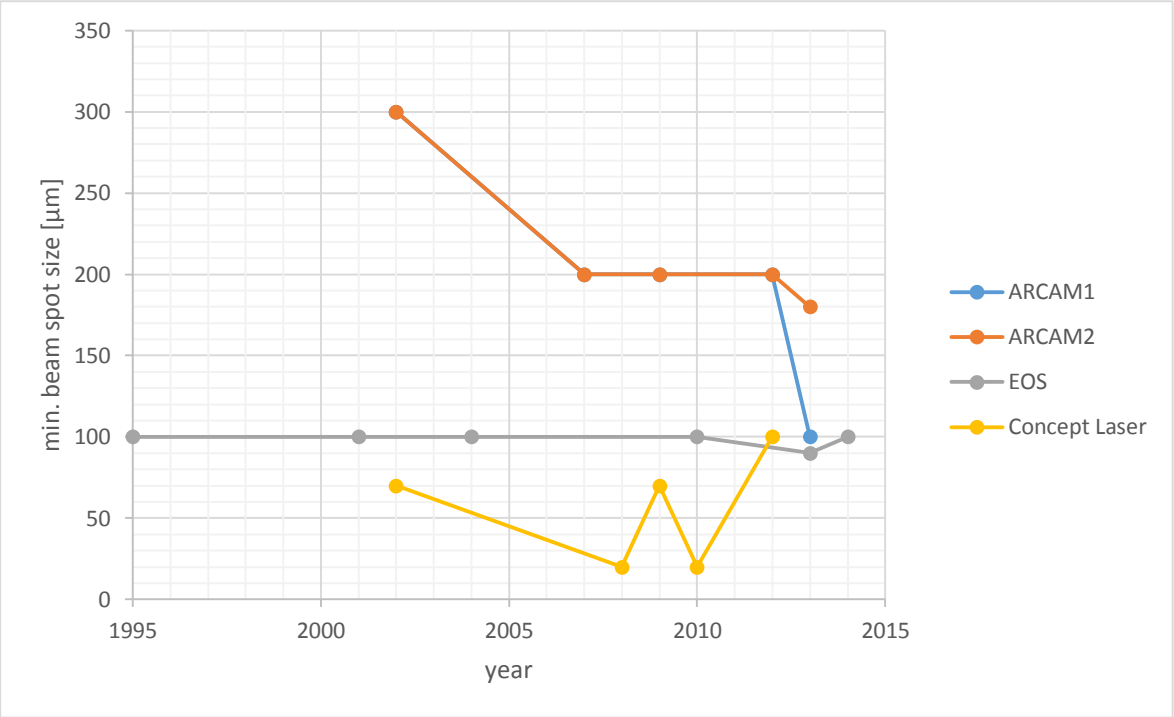

Figure 4.5: Development of the min. beam spot size 1995 to 2014

It examines that EOS systems stayed consequently on the same minimum spot size levels between 90 and 100 µm, while Concept Laser developed two systems with minimum diameters of 20 µm, particularly for elaborated structures like jewelry. Arcam was able to reduce their minimum beam spot sizes during the observed period, enabling a minimum beam spot size of 100 µm in the latest Q10 version.

The minimum beam spot size represents one of the major parameters determining accuracy and surface finish in AM. Otherwise, quality problems in decreasing the beam spot diameters occur for EBM systems (see Figure 4.6).

In Figure 4.6 thin walls were produced with beam spot sizes decreasing (from a to b).

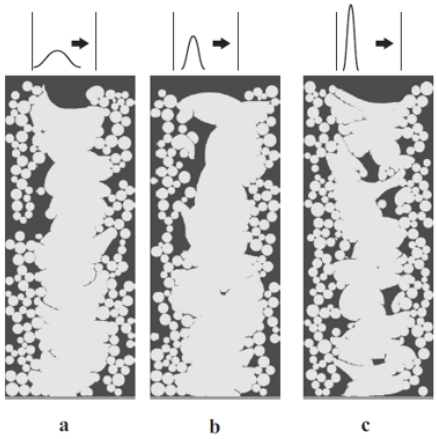

Figure 4.6: Decreasing beam spot diameters affecting wall quality (Attar, 2011, p.92)

This causes higher intensity levels leading to deeper melt pools and higher scan speeds. Hence, irregular wall thicknesses with high porosity can be observed (Attar, 2011, pp.90–92).

Mechanical properties and bulk hardness

In Figure 4.7 strength, elongation and bulk hardness parameters for Ti-6Al-4V specimens are presented by using different fabrication methods. In addition, EBM and DMLM as well as conventional methods (cast, wrought) methods are compared. For this reason, the AM specimens were produced with an EOSINT M270 and an Arcam A2, both machines commercialized around ten years ago.

As it was shown by Koike (2011), significant deviations between EBM and DMLM as well as AM methods and conventional methods in terms of strength cannot be observed. However, elongation in conventional wrought fabrication methods differ considerably from all other presented methods. It can reach up to 14%, whereas casting indicates 4%, DMLM 7% and EBM 3%. Comparing AM methods, DMLM points out small advantages in stress and significant ones in elongation. Additionally, Koike reports that better bulk characteristics can be seen in AM methods, both EBM and DMLM methods provide advantages.

Figure 13. Mechanical properties of metals using different fabrication methods.

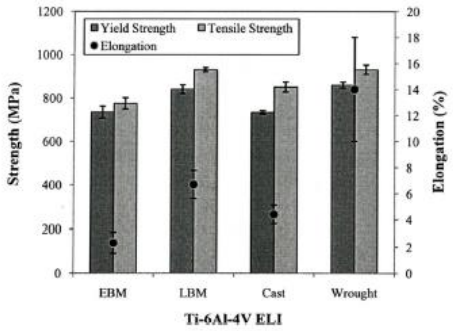

Figure 14. Bulk hardness of Ti-6Al-4V ELI specimens using different fabrication methods.

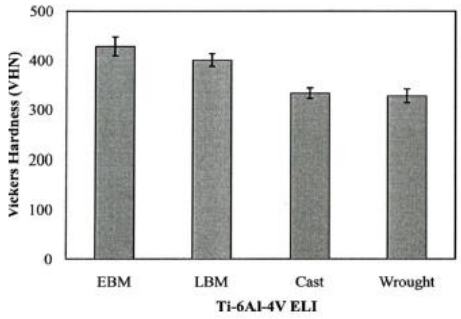

Figure 4.7: Mechanical properties and bulk hardness of Ti-6Al-4V (Koike et al., 2011, p.1788)

Further characteristics

Table 4.7 describes further differences between EBM and DMLM regarding several characteristics such as atmosphere, scanning and scan speeds. Whereas the scanning in EBM performs with deflection coils using magnetism, DMLM consists of mechanically operating galvanometers. This results in much faster scan speeds than in DMLM. Nevertheless, DMLM offers much better surface finish qualities and feature resolution, the range of materials is more versatile and a vacuum environment is not required.

Table 4.7: Main characteristics of EMB and DMLM (Gibson et al., 2010, p.127)

Characteristic	Electron beam melting	Selective laser melting
Thermal source	Electron beam	Laser
Atmosphere	Vacuum	Inert gas
Scanning	Deflection coils	Galvanometers
Energy absorption	Conductivity-limited	Absorptivity-limited
Powder pre-heating	Use electron beam	Use infrared heaters
Scan speeds	Very fast, magnetically-driven	Limited by galvanometer inertia
Energy costs	Moderate	High
Surface finish	Moderate to poor	Excellent to moderate
Feature resolution	Moderate	Excellent
Materials	Metals (conductors)	Polymers, metals and ceramics

In a study of Morris Technologies, an American AM company, a comparison between DMLM and EBM based on a list of characteristics was outlined (A6). This table was published in 2012, however, the values of examined characteristics have to rely on more current machine data. As a consequence, the newest EOS machine (EOS M290) will be compared to the newest Arcam machine (Q20) based and modified on the study of Morris Technologies.

As shown in Table 4.8, a comparison between current AM metal printers demonstrates advantages and disadvantages of the examined systems. It is comparing the previous table of Morris Technologies (A6) with the current one in table 4.8. Current values evidence that the balance of power is shifting to DMLM systems. Improvements were basically transacted in build envelope sizes, residual stresses as well as surface finish parameters. As a conclusion, DMLM technology is more sufficient for a wide variety of applications, whereas EBM supplies niche markets. The previous main advantage of EBM systems, its faster build rates, cannot be overserved in current metal based AM systems.

Table 4.8: EOS M290 vs. Arcam Q20 (A7 and A8)

Characteristic	**EOS M290**	**Arcam Q20**	**Result**
Build envelope	20312.5 ccm	9140 ccm	DMLM
Beam power	400 W	3000 W	EBM
Min. Beam spot size	100 µm	180 µm	DMLM
Mechanical properties* (Strength & Elongation)	850-950 MPa 7 %	750-800 MPa 3 %	DMLM
Bulk Hardness*	400 VHN	450 VHN	EBM
Atmosphere	Inert gas (nitrogen/ argon)	Vacuum	DMLM
Scanning	Galvanometers	Deflection Coils	EBM
Surface finish/ Detail resolution	Very good/ good	Fair	DMLM
Approved materials	Light metals, stainless and tool steel, superalloys	Titanium & Cobalt-Chrome alloys	DMML

In Chapter 4.3.1, main characteristics of DMLM and EBM were pointed out and compared with each other. Therefore, the publication date and important features of EOS, Concept Laser and Arcam systems were examined. As a result, DMLM systems produce bigger build sizes, perform with less beam power and show higher surface finish parameters. Additionally, further differences like in the scanning process, the atmosphere and the applicable materials were mentioned. In order to expand the knowledge of metal-based AM, the focus will lie on its costs and complexity in the following chapter.

4.3.2 Economic characteristics

Machine prices and costs for materials play a major role in cost analysis for DMLM and EBM processes (Table 4.9). They are represented as two critical factors for the final cost per part and vary significantly on which machine is purchased and which material is used for the production.

Table 4.9: Prices, materials and build volumes for current metal 3D printing machines (Wohlers, 2014, pp.254–266)

Name	**Power [W]**	**Price [€]**	**Materials**	**Build volume [mm^3]**
Arcam Q10	3000	565000 €	Titanium, cobalt-chrome	200 x 200 x 180
Arcam Q20	3000	800000 €	Titanium	350 dia. X 380
Concept Laser M2 Cusing		750000 €	Stainless steel, tool steel, CoCr alloys, nickel-based alloys, aluminum alloys, pure titanium	250 x 250 x 280
Concept Laser X line 1000 R	1000	1500000 €	Aluminum alloys, titanium alloys, nickel-based alloy	600 x 400 x 500
EOSINT M 280	400	415000 €	Cobalt-chrome, titanium, stainless and tool steel, Inconel, aluminum	250 x 250 x 325
EOSINT M 400	1000	1250000 €	Inconel, aluminum	400 x 400 x 400
SLM Solutions 280 HL	1000 + 400	450000 €	316L stainless steel, 17-4PH, H13 tool steel, Al-Si-12, Al-Si-10, AlSi7Mg, titanium, Ti-6Al-4V, Ti-6Al-7Nb, Hastaloy X, cobalt-chrome, Inconel 718/625	280 x 280 x 350
SLM Solutions 500 HL	1000+1000 +400+400	700000 €	Same as above	500 x 280 x 320
3D System ProX 100	50	226000 €	Steels, titanium alloys, cobalt-chrome, and other metals	100 x 100 x 80
3D System ProX 300	500	684300 €	Steels, titanium alloys, cobalt-chrome, and other metals	250 x 250 x 300

The range of machine prices varies for relevant and current machines from 415000 € for an EOSINT M 280 machine to 1500000 € for a Concept Laser X line 1000 R, dependent on the build volume, system manufacturer, implemented beam power and the range of materials.

Numerous different metals can be used for metal-based AM processes, such as tool steels, stainless steels, pure and alloyed titanium, aluminum alloys, nickel-based alloys, cobalt-chromium alloys, copper-based alloys and also gold and silver (Wohlers, 2013, p.56). Material costs significantly vary on the used material for the printing process. Prices for 2014 were ranging between 70 €/kg for tool steels and up to 785 €/kg for pure titanium. A list of important materials being used in metal-based AM can be seen in table 4.10.

Table 4.10: Material prices in $ and € based on a currency exchange rate of 1 $ = 0,8915 € (Wohlers, 2014, pp.54–55)

Name	**Price range [$/kg]**	**Price range [€/kg]**
Tool steel, stainless steel, aluminum alloy	78 - 120	69,5 – 107
Cobalt-chrome alloy	120 - 545	107 – 485,9
Nickel-based alloy	210 - 275	187,2 – 245,2
Pure titanium and titanium alloys	340 - 880	303,1 – 784,5

Exemplary prices being used in cost estimation models amounted 89 EUR/kg for 316L stainless steel powder (Roland Berger Strategy Consultants, 2013, p.28), 108 €/kg for stainless steel 17-4 PH (Baumers et al., 2012, p.938) and 145 €/kg for aluminum alloys (AlSi10Mg) (Atzeni and Salmi, 2012, p.1154). Prices used in this study are 89 €/ kg for maraging steel 1.2709 (density of 7.7 g/cm^3), 107 €/ kg for aluminum alloy AlSi10Mg (density of 2.68 g/cm^3) and 400 €/ kg for titanium alloy Ti6Al4V (density of 4.45 g/cm^3).

In this research, material prices, build volumes and machine prices represent mandatory input variables to set up an AM cost model analysis. Each value has an effect on the future cost per part and the cost development over the number of parts.

4.4 Cost analysis models

This chapter presents relevant cost functions in AM and explains its main principles. In 1998, first cost models for AM were presented by Alexander et al. offering basic process characteristics, giving information about the part orientation and support structures as well as including pre- and post-processing steps.

Exact costs for the number of parts being produced and a broader range (metals) of materials was not taken into account (Rickenbacher et al., 2013, p.208). In 2003, Hopkinson and Dickens introduced a model for SLS able to calculate the break-even point with conventional

manufacturing. Assumptions were based on a constant production time for same parts by dividing total indirect costs through the number of produced parts. This results in a stable cost per part function over an increased batch size. Nevertheless, the course of the curve in conventional manufacturing is described as decreasing in costs per part. The authors assume costs for the mould in conventional manufacturing to be paid off according to the batch size (Ruffo et al., 2006, p.1418).

Because of the questionable assumptions of indirect costs in the study of Hopkinson and Dickens, a more accurate cost model in AM was presented by Ruffo and Hague in 2007. It describes costs for low production volumes more precisely and is applicable for different components printed in the same time.

In figure 4.8 a low-volume production of spring clip is described. Generally, the cost function consists of direct and indirect costs, the manufacturing and working time as well as the mass units. This exemplified cost function decreases rapidly for the first 40 parts and is followed by an approximation to a specific cost value of 10 € per part. It contains a batch size of 40 parts for each printing procedure. Printing only one part leads to its highest possible costs, because indirect costs and time costs will not be divided through several parts. Consequently, the costs per part decreases with a higher number of parts. After the first batch is processed, the cost function increases, resulting from a low packing density for the second batch in the beginning. Finally, a higher part number has a positive effect on the part price until a new batch is started (Ruffo and Hague, 2007, p.1587).

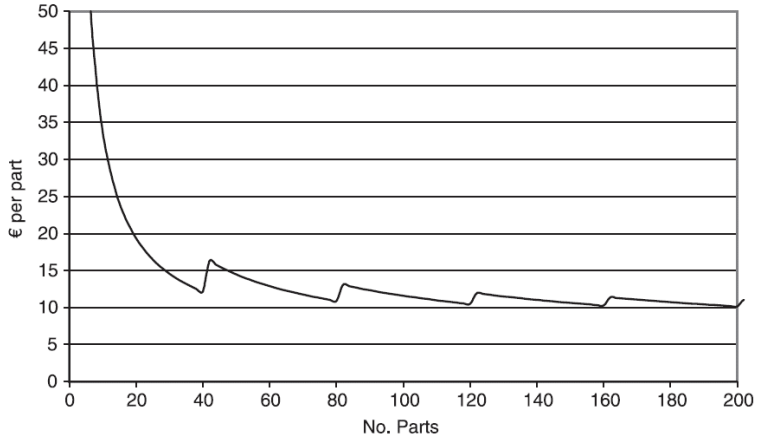

Figure 4.8: Exemplified low-volume cost function in AM (Ruffo and Hague, 2007, p.1590)

Basic formulas of the cost model can be seen in Figure 4.9, determining the cost function in Figure 4.8. Whereas direct costs are dominated by material costs, indirect costs contain labor costs, machine costs as well as production and administrative overhead costs. The coefficient m_B is calculated by multiplying the density of material ρ with the volume of the build V_B. The total time of the build t_B consists of the time to laser scan t_{xy}, the time to add layers t_z and the heating time before scanning t_{HC}.

$$Cost_B = Cost(t_B) + Cost(m_B) \quad (1)$$

where

$$Cost(m_B) = \frac{direct\_Cost}{mass\_unit} m_B \quad (2)$$

$$Cost(t_B) = \frac{\sum indirect\_Costs}{working\_time} t_B \quad (3)$$

Figure 4.9: cost estimation relationships (Ruffo et al., 2006, p.1420)

Higher production volume leads to a constant part price, which has advantages as well as disadvantages at the same time. In AM, low-volume production triggers highly economic part prices, but high-volume production has shown not to be competitive versus conventional methods so far (Garrett, 2013, p.6).

Main cost factors are observed differently in literature. While Wohlers and Grimm claim indirect costs to serve as the essential cost drivers in Rapid Manufacturing, Ruffo points out the importance of regarding time as the most important key value (Munguía et al., 2009, p.995).

Disadvantages in all existing models can be seen in its limitations in the material, timeliness and the specific DMLM process. Most of the models are concentrated on plastics, not using present direct and indirect cost values (e.g. material price) applicable on DMLM. As a consequence, an adjustment for a DMLM cost model is reasonable. This illustrates once again the main research question (RQ) in Chapter 3.3.

RQ1: How can several current metal-based Additive Manufacturing machines up to 3000 W be compared and evaluated with each other in terms of cost and feasibility?

Figure 4.10 provides a cost model used for DMLM. In the study of Atzeni and Salmi in 2012, costs of an EOSINT 270 machine were analyzed. The most critical parameter observed in this model is the build time T. The total cost per assembly reacts sensitively on this parameter, an exact estimation of time necessary for the printing process is essential.

Further disadvantages in this model can be seen in ignoring occurring waste of the PBF process. A recycle rate between 95 to 98 % for metal parts leads to waste factors ranging from 2 to 5 % (Berman, 2012, p.157). However, this percentage has to be calculated over the full powder bed and has potential to play a significant role for total material cost estimation. Therefore, the recycle rate will be part of the outlined cost model in Chapter 5. Also, the fact that support structures are essential for the fabrication of metal parts by PBF is neglected. Consequently, a support structure factor will be considered in the cost model presented in Chapter 5. In general, the amount of support structure for each part is related to its complexity degree and leads to increased built-up times and material usage.

Table 2 Evaluation model of part cost for selective laser sintering

Number of parts produced per job	(−)	*N*	*Magics RP software*
Material cost per kg	(EUR/kg)	*M*	Given by supplier
Part volume	(mm^3)	*V*	Magics RP software
Density of the sintered material	(g/mm^3)	*D*	
Mass of material per part	(kg)	*U*	$D \times 1.1 \cdot V$
Material cost per part	(*EUR*)	*MP*	$U \times M$
Machine operator cost per hour	(EUR/h)	*O*	
Set-up time per build	(h)	*A*	
Pre-processing cost per part	(*EUR*)	*AP*	$O \times A/N$
Depreciation cost per year	(EUR/year)	*C*	Given by supplier
Hours per year	(h/year)	*H*	5,000
Machine cost per hour	(EUR/h)	CH	*C/H*
Build time	(h)	*T*	EOS machine software
Machine cost per build	(EUR)	CB	$CH \times T$
Processing cost per part	(*EUR*)	*CP*	*CB/N*
Machine operator cost per hour	(EUR/h)	*O*	
Post-processing time per build	(h)	*B*	
Heat treatment cost per build	(EUR)	HT	
Post-processing cost per part	(*EUR*)	*BP*	$(O \times B + HT)/N$
Total cost per assembly	**(EUR)**	**P**	**MP+AP+CP+BP**

Figure 4.10: Part cost evaluation model for DMLM (Atzeni and Salmi, 2012, p.1150)

Assumption models to estimate the build time are published in several studies, e.g. (Munguía et al., 2009, p.998) and (Rickenbacher et al., 2013, p.210). Main disadvantages can be seen in the limitation on specific printers and adjustments of the build time by implementing coefficients into build time formulas. A generalized model for build time estimation in order to show several parameters for several printing machines is not described. Further, a comparison in build time and consequently costs between printing machines is not presented. Nevertheless, Munguia et al. achieved important findings according to build time correlation parameters. The author discovered a high correlation between the z-height and the build time. Increasing height of parts leads to higher build times in AM. The second best build time input parameter is described as the part volume, which also leads to suitable results. However, this correlation model was developed for plastic parts (Duraform PA). Hence, these observations can partly be transferred to DMLM and EBM, but have to be seen critical (Munguía et al., 2009, p.998).

Compared to traditional manufacturing, a main advantage of AM is represented by lower cost for a small production volume. Nevertheless, further benefits are located in the structural improvements resulting in reduced weight and the ability to produce high complex parts.

4.5 Structural improvement potential

One major advantage of 3D printing is based on its structural improvement potential. Parts that used to be not producible or became too expensive due to their high complexity level, can be produced efficiently by 3D printers. Thus, the complexity level is not resulting in higher part prices, which is leading to the term "complexity for free" (Gibson et al., 2010, p.7). Figure 4.11 presents a comparison between AM and conventional manufacturing, in which this potential is outlined.

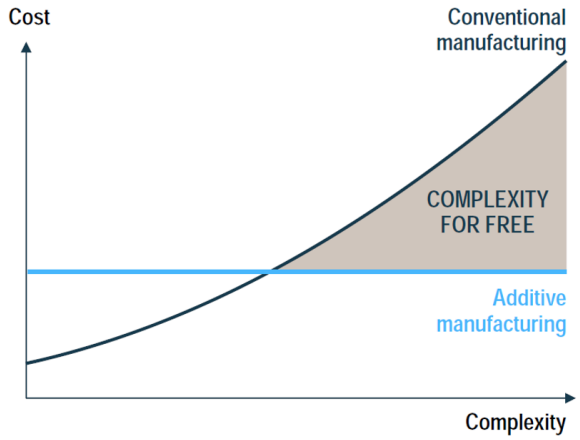

Figure 4.11: Complexity comparison of AM and conventional manufacturing (Roland Berger Strategy Consultants, 2013, p.12)

Whereas costs in AM stay constant regarding higher complexity (blue line), costs in conventional manufacturing rise over increasing complexity levels (black line). Hence, a cost intersection point is described as the starting point for the "complexity for free". Highly complex parts show cost advantages in AM, costs for complexity can be saved. Furthermore, molding is not crucial anymore for the fabrication process. Additionally, parts do not have to contain exclusively positive drafts. The number of design rules is decreased significantly, resulting in time savings for the product planning process. Previous problems for producing e.g. initial channels do not occur by implementing DMLM or EBM machines.

These changes are leading to a high redesign potential of products. The focus rests on saving material and weight of products (light weighting) by maintaining steady or improved mechanical characteristics. Consequently, less material produces less costs and lighter products. Especially for airplanes and cars the light weighting effect includes high cost savings by lowering the consumption of petrol (Garrett, 2013, p.4). As an example, Airbus was achieving up to 50% weight reduction for some of their airplane parts (Madeley and Chaphalkar, 2013, p.10).

However, all potential advantages like "free complexity", new structures and low costs for a small production volume are dependent on the time of the building process, which is mainly influenced by build volume rates.

4.6 Build volume rates

Figure 4.12 shows the increase of volume build rates between 1997 and 2012. Whereas the improvements in build rate can be described as very slow in the time between 1997 and 2003, significant technological developments enabled a step from approximately 2 mm^3/s in 2003 to 12 mm^3/s in 2010.

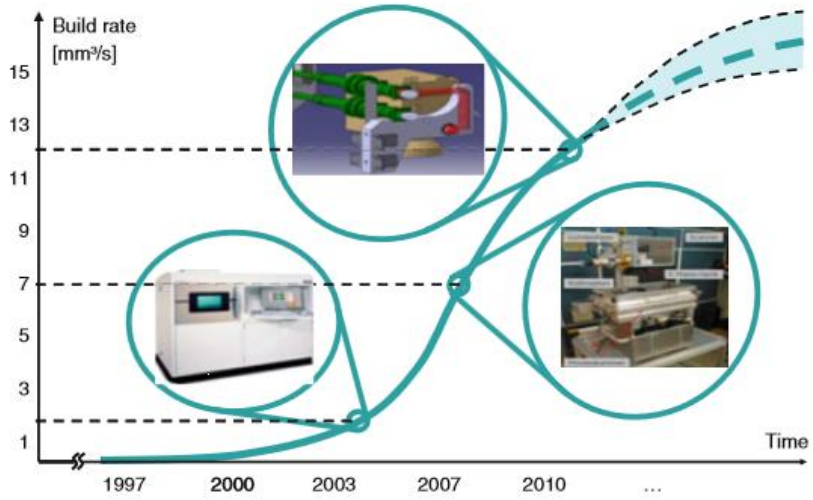

Figure 4.12: Development of volume build rates for DMLM between 1997 and 2010 (Schuh et al., 2012, p.144)

In general, build volume rates $\dot{V}$ $[\frac{mm^3}{s}]$ are described by the material volume created out of the metal powder over time. They represent the main factor for productivity and finally generate lower costs in terms of machine time savings. The competitiveness to conventional methods is in many cases not given due to not suitable build volume rates and the implementation of 3D metal printers is only economically reasonable regarding high complex parts (Figure 4.11). In addition to cost consideration, part quality is connected heavily to build volume rates. Theoretic build volume rates can be calculated by multiplying the layer thickness D_S [µm], the scan speed v_{scan} $[\frac{mm}{s}]$ and the scan line spacing (distance between parallel laser tracks) Δy_s [µm].

$$\dot{V} = D_S \times v_{scan} \times \Delta y_s$$

(Schleifenbaum et al., 2010, p.162)

Moreover, the scan line spacing is formulated as $\Delta y_s = 0{,}7 * d_s$, where d_s is the focus diameter (Schleifenbaum et al., 2010, p.162). Too small scan spacings are resulting in cracks, whereas too large spacings are leading to not fully consistent layers (Dewidar et al., 2003, p.1655).

The parameter v_{scan} $[\frac{mm}{s}]$ is dependent on the incident intensity $[\frac{W}{mm^2}]$ and the required layer thickness [µm]. If intensity is high and the required layer thickness is low, high scan speeds will be achieved. Accordingly, low intensities and large layer thicknesses are leading to lower scan speeds. This phenomena arises from the heat diffusion process described by Navier-Stokes equations. When the solidus temperature of metal is exceeded, the material starts to melt and is transferred into the liquid phase. Additionally, the depth of the affected area is growing over time. After the required layer thickness is reached, the laser beam is scanning consecutive areas and the material begins to solidify (Attar, 2011, p.92).

Furthermore, intensity is representing the quotient of laser power [W] and area [mm^2]. The affected area can be calculated by $\frac{1}{4} \times d_s^2 \times \pi$. This shows that a given laser power is directly affecting scanning speeds v_{scan} as well as beam diameters d_s.

Figure 3.11 explains differences in part quality varying by increasing scan speeds and laser power. Five different zones can be observed, zones of no marking, partial marking, melting with balling, melting with breakage and a "high quality" zone with continuous melting. However, the relation between scan speeds and laser powers is described as a very complex phenomena, dependent on many parameters and differing for every single material.

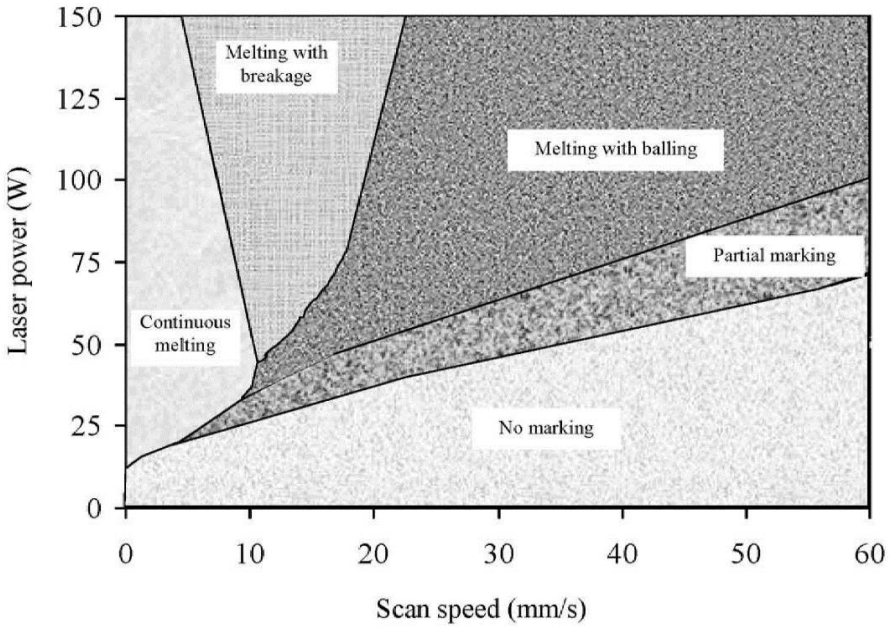

Figure 4.13: Single-line melting process map with a 150 W laser (Dewidar et al., 2003, p.1655)

Taking density as a quality parameter in metal-based AM, figure 4.14 shows density dependencies on increasing scanning velocities. Each curve represents a specific power level, starting with 300W and ending up at 1000W.

In order to produce fully dense parts, the density percentage has to reach nearly 100%, which leads to the result that for a 300W laser power system a scanning velocity of 500 mm/s is applicable, 500W enables 1200 mm/s, 700W induces 1600W and 1000W allows a scanning velocity of 2200 mm/s.

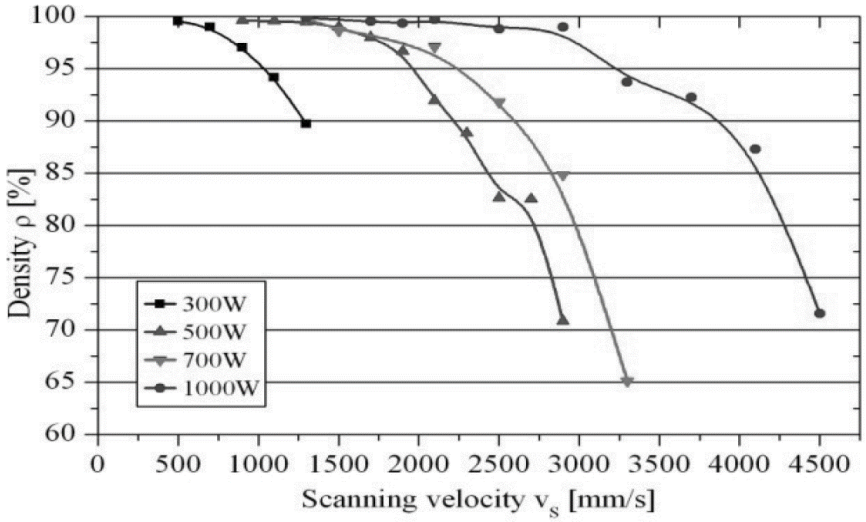

Figure 4.14: Density dependency on scanning velocity with a layer thickness of 50 µm and a hatch line spacing of 150 µm for aluminum alloys (Buchbinder et al., 2011, p.274)

As a consequence, an implementation of these numbers into the formula $\dot{V} = D_S \times v_{scan} \times \Delta y_s$ respective a constant layer thickness of 50 µm and constant hatch line spacing of 150 µm, build volume rates of 4 mm^3/s (300 W), 9 mm^3/s (500 W), 12 mm^3/s (700 W) and 16 mm^3/s (1000 W) are made possible. Figure 3.13 compares increasing beam powers with feasible scanning velocities. Therefore, a constant rise of the scanning velocity can be observed.

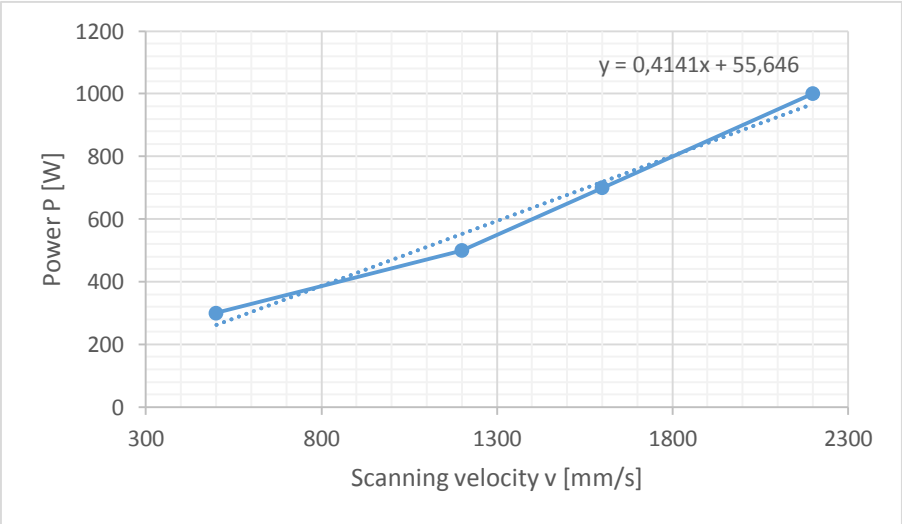

Figure 4.15: Relation between scanning velocity and beam power of aluminum alloys to obtain acceptable quality levels

Nevertheless, the idea behind estimating build times based on volume rates is represented by taking the laser power and layer thicknesses into account. These parameters are relatively easy accessible in literature and allow general statements about several 3D metal-based printing machines. Therefore, the layer thickness symbolizes part accuracy and the laser power stands for heat diffusion rates and consequences for the build volume rate.

A main parameter of total cost estimation is represented by build volume rates [mm^3/s]. They result from an interaction between beam power, hatch size, material and layer thickness. In order to quantify this parameter, a minimum relative density of 98 % is assumed to produce "fully dense" components. Furthermore, high density generally induces sufficient stress and elongation measurements. This assumption allows conclusions about maximum scan speeds of several materials. Due to the fact that the estimation of volume rates is complex and literature shows lacks in sufficient material testing, the focus will lie on three important materials, maraging steel 1.2709, an aluminum alloys (AlSi10Mg) and titanium alloy (Ti6Al4V).

4.6.1 Maraging Steel 1.2709

As an example, figure 4.16 shows on the left side relative densities of five layer thicknesses by increasing scan speeds for maraging steel. For 60 µm layers, 98 % density is reached with scan speeds of 100 mm/s, 50 µm layers contain 150 mm/s, 40 µm layers allow 200 mm/s and 20 µm can be produced by scan speeds of 250 mm/s. With a hatch scanning width of 0.126 mm, build volume rates of 0.76 mm^3/s (60 µm), 0.945 mm^3/s (50 µm), 1.008 mm^3/s (40 µm) and 0.945 (30 µm) are realized for 100 W and 200 W lasers (Yasa and Kruth, 2009, p.5).

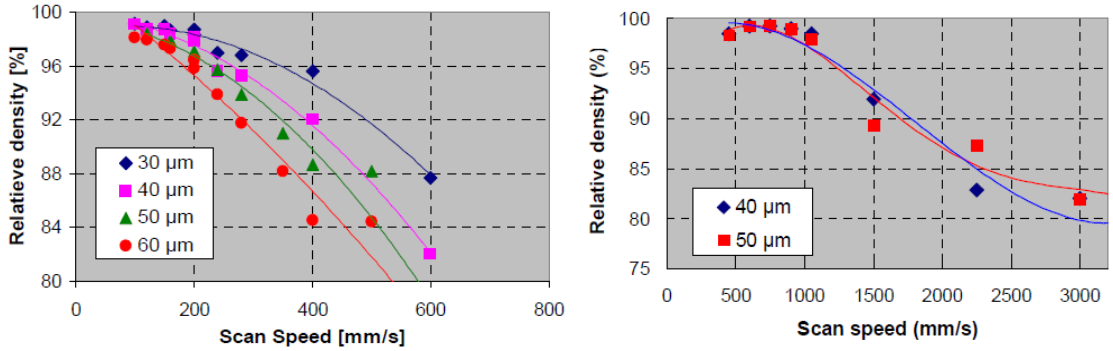

Figure 4.16: Effect of scan speeds on relative densities for several layer thicknesses of a 100 W (left) and a 200 W (right) laser system for maraging steel 300 (Yasa and Kruth, 2009, p.5)

On the right side, 40 and 50 µm layers were produced with increasing the scan speed. A relative density rate of 98 % is measured by a scan speed of 900 mm/s for both 40 and 50 µm layers, which represents build volume rates of 4.54 mm^3/s (40 µm) and 5.67 mm^3/s (50 µm). In addition, higher relative density rates can be achieved by lowering the scan speed, e.g. scan speeds of 600 mm/s (99 % density) result finally in 3.02 mm^3/s (40 µm) and 3.78 mm^3/s (50 µm).

Moreover, machine manufacturers, such as EOS and Concept Laser present recommended parameters for their sold machines. For maraging steel powder, 30-40 µm layers can be processed with scan speeds of 750 mm/s and a scan spacing of 100 µm for the EOSINT 270, whereas Concept Laser outlines 200 mm/s and 30 µm layers for their Concept Laser M3 Linear machine. A build volume rate calculation of these parameters leads to 2.25 mm^3/s (30 µm) and 3 mm^3/s (40 µm) for the EOSINT M270 and 0.6 mm^3/s for the Concept Laser machine. This massive difference in volume build rates between these two machines arises from the laser beam power. Whereas the EOSINT M270 is equipped with an 200 W laser, the Concept Laser machine only comprises a 100 W laser system (Yasa and Kruth, 2009, pp.1–5).

Other reports claim that components out of maraging steel were produced with 40 µm layers, scan speeds of 750 mm/s for a beam power of 200 W. Assuming scan line spacings of 0.126 mm, a build volume rate of 3.78 mm^3/s can be achieved (Sanz and García Navas, 2013, p.2127). Additionally, EOS presents volume build rates of 3 – 3.6 mm^3/s for 40 µm layers for the EOSINT M 270 system (EOS, 2007, p.2). Another EOS source points out recommendations of 1.6 mm^3/s for 20 µm layers and 3 mm^3/s for 40 µm layers with a 200 W EOSINT M 270 and 4.2 mm^3/s for 40 µm and 5.5 mm^3/s for 50 µm with a EOS M 400 (400W) machine (EOS, 2011a, p.3).

While build volume rate data is available for 100 W and 200 W laser systems, only very few published sources are tangible for higher beam powers. Reasons for that can be seen in high prices of these high power laser machines as well as their novelty on the market. Nevertheless, theoretical volume build rates are calculated for 1000 W and 1500 W regarding several layer thicknesses. As a result, 1000 W laser systems provide volume build rates of 8 mm^3/s (60 µm), 11 mm^3/s (90 µm), 12 mm^3/s (120 µm) and 15 mm^3/s (150 µm). Likewise, 1500 W systems can achieve 12 mm^3/s (60 µm), 13 mm^3/s (90 µm), 17 mm^3/s (120 µm) and 22.5 mm^3/s for 150 µm layers. In addition, this report presents strength and elongation parameters, which fulfill high quality standards (Brecher, 2015, pp.57–58).

4.6.2 Aluminum alloy AlSi10Mg

Low residual porosity 0.7 - 0.8 % and suitable stress and elongation parameters were achieved with scan speeds of 900 mm^3/s respectively 800 mm^3/s, beam powers of 120 W respectively 195 W and a hatching distance of 0,1 mm respectively 0,17 mm for layer thicknesses of 30 µm (Manfredi et al., 2013, p.859). Therefore, evaluated build volume rates lead to 2.7 mm^3/s (120 W) and 4.08 (195 W).

In a study of Read et al. (2015), the interaction between scan speeds, laser power and porosity is visualized. Figure 4.17 outlines highest porosity levels for increased scan speeds and decreased laser power. However, best results are presented with high laser powers (175 W) and scan speeds of 1025 mm^3/s. Moreover, a table of porosity levels is shown in this study, which outlines all relevant measured parameters for a proper volume build rate estimation.

A porosity under 2 % stands for at least 98 % fully dense components, this quality characteristic can be fulfilled with a laser power of 175 W, scan speed of 1025 mm/s and a hatch spacing of 97.5 µm (build volume rate of 2.99 mm^3/s). Additionally, parts with a relative porosity of 0.8 % were produced for 200 W, 1350 mm/s scan speed and a hatch spacing of 75 µm, which results in a volume build rate of 3.04 mm^3/s. All specimens were fabricated with a layer thickness of 30 µm. Additionally, optimized process characteristics were provided for 200 W with scan speeds of 1400 mm/s, scan spacing of 105 µm and 30 µm layers (build volume rate of 4.41 mm^3/s) and for 50 µm layers with 500 mm/s and 150 µm scan spacing used for a laser power of 250 W, resulting in a volume build rate of 3.75 mm^3/s (Read et al., 2015, pp.420–426).

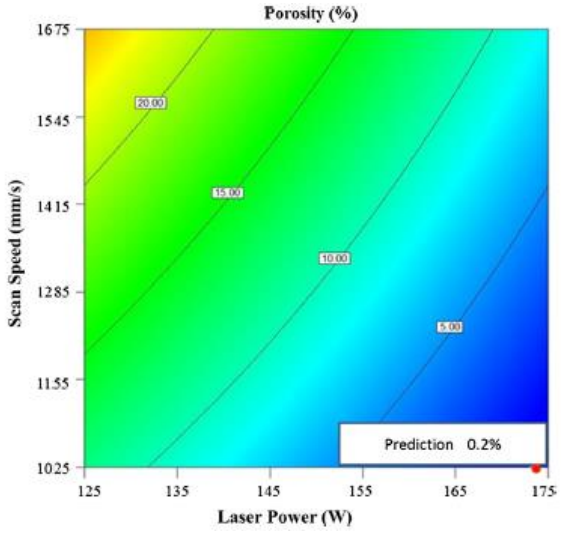

Figure 4.17: Interaction between laser power, scan speeds and porosity between 125 W and 175 W for AlSi10Mg and 30 µm layers (Read et al., 2015, p.419)

Furthermore, Krishnan and Atzeni (2014) suggests that components with high relative density parameters can be manufactured with 195 W, 700 mm/s, 0.12 mm scan line spacing and a layer thickness of 30 µm, leading to a build volume rate of 2.52 mm^3/s. Also scan speeds of 900 mm/s, a scan line spacing of 0.1 mm shows appropriate results, giving a build volume rate of 2.7 mm^3/s. Surprisingly, a fast build volume rate was provided through a laser beam power of 180 W. Therefore, scan speeds of 700 mm/s and scan line spacing of 0.17 mm were implemented, resulting in a volume build rate of 3.57 mm^3/s (Krishnan et al., 2014, p.453).

According to Aboulkhair et al. (2014), highest quality parts of over 99.5 % relative density were produced with a 100 W system for 40 µm layers, scan speeds of 500 mm/s and hatch spacing of 50 µm, causing a build volume rate of 1 mm^3/s (Aboulkhair et al., 2014, p.58). Moreover, EOS points out build volume rates AlSi10Mg of 4.8 mm^3/s for their EOSINT M270 machine (200 W and 40 µm layers (EOS, 2009, p.2)) and 7.4 mm^3/s for their EOSINT M280 system (400 W and 40 µm layers (EOS, 2014a, p.3)).

In a study of Kelbassa et al. (2014) parameters for high power DMLM of AlSi10Mg were presented. Using the skin-core technology, skin parts was manufactured with a laser power of 200 W, scan speeds of 800 mm/s and a scan line spacing of approximately 0.14 mm (0.7 times of the 200 µm diameter). Respective a layer thickness of 50 µm, volume build rates of 5.6 mm^3/s are calculated. The impact of lower accuracy preconditions for the core parts allows laser beam powers of 1000 W with beam diameters of 200 µm and scan speeds of 2000 mm/s, for up to 200 µm layer thickness, causing build volume rates of 24 mm^3/s for 100 µm layers and a assumed scan line spacings of 120 µm (Kelbassa et al., 2014, p.36).

Furthermore, calculated volume build rates of Buchbinder et al. (2011) with relative porosity levels of over 98 % for high laser beam powers were taken from Figure 4.14. Bremen et al. (2012) outline high density levels for a 1000 W laser machine with scan speeds of 1700 mm/s, scan line spacings of 0.15 mm and 0.2 mm for 50 µm layers, resulting in build volume rates of 12.75 mm^3/s and 17 mm^3/s (Bremen S. et al., 2012, p.35).

In the final report of Fraunhofer ILT (2007), it is reported that 99.5 % dense parts with a layer thickness of 50 µm were manufactured with scan line spacings of 0.15 mm for a 200 W laser system. Therefore, a scan speed of 450 mm/s was suggested. Also, 98 % dense AlSi10Mg components were produced with a scan speed of 640 mm/s. As a result, volume build rates of 3.375 mm^3/s (450 mm/s) and 4,8 (640 mm/s) are achieved (Fraunhofer ILT, 2007, p.25). Rosenthal et al. (2014) were evaluating part quality measurements on a 400 W laser system for AlSi10Mg and gained from suitable results. They were creating their specimens with a scan velocity of 1000 mm/s and a scan line spacing of 200 µm. The layer thickness was not mentioned directly, but the particle size between 25 – 50 µm was given. Therefore, a layer thickness of probably 70 µm can be expected, which leads to a volume build rate of 14 mm^3/s (Rosenthal et al., 2014, pp.448–450).

In a study about AM machines available on market, typical volume build rates of 0.5 – 1.5 mm^3 are reported for 100 W laser system with typical layer ranges between 10 to 30 µm. Consequently it is assumed, that a volume build rate of 0.5 mm^3/s is achieved with 10 µm and a volume build rate of 1.5 µm is achieved with a layer thickness of 30 µm (Frick, 2011, p.4). Moreover, the company Concept Laser maintains that the maximum volume build rate of the model “X line 1000R” including 1000 W laser power is 27.78 mm^3/s for AlSi10Mg (Concept Laser, 2012, p.2).

4.6.3 Titanium alloy Ti6Al4V

All build volume rates for the titanium alloy Ti6Al4V were taken from the company EOS due to a lack of data in literature. A build volume rate of 3 mm^3/s for 200 W laser systems is suggested (EOS, 2008, p.2). Additionally, build volume rates for 200 W of 3.75 mm^3/s and 9 mm^3/s for 400 W systems are outlined (EOS, 2011b, p.2). The same company presents build volume rates for 200 W laser systems and 30 µm layer thickness of 3.8 mm^3/s and 8.2 mm^3/s for 400 W laser systems and 60 µm layer thickness (A9).

Because most volume build data points are available for the aluminium alloy AlSi10Mg, a build volume rate function for this material is established and based on this function, conclusions for MS 1.2709 and Ti6Al4V are presented in figure 4.21.

4.6.4 Derivation of volume build rates

Measured scan speed values for porosity levels under 2 % were taken from scan speed – porosity diagrams. Subsequently, build rates were calculated by multiplying scan speed, layer thickness and scan spacing. An estimated build volume rate is shown over the beam power in figure 4.18.

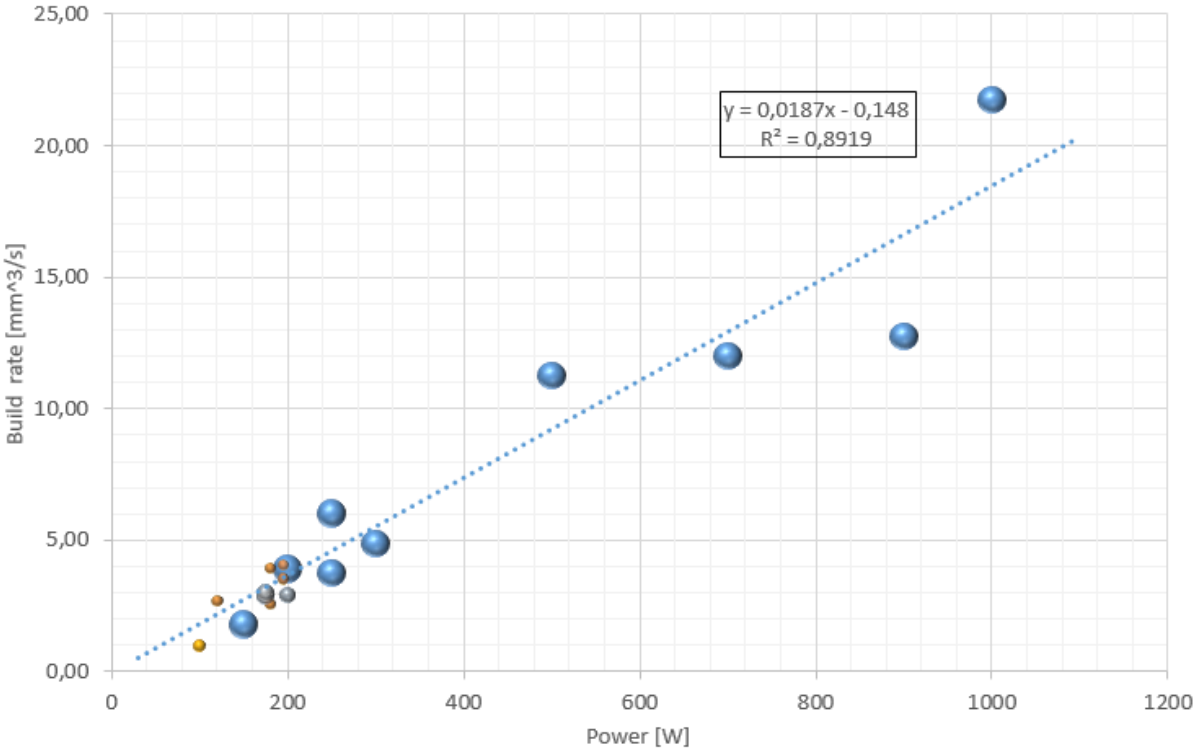

Figure 4.18: Effect of power on build rate for AlSi10Mg

As a result, increased beam power leads to constantly growing build rates. This curve progression can be approximated linearly to y = 0,0187x – 0,148.

This indicates a slope of 1.87 % and nearly ends up in the zero point. The area of the measured values (bubble) symbolizes the scanned volume of the laser spot, resulting in a cylinder of $V = \frac{1}{4}d^2\pi h$, taking the beam diameter d and the layer thickness h as a combined quality criteria into account, which is describing the surface feature. This parameter is meant, when talking about accuracy in this study. Accordingly, the accuracy for beam powers over 200 W is low, whereas the range between 0 and 200 W outlines much higher accuracy levels.

A direct effect between accuracy and build volume rate for same power levels cannot be observed, e.g. at a power level of 150 W lower build speeds are found for lower accuracy than for higher one. Consequently, this figure will be divided into two accuracy areas. High accuracy and lower build speeds between 0 and 200 W and low accuracy levels but higher build rates between 200 and 1000 W. As an effect, 1000 W lasers are downgraded to 200 W and 3.59 mm^3/s for highly accurate areas.

For this reason, 100 W laser systems work with a volume build rate of 1.72 mm^3/s and 200 W lasers with 3.59 mm^3/s. 400 W laser with low accuracy reach 7.33 mm^3/s, but will be downgraded for high accuracy to 3.59 mm^3/s. The same adjustment occurs for 1000 W laser systems, in which low accuracy allows 18.55 mm^3/s, while high accurate areas have to be produced with 3,59 mm^3/s.

In figure 4.19, the volumetric energy density is defined as $\epsilon = \frac{P}{vxh}$ [J/mm^3] and expresses induced work per volume, where P is the power [W], v the scan velocity [mm/s], x the layer thickness [mm] and h the hatch distance [mm].

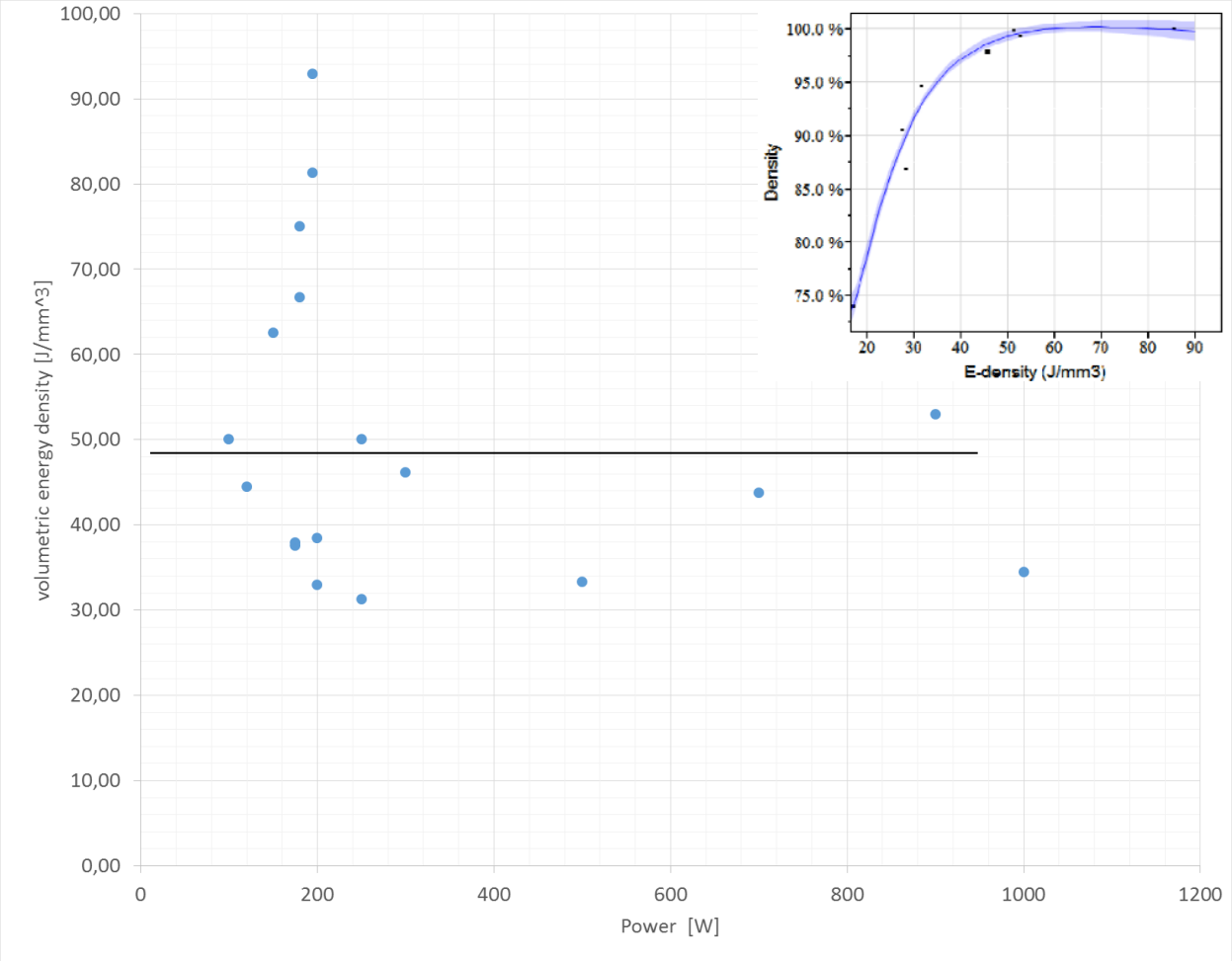

Figure 4.19: Relations between volumetric energy density and power respectively density for AlSi10Mg (Spierings et al., 2012, p.3)

Power is divided through scan speed v, scan line spacing x and layer thickness h. Volumetric energy density for AlSi10Mg varies between 30 to 94 J/mm^3, the average value contains 50.64 J/mm^3 (Hinduja and Li, 2013, p.366). This leads to the conclusion that a volumetric energy density of at least 30 J/mm^3 has to be induced to melt AlSi10Mg powder particles in layer thicknesses ranging from 30 to 50 µm. Moreover, the relation between volumetric energy density and density/porosity is presented. Suitable density results (approximately 99 % density) will be achieved over 50 J/mm^3 (Spierings et al., 2012, p.3).

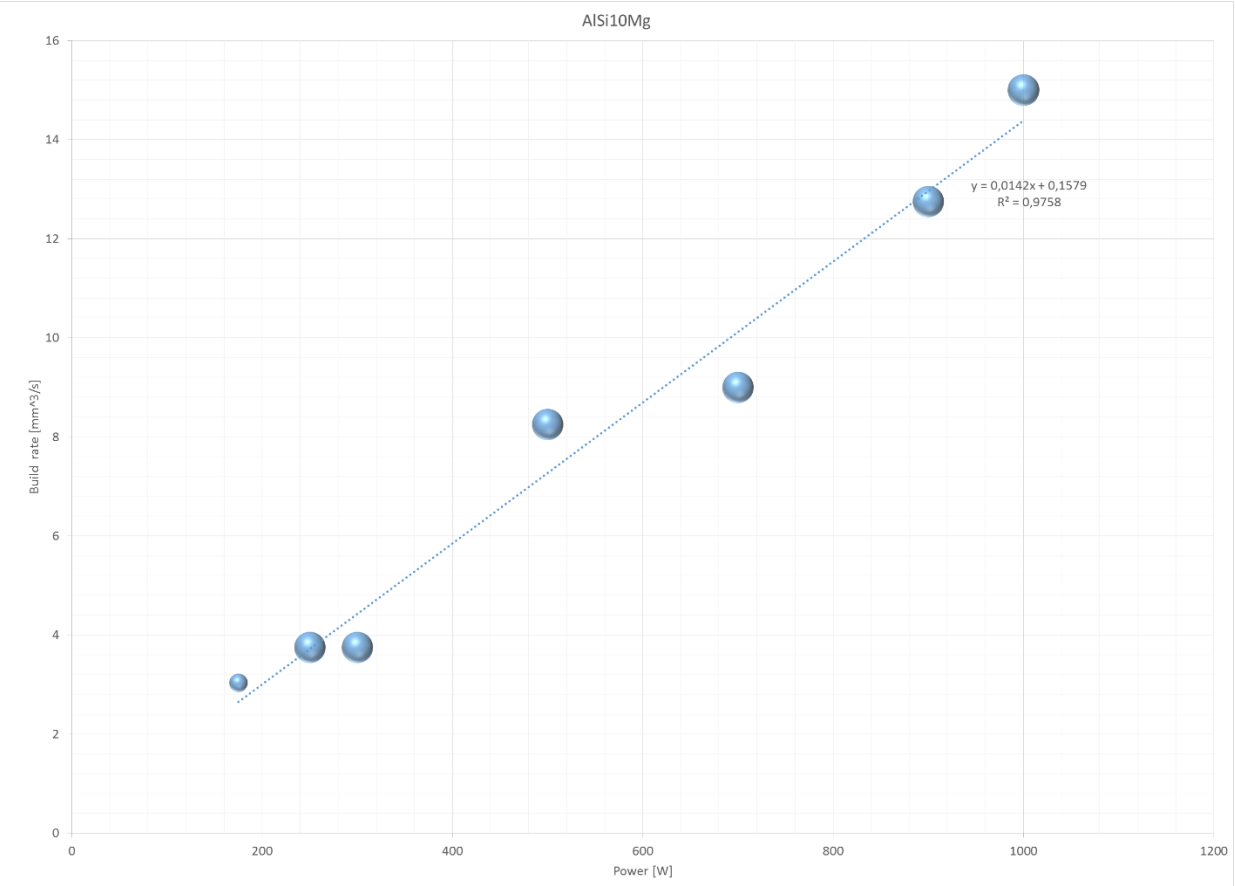

Figure 4.20: build rate function for AlSi10Mg with a density over 99.5 %

A linear regression to describe this function is y = 0.0142x+0.1579 with a slope of 1.42 per cent for a density over 99.5 %. While a sufficient amount of data points for the material AlSi10Mg for several density rates was available (over 98 % and over 99.5 %), this was not the case for Maraging Steel 1.2709 and the titanium alloy Ti6Al4V. Therefore, all data points for the mentioned materials with density levels over 98 % are shown in figure 4.21.

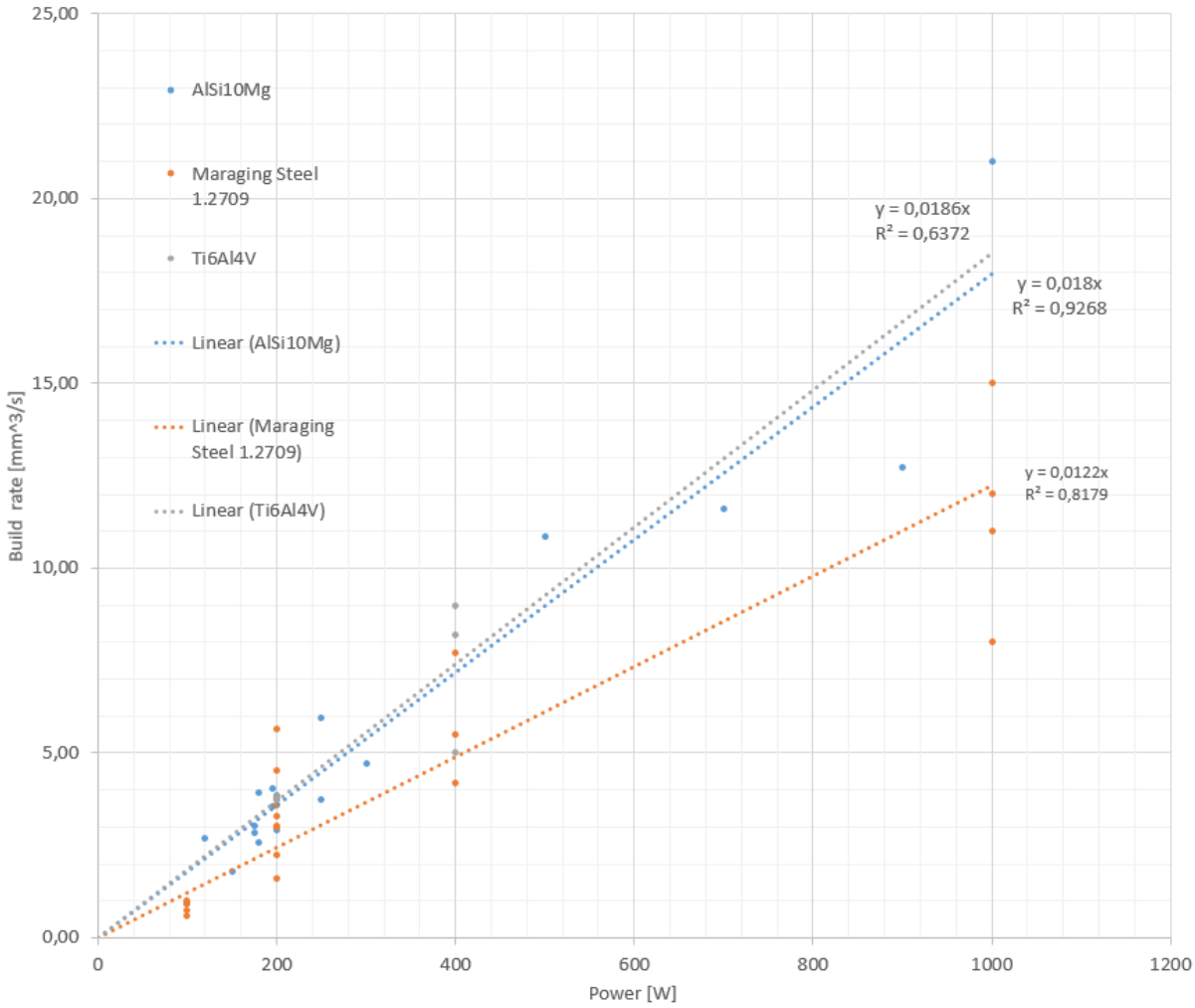

Figure 4.21: Build volume rates for MS 1.2709, AlSi10Mg and Ti6Al4V for porosity levels under 2 %

It can be observed that the titanium alloy Ti6Al4V indicates highest build rates with a slope of 1.86 % and a build volume rate of 18.6 mm^3/s. The second fastest build volume rates can be achieved by using aluminum alloys (AlSi10Mg) with a volume build rate slope of 1.8 % and volume build rate of 18 mm^3/s for 1000 W lasers. However, slowest volume build rates are described by maraging Steel 1.2909 with a slope of 1.22 % and a volume build rate of 12.2 mm^3/s. All trend lines were centered to the zero point and linear progression is assumed, leading to coefficients of determination between 64 and 93 %. The reason for high volume build rates of AlSi10Mg is determined by low melting points of 600 °C, compared to melting points of 1600 °C of Ti6Al4V and 1423 °C of maraging steel 1.2709. Moreover, several parameters like the degree of absorption or the particle size result in deviating build volume rates.

In order to present build volume rates for maraging steel 1.2709 and titanium alloys Ti6Al4V with highest density levels over 99.5 %, the gap between AlSi10Mg for a density of 98 % and 99.5 % is calculated. Thus, the equations of y = 0.018x (AlSi10Mg 98% density) and y = 0.0142x are subtracted from each other and the percentage difference of both equations is evaluated.

$$percentage\ difference\ (\%) = \frac{0{,}018x - 0{,}0142x}{0{,}18x} = 21{,}1\ \%$$

This decline in the volume build rate is taken for the titanium alloy as well as the maraging steel to increase the density for these materials to over 99.5 %. Consequently, following values for the volume build rates can be evaluated.

Table 4.11: Volume build rates of MS, AlSi10Mg and Ti6Al4V

Power [W]	MS 1.2709 [mm^3/s]	AlSi10Mg [mm^3/s]	Ti6Al4V [mm^3/s]
50	0,48	0,71	0,73
100	0,96	1,42	1,47
150	1,44	2,13	2,20
200	1,93	2,84	2,94
250	2,41	3,55	3,67
300	2,89	4,26	4,40
350	3,37	4,97	5,14
400	3,85	5,68	5,87
450	4,33	6,39	6,60
500	4,81	7,10	7,34
550	5,29	7,81	8,07
600	5,78	8,52	8,81
650	6,26	9,23	9,54
700	6,74	9,94	10,27
750	7,22	10,65	11,01
800	7,70	11,36	11,74
850	8,18	12,07	12,47
900	8,66	12,78	13,21
950	9,14	13,49	13,94
1000	9,63	14,20	14,68

The Matlab model is based on these material-dependent build volume rates. Higher values cause lower costs per part, whereas low build volume rates have a negative effect on costs. Nevertheless, machines like the SLM Solutions 500 HL and the Arcam Q10 show higher beam powers with up to 2800 W respectively 3000 W for EBM. However, the linear trend of increasing volume build rates between 0 and 1000 W cannot be transferred to the range between 1000 and 3000 W. According to SLM Solutions, their laser-based system SLM Solutions 500 HL reaches volume build rates of 70 ccm/h (19,44 mm^3/s) by implementing two 1000 W lasers and two 400 W simultaneously (SLM Solutions, 2012). However, Arcam reports of even higher volume build rates of up to 80 ccm/h (22.2 mm^3/s), increasing productivity significantly but also lowering the surface feature. Table 4.6 shows predicted build volume rates for metal-based AM machines over 1000 W being based on a logarithmic interpolation (A10).

Table 4.12: Volume build rates of MS, AlSi10Mg and Ti6Al4V (A10)

Power [W]	MS 1.2709 [mm^3/s]	AlSi10Mg [mm^3/s]	Ti6Al4V [mm^3/s]
2800	15,8	20,1	17,7
3000	16	20,6	18

The aluminum alloy AlSi10Mg indicates highest build volume rates of up to 20.6 mm^3/s for a beam power of 3000 W, whereas Ti6Al4V allows build volume of 18 mm^3/s and MS 1.2798 with 16 mm^3/s. The difference in build volume rates can be explained due to varying melting points, heat absorption and heat conductivity rates for each material.

The reason for the logarithmic development for build volume rates of power ranges between 50 and 3000 W could lie in the implementation of beam laser powers of not more than 1000 W in DMLM. In order to reach laser beam powers over 1000 W, several lasers are installed in one machine. These lasers do not necessarily work at the same time, leading to slower build volume rates and explaining a break in the linear behavior in power levels from 0 to 1000 W.

In chapter 4, metal-based Additive Manufacturing, firstly market shares in metal-based AM machine purchases were presented. Accordingly, the companies EOS, Concept Laser and Arcam are described as the market leaders. Subsequently, main characteristics of current DMLM and EBM machines are outlined and compared in terms of performance and mechanical properties. Accordingly, build sizes of DMLM machines were constantly increased whereas EBM machines stayed on the same level.

Build sizes of DMLM machines are in most cases much larger than in EBM machines, leading to higher batch sizes. Regarding beam powers, EBM machines originally contain high power levels by implementing a laser beam (3000W) into the machine system. On the other hand, DMLM machines started with low power level lasers (100W), but increased the level to up to 2800 W by using several high power lasers at the same time. A comparison of beam spot sizes, a parameter for surface quality, elaborated significant differences. DMLM generally provides higher accuracy levels, while EBM can only compete on equal levels with the latest Q10 machine. Concerning mechanical parameters, major differences in strength between EBM and DMLM machines as well as AM and conventional machines could not be observed.

Nevertheless, a closer look at elongation parameters has shown deviations. With this knowledge, a direct comparison between an EOS M290 and an Arcam Q20 offered exact statements of advantages and disadvantages in each system. As a result, EBM concentrates on specific applications in medical and aerospace industries, whereas DMLM machines cover a wider field of industry fields. In the following chapters, main economic characteristics like machine prices, material and labor costs were presented. Additionally, the cost potential of structural improvement was described.

Based on previous chapters, cost analysis models were explained and specific low volume cost functions introduced, showing that the build time is a major and critical factor in cost estimation, because of material, machine and accuracy dependencies. The build time can be calculated by developing build volume rates, which can theoretically be estimated by multiplying layer thicknesses, scanning speeds and scan line spacings.

Parameters like scanning speeds and beam power are always limited in quality problems, the relation between them is based on several constants and assumptions. Additionally, the density decreases with higher scanning velocities, optimal values were presented in figure 4.14. Evaluated build volume rates for MS 1.2709, AlSi10Mg and Ti6Al4V are shown in figure 4.21.

5 Mathworks Matlab metal-based Simulation tool

In this thesis, an existing cost model of Ruffo et al. (2006) is used as an initial point. It consists of direct and indirect costs. Direct costs are described as material containing the part volume and additional waste. Indirect costs include labor, machine costs, administrative overhead costs and production overhead costs. Labor exclusively contains the technicians' salaries, whereas machine costs are divided into the purchase absorption, maintenance costs as well as software and hardware costs. Due to the reason that production and administrative costs are varying significantly from several circumstances, such as location and type of the company, they will not be part of this cost model. Indirect costs are dependent on the process time. Consequently, the cost of the build is represented by a summation of direct and indirect costs.

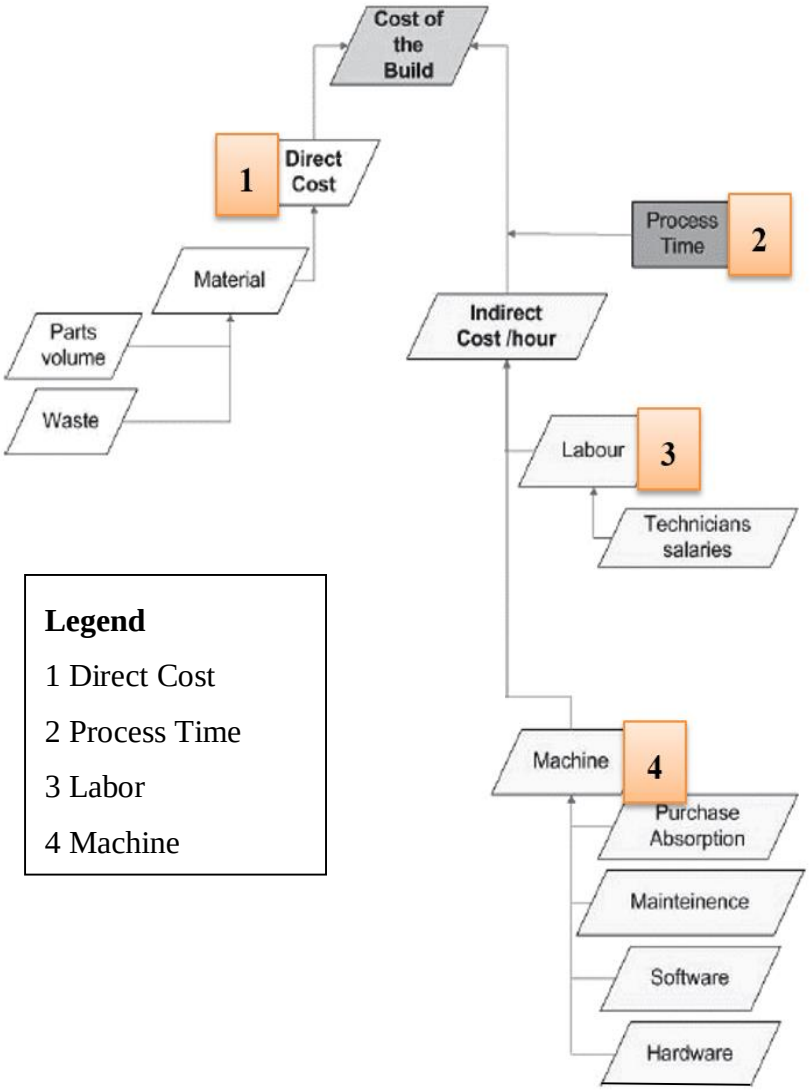

Figure 5.1: Initial point for the cost model in this study (Ruffo et al., 2006, p.1421)

Based on the model in figure 5.1 an elaborated cost model is presented in figure 5.2. The cost of part (cop) is basically calculated through the summation of “Expenses on Machine”, “Expenses on Worker” and “Material cost”. These costs have a different origin and are called cost types.

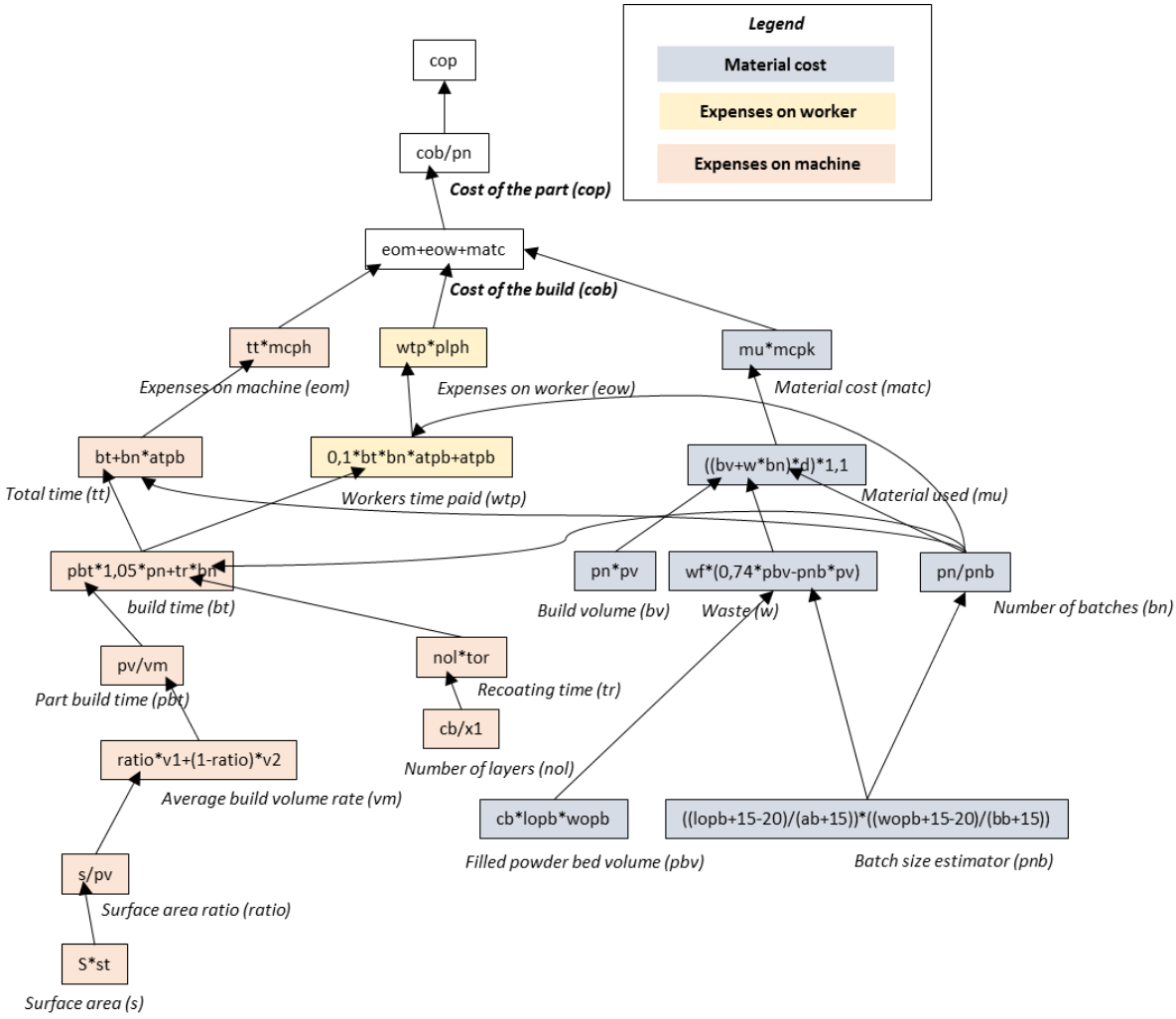

Figure 5.2: Elaborated cost model

In order to understand each cost type and its origin, they will be described more precisely in the following chapters.

5.1 Material costs

Batch size estimator (pnb)

Batch size describes the number of products being manufactured during one set (batch). This number is always limited to the bounding box of the machine. Dependent on the planned way of placing the parts into the powder bed, a specific number of parts (N) can be calculated through:

$$N = \left(\frac{PL_x + g_x - 20}{bb_x + g_x}\right)\left(\frac{PL_y + g_y - 20}{bb_y + g_y}\right)$$

Figure 5.3: Formula for a batch size estimation including gaps (Gibson et al., 2010, p.377)

Where PL_x is representing the horizontal direction of the powder bed [mm] and Pl_y the vertical direction of the powder bed. Gaps between the bounding boxes are symbolized by g_x in horizontal direction and g_y in vertical direction [mm]. Finally, bb_x and bb_y describe the x and y – direction of the bounding box [mm]. 15 mm are assumed for the gaps between the bounding boxes in x and y – direction. In figure 5.2, PL_x is represented by "lopb", bb_x by "ab", PL_y by "wopb" and bb_y by "bb".

Filled powder bed volume (pbv)

The height of parts "cb" is multiplied with the length of the powder bed "lopb" and the width of the powder bed "wopb". Consequently, a filled up build chamber is calculated without inserted parts.

Waste (w)

Unused powder of the filled up powder bed can be recycled with a range between 95 to 98 % (Berman, 2012, p.157). This factor is called "waste factor wf" in this study. As a result, the volume of the filled powder bed is calculated by assuming a hexagonal closest particle packing ratio of 74 %. This percentage is multiplied with the length and height of the specific powder bed and its fill-up height dependent on the part height. Subsequently, the number of produced parts multiplied with the volume of each part is deducted from the theoretical filled powder bed. This result is calculated with a waste factor of 2 % and finally leads to the wasted material.

$$w = wf * (0{,}74 * pbv - pbn * pv)$$

Where "w" stands for the waste, "wf" represents the waste factor, "pbv" the filled powder bed volume, "pbn" the batch size estimator and "pv" the part volume.

Build volume (bv) and number of batches (bn)

The build volume is calculated by multiplying the part number "pn" and the part volume "pv". To evaluate "bn", the part number "pn" is divided through the number of parts in each bed "pnb", which was defined by the batch size estimator.

Material used (mu)

The total volume, consisting of build volume "bv" and waste "w", is evaluated over the density for each material and additional support structure. The initial point for this dependency is described by

$$m_B = \rho * V_B$$

Where "m_B" outlines the mass of the part, "ρ" the density and "V_B" the volume of the part. Additionally, support structures have to be established for structural stability during the printing process. This issue is respected by adding a constant factor of **10 %** (α) extra to the part volume.

Material costs (matc)

Estimated mass "mu" has to be multiplied with the cost per each kg "mcpk", which differs significantly according to the type of material being used. Maraging Steel 1.2909, AlSi10Mg and Ti6Al4V can be selected as the material being used in the AM tool.

5.2 Expenses on machine

Surface area ratio (ratio)

The surface area "s" is evaluated by multiplying the surface area "S" and the width of the skin area "st". In order to receive a ratio between skin and core area, the surface area has to be divided through the part volume "pv". This ratio is based on selected accuracy levels and has an effect on all accuracy levels. Dependent on the evaluated ratio, a specific build volume rate will massively influence the build time.

- ***High accuracy (ratio = 1)***

High accuracy levels are assumed for smaller beam diameters around 200 µm and layer thicknesses between 30 and 50 µm. These sets of parameters are typically used for beam powers below and up to 200 W.

Consequently, higher beam powers over 200 W are downgraded to 200 W to achieve high accurate quality parts. As a result, the build volume rate decreases significantly, leading to higher build times and cost.

- ***Low accuracy (ratio = 0)***

Low accuracy guarantees high build volume rates but does not necessarily fulfill required quality parameters. Inserted beam powers operate with full power and will not be downgraded as it is the case for high accurate parts. Beam diameters over 200 µm and layer thicknesses above 50 µm are reducing build time and cost, but suffer from low precise surfaces.

- ***Skin-core accuracy (ratio = 0-1)***

The skin-core technology enables fast volume build rates with high surface quality characteristics. Therefore, the inner "core" area of parts is built with bigger beam diameters, thicker layers and higher beam powers.

Consequently, this area shows poor results in terms of surface quality and accuracy. In order to avoid quality issues, the outer "skin" area is manufactured by using smaller beam diameters, thinner layers and lower beam powers. Typical parameters are represented by a layer thickness for the skin area of 100 to 200 µm and a layer thickness of 50 µm for the core area. Hence, productivity could be increased to up 1000 % compared to current build up technologies.

Nevertheless, the skin-core technology requires overlaps between the skin and the core area. Moreover, the layer thickness ratio between inner and outer areas cannot extend 1:4. This means that by using a skin layer thickness of 50 µm, the core layer thickness is limited to 200 µm. Suitable porosity levels only occur by including an overlap area between inner and outer layer thicknesses. For skin-core ratio of 1:2 the overlap area is typically 0.5 mm, whereas an overlap of 0.75 mm is necessary for a skin-core ratio of 1:4. Furthermore, a width of the skin area can be expected to amount approximately 3 mm (Schuh et al., 2012, pp.164–166).

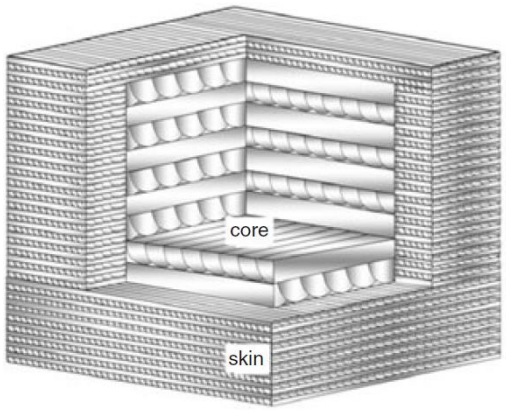

Figure 5.4: skin-core principle (Schuh et al., 2012, p.163)

Average build volume rate (vm)

The average build volume rate is dependent on the explained ratio "ratio", which maintains, if a slow build volume rate for accurate parts with good feature resolution or a fast build volume rate for low accurate parts with low feature resolution is implemented into the cost model. The skin-core technology describes a middle course by combining high and low build volume rates at the same time. As mentioned before, low accurate parts are allocated by a ratio of 0, which means that the value v1 will not influence the average speed vm. However, high accuracy with a ratio of 0 leads to an average speed exclusively containing v1.

```
vm = ratio*v1+(1+ratio)*v2
```

Where "vm" represents the average speed, "ratio" the skin-core ratio, "v1" the high-accurate build volume rate and "v2" the low-accurate build volume rate.

Build time (bt)

The build time includes three major different build time types, which are represented by the scan time T_S, the recoating time T_r and the delay time T_e. This leads to the formula

$$T_b = T_s + T_r + T_e$$

Figure 5.5: Formula for the build time estimation (Gibson et al., 2010, p.376)

Transferring this formula to the cost model presented in this study, the delay time amounts 5 % and is added to the scan time.

```
bt=pbt*1,05*pn+tr*bn
```

Where "bt" stands for the build time, "pbt" outlines the part build time, "pn" the part number, "tr" the recoating time and "bn" the number of batches.

Recoating time is calculated over the number of layers (nol), which slices the height of the part (cb) into constant layer thicknesses (x1). The layer thickness parameter is determined by 50 µm for all parts and is consequently not dependent on the accuracy level. Moreover, the recoating time is including a constant recoating time factor of 4.5 seconds per layer. This factor was taken from an online video showing the DMLM process. Consequently, the recoating time factor has to be multiplied with the number of layers (nol).

Expenses on machine (eom)

The total time (tt) is calculated by taking the build time (bt) and adding additional times per batch (atpb) and the batch number (bn) into account. Additional times per batch are based on study of Rickenbacher et al. (2013) and assumed for all printing processes in this study. These numbers have to be taken for each batch. A preparation time of T_{prep} = 0,25 h, a build job time of $T_{Buildjob}$ = 0,25 h, a setup-time of T_{Setup} = 0,75 h, removal time of $T_{Removal}$ = 0,5 h, post-processing time of T_{Postp} = 0,1 is taken into account. This results in a total labor time for each batch of **atpb = 1,85 h/batch** (Rickenbacher et al., 2013, p.213).

To estimate expenses on machine (eom), the total time (tt) is multiplied with the parameter machine cost per hour (mcph).

Machine cost per hour (mcph)

DMLM and EBM machines in this study are 120 h/week in use, which represents a 24 h usage during the five working days of a week. Furthermore, a maximum machine usage of 51 weeks each year leads to 6120 h/year of possible machine utilization. Taking into account that one year consists of 8736 hours, the outlined machine utilization of 6120 h/year **(mh)** results in an utilization rate of 70 %, which is assuming that the production is also running during nights and delays for reparations are not existing. Nevertheless, bigger manufacturing companies also produce goods on weekends, hence, an utilization rate of 70 % is imaginable for modern manufacturing companies.

Purchase absorption **(pc)** is calculated with 8 years for production machines and 5 years for software. Hence, the purchase price has to be divided through 8 and the software purchase price through 5. This value varies from machine to machine and contains a significant impact on the total cost per part. Maintenance, software and hardware costs were transferred from Ruffo et al. (2006) and are assumed to be constant values. Therefore, according to a depreciation time of 5 years for each of them, 21750 € have to be spent on maintenance each year **(mc)**, 1450 €/year for software **(sc)** and 870 €/year hardware **(hc)**.

Table 5.1: Cost assumptions (Ruffo et al., 2006, p.1420)

Machine costs	*€*
Maintenance/year **(mc)**	21750
Software cost/year **(sc)**	1450
Hardware cost/year **(hc)**	870

Machine cost values are taken from table 5.1. In order to calculate machine costs per hour, following formula is being implemented into the simulation tool.

$$mcph = \frac{pc + mc + sc + hc}{mh}$$

mcph = machine cost per hour; mc = maintenance cost per year; sc = software cost per year; hc = hardware cost per year; mh = machine hour

Machine costs in this study exclusively vary from each other because of different machine costs, all additional costs are assumed to stay constant for differing machines.

5.3 Expenses on worker

Workers time paid (wtp)

Labor costs are calculated on the average salary for a technician in mechanical engineering in Germany, which is 3150 € per month (Maschinenbautechniker.eu). Consequently, 37800 € each year a company pays for salary. Additionally, employer contributions of 22 % extra are added, resulting in a total labor cost of 46116 €/year (Ruffo et al., 2006, p.1420). This number is divided though the machine utilization of 6120 h/year **(mh)**. As a result, the production labor cost per hour **(plph)** is evaluated.

It is assumed that the employer is not working full time for the manufacturing process. More precisely, the employer will be paid for the setup-time and the reprocessing time for each batch and a monitor-time during the printing process of **10 %.** This factor has to be multiplied with the build time (bt). Additionally, the additional time per batch (atpb) respectively the number of batches is added

Expenses on worker (eow)

This value is calculated as the product of the workers paid time (wtp) and the production labor cost per hour (plph). Expenses on worker vary massively on the objected country and the required qualification of the employee. This parameter concludes all necessary values for the elaborated cost model.

Summarizing expenses on worker (eow), expenses on machine (eom) and material cost leads to the total cost of the build (cob).

5.4 Representation of a software tool based on “MathWorks Matlab”

5.4.1 Graphical User Interface (GUI)

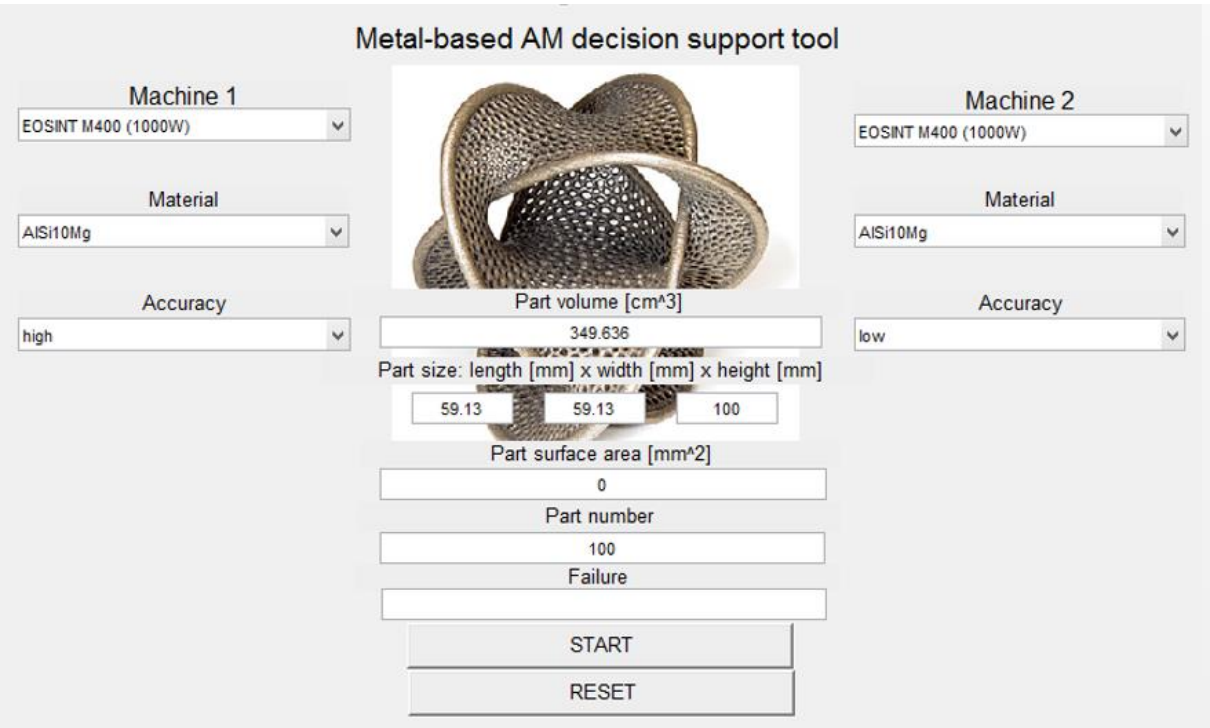

Figure 5.6: Graphical User Interface

On the left side, input data for machine 1 has to be selected. First of all the machine, then the material and additionally the accuracy level have to be chosen consecutively. On the right side, same has to be done for machine 2. In the middle, the part volume, part size, the surface area and the production volume has to be implemented. However, if a skin-core analysis as the selected accuracy level is not selected, the part surface area value is not playing a role in the calculation. Therefore, the value “0” can be implemented and the “Start” button begins the calculation. If input data is not fulfilling machine criteria, a failure code is requesting a change in the input data in order to start the simulation. After the simulation, a new evaluation round can be started through the “reset” button.

5.4.2 Output figures

Figure 5.7 outlines the cost per part over the number of parts for machine 1 and machine 2. This function stabilizes after approximately 20 parts. The reason for higher costs at the beginning is the low amount of parts in the powder bed and additional time for the set-up of the machine and existing post-processing time, which is calculated only over one piece. Tiny fluctuations after 20 parts represent new rounds of batches, hence cost per part values increase slightly.

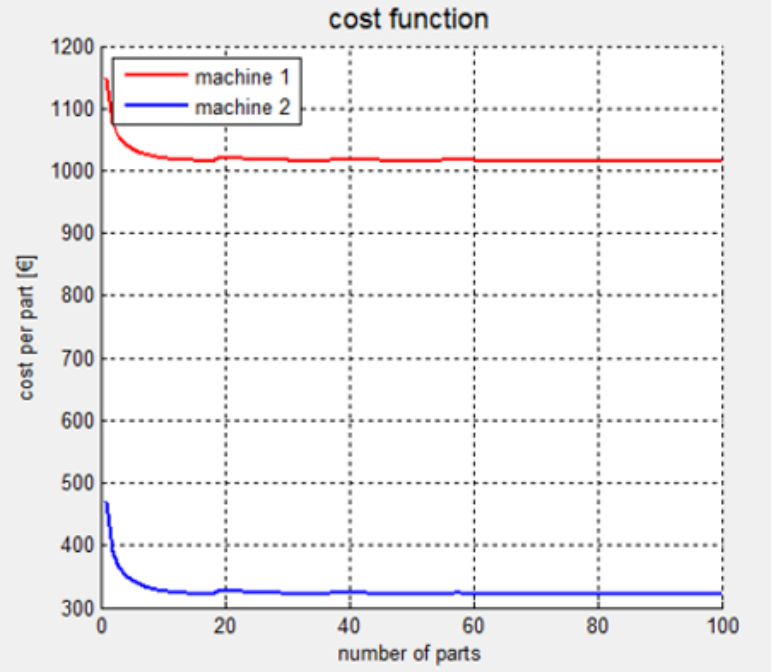

Figure 5.7: cost function

Figure 5.8 shows total costs on the vertical axes for machine 1 (on the left) and machine 2 (on the right). Moreover, a distinction between “machine”, “material” and “employee” cost types is made and a relation between both machines is presented. Typically, machine costs indicate the highest ratio of total costs. Nevertheless, in a few cases material costs can exceed machine costs, e.g. if high-costly materials like titanium are used. Due to the fact that employee costs are calculated with a monitoring factor of 10 %, this cost ratio is kept small. In this example, total costs of machine 1 are much lower than of machine 2. Especially machine and employee costs are decreased massively. The reason for this lies in the build volume rate. The time used for the build-up of the part is much lower on machine 2, consequently also employee costs are shrinking significantly.

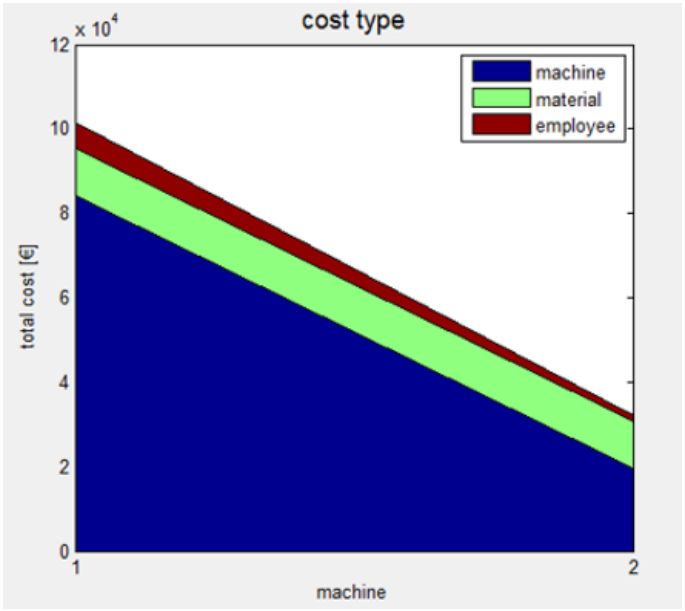

Figure 5.8: cost type

In figure 5.9, the total time function respectively the produced number of parts is represented. The slope of this function is a criteria for time used to manufacture the parts. In this case, machine 2 (blue line) needs much less time for the same parts than machine 2 (red line).

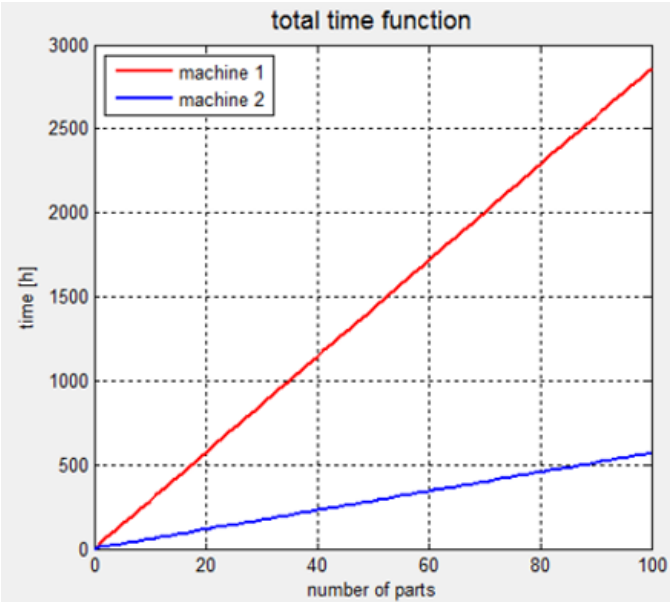

Figure 5.9: build time function

In general, the three output functions enable cost per part, cost type and time evaluations for two machines at the same time. Subsequently, Chaper 6 outlines the Design of Experiments

6 Design of Experiments

6.1 Sensitivity analysis

A mass- and building height sensitivity analysis shows the effect of mass and the effect of the building height on costs. As input parameters, an EOSINT M400 (1000 W) machine was used, producing parts out of AlSi10Mg with low accuracy. To achieve stable cost and avoid the low production fluctuating zone, a production volume of 100 parts was selected.

In an initial approach mass is increased by +25% and +50% and decreased by -25% and -50%, while the height of the part (c_0 to c_4) is kept constantly. Consequently, the length (a), width (b) and volume (V) of the part changes, resulting in varying cost values (cost/part).

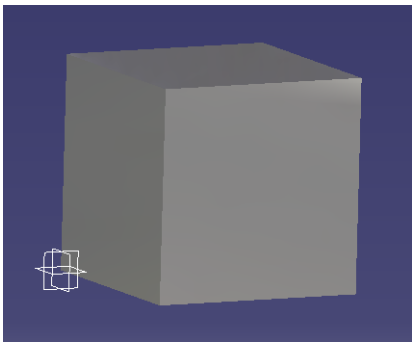

Figure 6.1: aluminum cuboid ($\rho_{AlSi10Mg}$ = 2.86 g/cm^3)

Table 6.1: constant building height, varying mass

m_0 = 1 kg	**m_1 = 1,25 kg**	**m_2 = 1,5 kg**	**m_3 = 0,75 kg**	**m_4 = 0,5 kg**
c_0 = 10 cm	c_1 = 10 cm	c_2 = 10 cm	c_3 = 10 cm	c_4 = 10 cm
a_0 = 5.913 cm	a_1 = 6.61 cm	a_2 = 7.242 cm	a_3 = 5.12 cm	a_4 = 4.18 cm
b_0 = 5.913 cm	b_1 = 6.61 cm	b_2 = 7.242 cm	b_3 = 5.12 cm	b_4 = 4.18 cm
V_0 = 349,636 cm^3	V_1 = 436,921 cm^3	V_2 = 524,466 cm^3	V_3 = 262,144 cm^3	V_4 = 174.724 cm^3

Cost/part (m_0) = 320 €	Cost/part (m_1) = 400 €	Cost/part (m_2) = 500 €	Cost/part (m_3) = 245 €	Cost/part (m_4) = 165 €

Figure 6.2 shows the effect of mass on costs. As a result, increased mass with a constant building height leads to higher cost. For masses between 0.5 and 1.5 kg, costs are accounted from 165 to 320 €, a cost difference of 155 €.

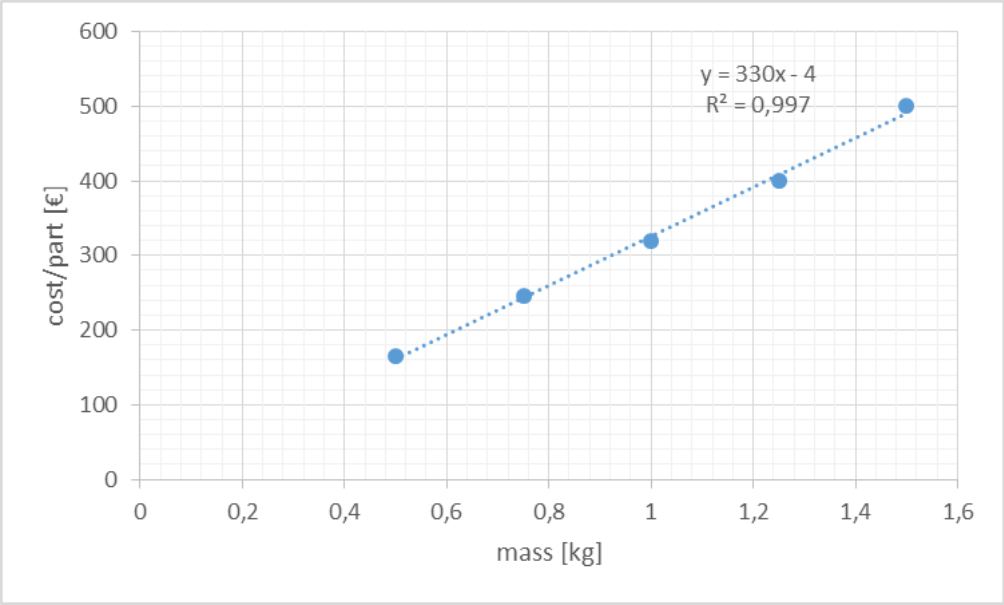

Figure 6.2: constant building height, varying mass

In the next approach, mass is kept constantly at 1 kg (m_0 to m_4) and the building height is increased by +25% and +50% and decreased by -25% and -50%. Hence, the length (a), width (b) and volume (V) of the part changes, resulting in varying cost values (cost/part).

Table 6.2: constant mass, varying building height

c_0 = 10 cm	**c_1 = 12,5 cm**	**c_2 = 15 cm**	**c_3 = 7,5 cm**	**c_4 = 5 cm**
m_0 = 1 kg	m_1 = 1 kg	m_2 = 1 kg	m_3 = 1 kg	m_4 = 1 kg
a_0 = 5,913 cm	a_1 = 5,29 cm	a_2 = 4,828 cm	a_3 = 6.828 cm	a_4 = 8,362 cm
b_0 = 5,913 cm	b_1 = 5,29 cm	b_2 = 4,828 cm	b_3 = 6,828 cm	b_4 = 8,362 cm
V_0 = 349,636 cm^3	V_1 = 349,636 cm^3	V_2 = 349,636 cm^3	V_3 = 349,636 cm^3	V_4 = 349,636 cm^3

Cost/part (c_0) = 320 €	Cost/part (c_1) = 325 €	Cost/part (c_2) = 330 €	Cost/part (c_3) = 315 €	Cost/part (c_4) = 310 €

Figure 6.3 describes the effect of varying building heights on the costs per part at constant mass values. Accordingly, costs increase with the building height and are ranging from 310 to 330 euros, which symbolizes a cost difference of 20 €.

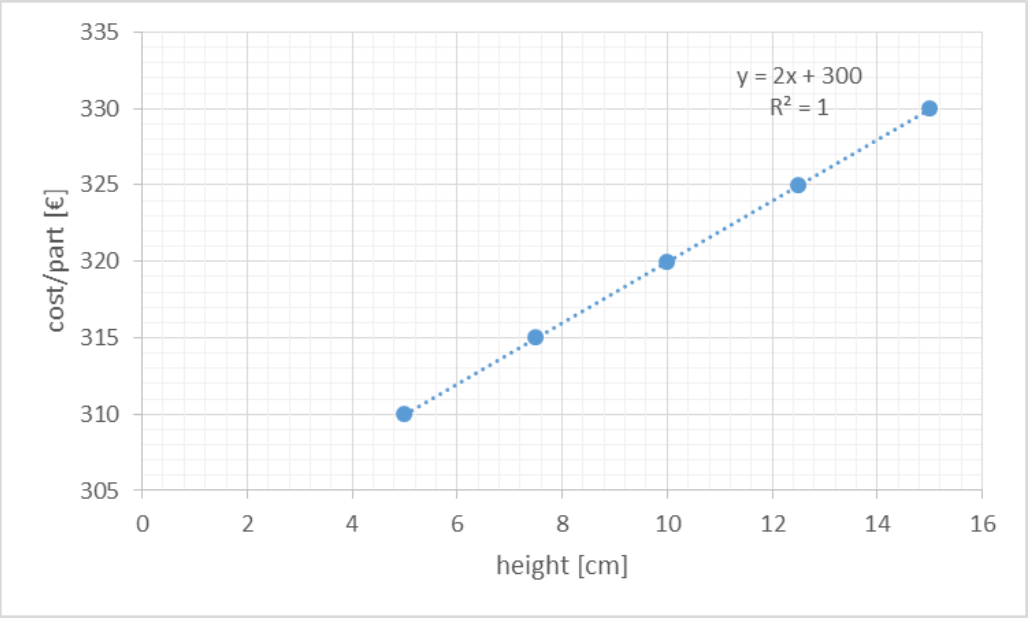

Figure 6.3: constant mass, varying building height

The sensitivity analysis between mass and building height shows that the effect of mass on costs is much stronger than the effect of building height on costs. Cost differences of 155 respectively 20 € occur in these calculations and indicate significant differences.

For this reason, material costs have a greater impact than the recoating time in metal-based AM. Compared to plastic-based AM processes, the building height is the main parameter to evaluate cost and time, due to low material costs. Additionally, the fusion time has a greater impact on time than the recoating time. Consequently, expenses on machine and employee increase and have an impact on the total cost of the build.

6.2 Skin-core analysis

To analyze the advantages in cost and time of the skin-core technology compared to parts with high accuracy, a simple cube with a 100 mm in length, 100 mm in width and 100 mm in height is tested on a SLM 500 HL system with AlSi10Mg as the input material (figure 6.4).

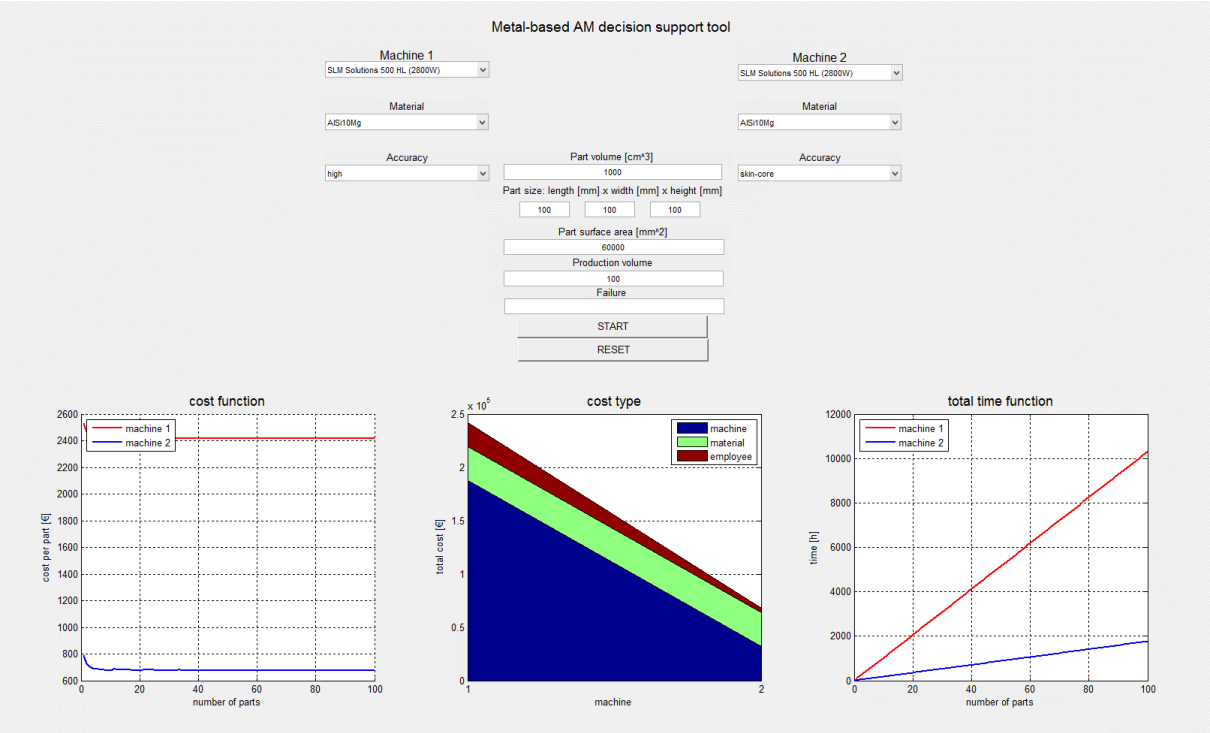

Figure 6.4: Skin-core analysis

As a result, costs per part are much lower by using the skin-technology resulting from higher average volume build rates. However, cost per part with high accuracy amount approximately 2400 €, while cost per part with the skin-core technology are lowered to 700 €. Due to a decreased build time, machine costs and expenses for the employee could be decreased massively. Less time on the machine is needed and monitoring time of the employee is shrinking.

6.3 DMLM and EBM comparison

A comparison between laser beam-based DMLM and electron beam-based EBM was conducted to evaluate differences in both systems. Therefore, an Arcam Q 10 was compared to an EOSINT M280. Cost and time values for a turbine wheel in figure 6.5 are presented in figure 6.6. The exemplary parts is manufactured out of Ti6Al4V with low accuracy.

Turbine wheel

Dimensions:
54 × 54 × 28 mm

Volume:
20618 mm³

Figure 6.5: Turbine wheel (Baumers et al., 2012, p.935)

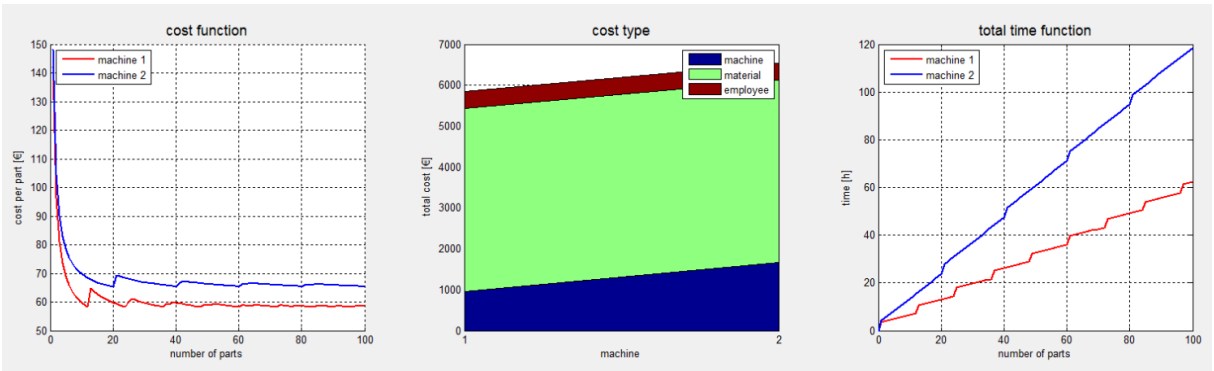

Figure 6.6: Exemplary comparison of DMLM and EBM

“Machine 1” represents the EBM machine, while “machine 2” stands for the DMLM machine. As a consequence, costs per part are lower for the EBM system, arising from higher volume build rates. Minute jumps in the cost function and the total time function represent the beginning of a new batch. However, according to a smaller build volume of the EBM system, this effect is more distinctive for electron beam-based systems.

6.4 Exemplary parts

6.4.1 Random test

In this random test, input parameters were selected randomly and 5 exemplary parts were tested in terms of costs. Therefore, all possible machines were evaluated with AlSi10Mg as the material of the parts and a production volume of 100 parts, comparing low quality parts with high quality parts. As a result, the cost per part of exemplary components of figure 6.7 are shown in table 6.3.

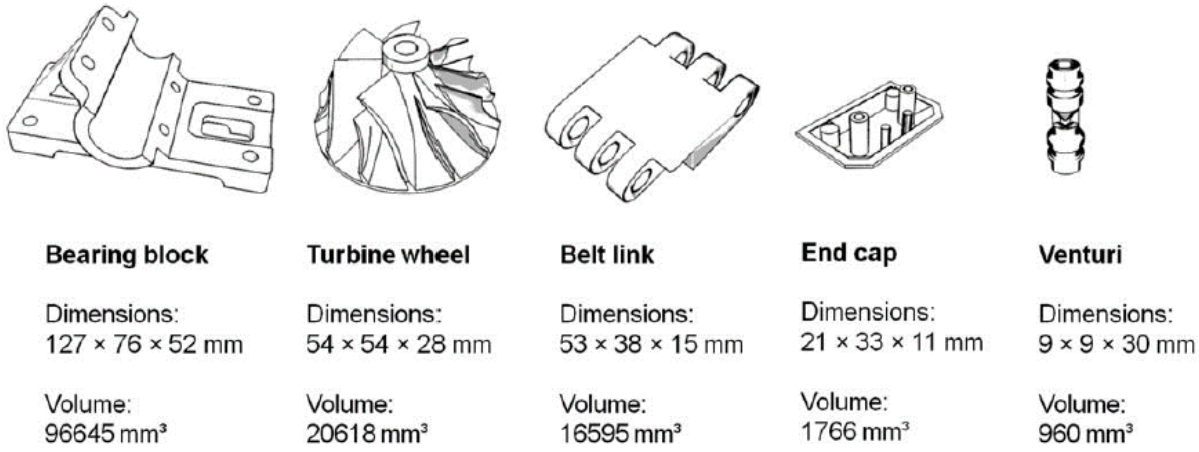

Figure 6.7: Set of exemplary parts (Baumers et al., 2012, p.935)

Low quality

Table 6.3: Cost per part with low quality (AlSi10Mg)

Machine	Bearing block [€]	Turbine wheel [€]	Belt link [€]	End cap [€]	Venturi [€]
3D Systems ProX 100 (50W)	Too big	118	90	16,5	11
Concept Laser M2 (400W)	158	37	28	4	3
EOSINT M280 (400W)	128	29	22	3,7	3
3D Systems ProX 300 (500W)	130	28	23	3,9	3
EOSINT M400 (1000W)	118	22	18	2,7	2
Concept Laser X line 1000R (1000W)	110	23	19	2,8	2
SLM Solutions 280 HL (1000W)	75	19	13	2,4	1,6
SLM Solutions 500 HL (2800W)	70	18	11	2	1,3
Arcam Q10 (3000W)	78	20	13,5	3,6	2,6

Consequently, cost per part is dependent on the volume and the three dimensions. The “venturi” part shows lowest costs, while the bearing block indicates the cost maximum. Figure 6.8 represents the effect of the beam power on average costs. To calculate average costs, all five cost values of each machine are summed up and divided through the number of different parts.

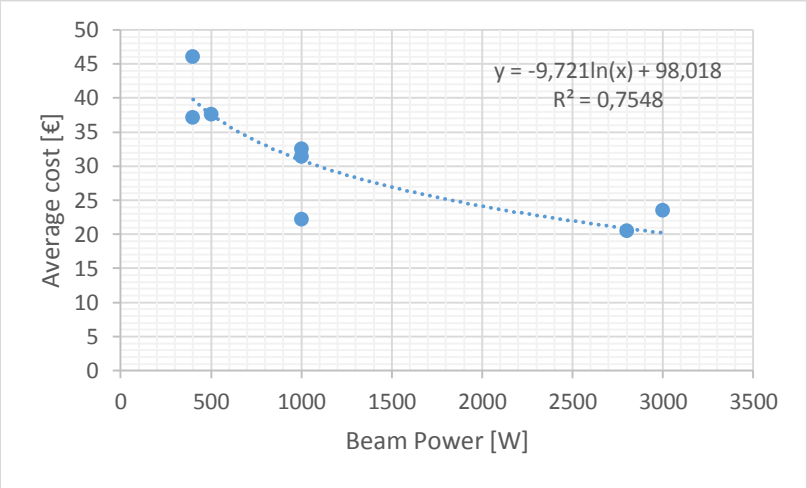

Figure 6.8: Influence of beam power on average costs

Accordingly, high beam powers result in lowered average cost values by the implementation of outlined random input parameters. A reason for this behavior can be seen in the selection of low quality parts. Thus, the volume build rate symbolizes the most influential parameter, which increases significantly for higher beam powers and also compensates higher machine prices. In figure 6.9, the effect of the build machine volume on average costs is represented. A relation between higher build machine volumes and average cost cannot be observed.

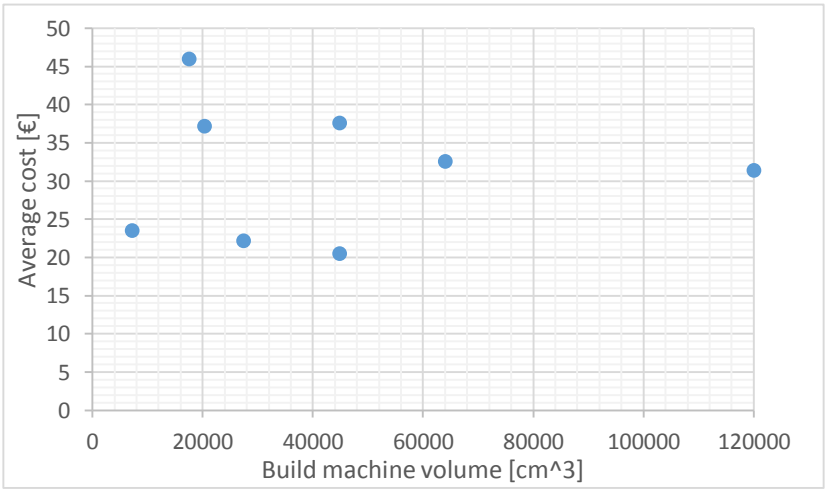

Figure 6.9: Influence of build machine volume on average costs

Figure 6.10 outlines all cost per part values of table 6.3 in one figure. Consequently, the 3D Systems ProX 100 shows highest costs, while the SLM Solution 500 HL indicates lowest cost values. Moreover, the bearing block is not able to be produced with the 3 D Systems ProX 100 because the size of the part does not fit into the powder bed.

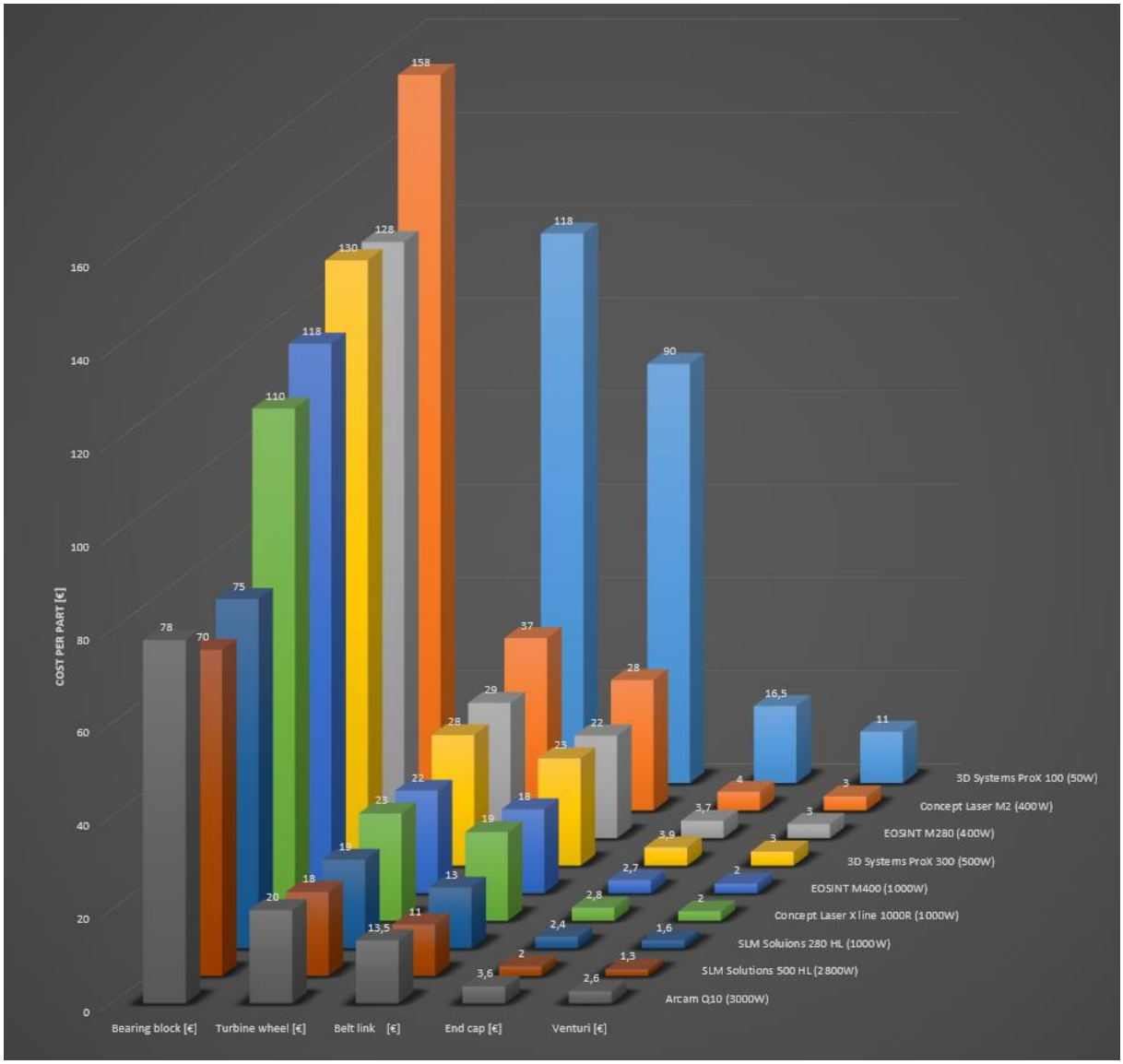

Figure 6.10: Cost per part machine comparison for several components

These results can be described as cost values for productivity. However, high quality parts lead to diverging conclusions.

High quality

In order to fabricate high quality parts with good feature resolution, metal-based AM machines above 200 W are downgraded to 200 W laser systems with decreased build volume rates. Nevertheless, quality parameters like the beam diameter are reduced resulting in a finer surface processing.

Table 6.4: Cost per part with high quality (AlSi10Mg)

Machine	Bearing block [€]	Turbine wheel [€]	Belt link [€]	End cap [€]	Venturi [€]
3D Systems ProX 100 (50W)	Too big	118	92	17	11
Concept Laser M2 (400W)	265	58	44	8	4
EOSINT M280 (400W)	210	46	35	6,5	3,5
3D Systems ProX 300 (500W)	250	54	41	6,7	3,7
EOSINT M400 (1000W)	405	78	60	8	5
Concept Laser X line 1000R (1000W)	400	88	70	8	6
SLM Solutions 280 HL (1000W)	195	43	35	6	4
SLM Solutions 500 HL (2800W)	245	53	42	6	4
Arcam Q10 (3000W)	230	53	40	7	4

Subsequently, same figures compared to low quality results are outlined. First of all, average cost over beam power is shown in figure 6.11.

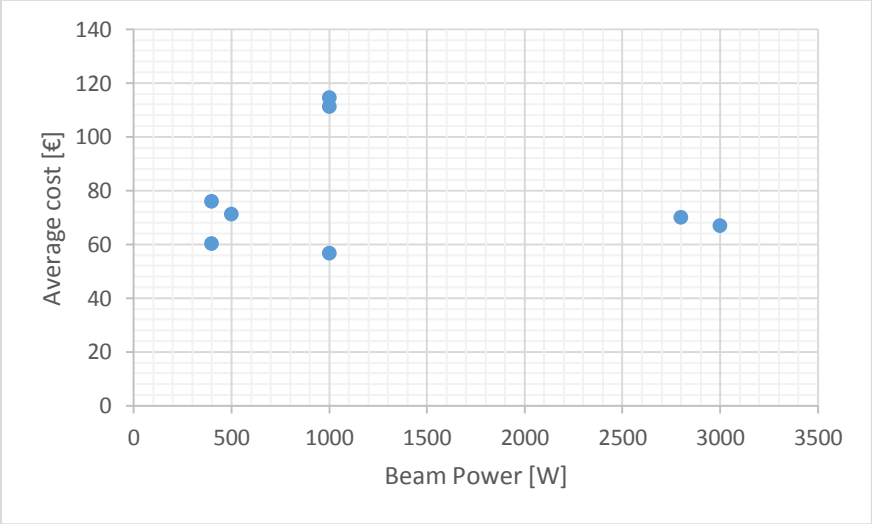

Figure 6.11: Influence of beam power on average costs

Any direct relation between average cost and beam power can be observed.

For this reason, average costs are presented over the build volume in figure 6.12. This figure shows that presented machines with smaller build volumes have cost advantages for high quality parts production.

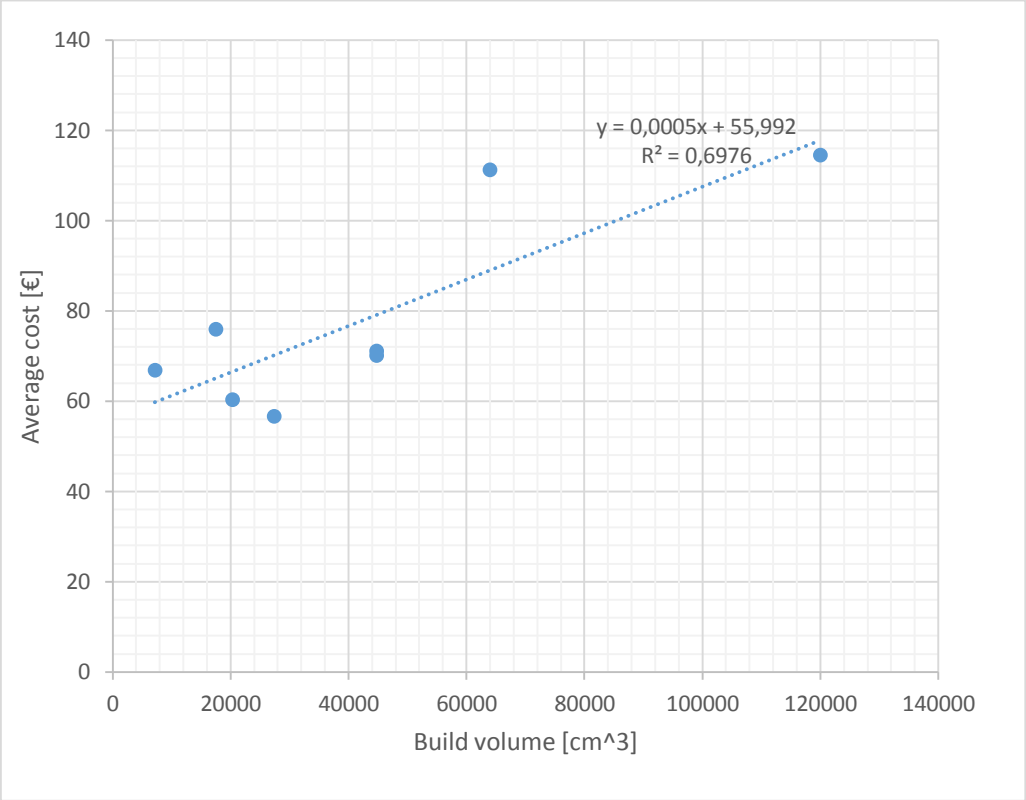

Figure 6.12: Influence of build machine volume on average costs

The reason can be seen in relatively high machine prices for big build volume chambers. A main advantage of big build volumes is a low amount of additional time being needed for preparing and post-processing for a new batch. However, if the build volume rate is relatively low, total time is increasing significantly and the importance of additional time is decreasing relatively. Hence, additional costs for higher build volumes have a bigger effect on average costs than additional time needed.

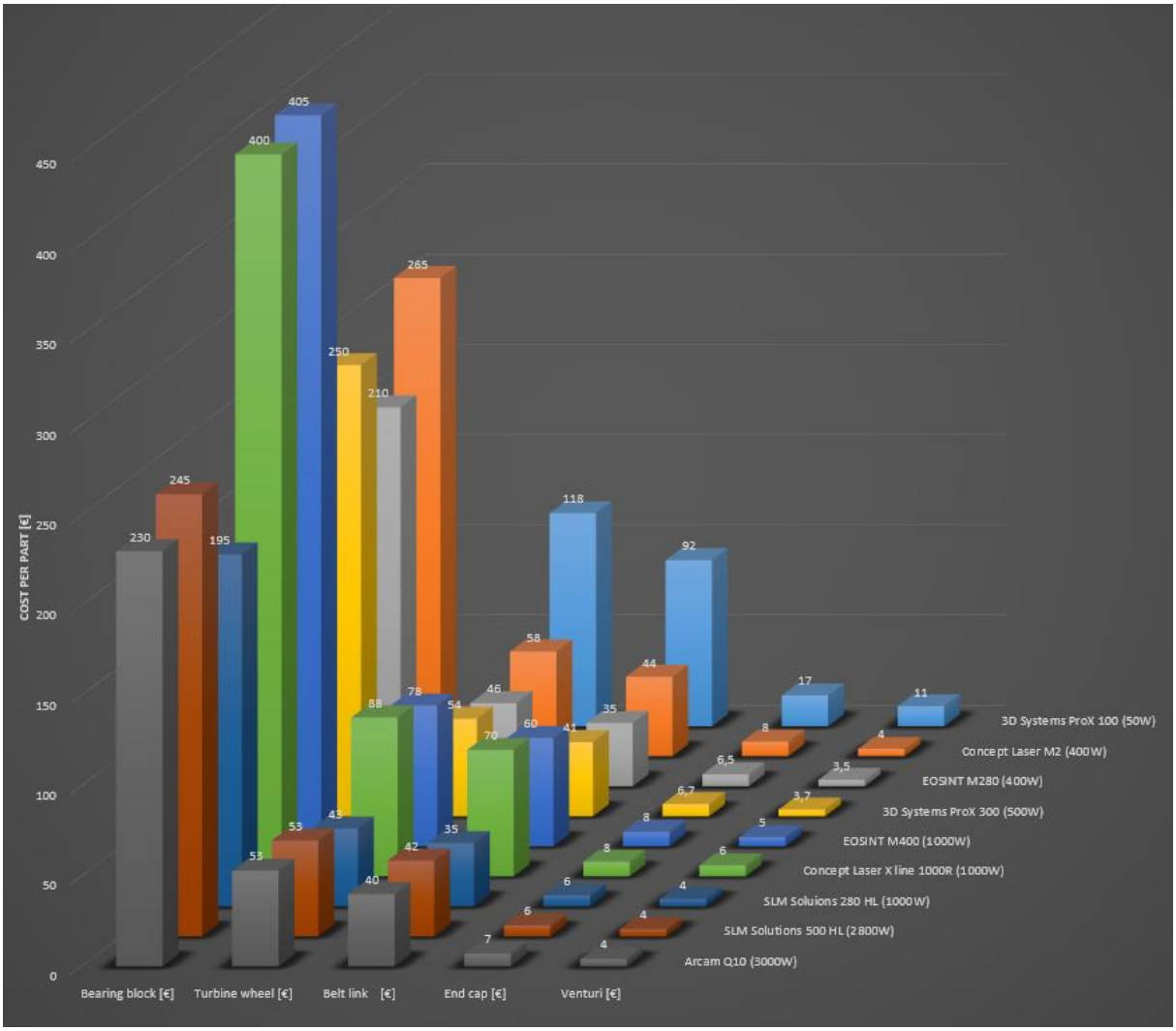

Figure 6.13: Cost per part machine comparison for several components

This figure shows that the Concept Laser X line 1000 R, the EOSINT M 400 and the 3D Systems ProX 100 lead to highest cost part values, whereas the SLM Solutions 280 HL and the EOSINT M280 show lowest costs. As a consequence, machines with smaller build volumes induce lower costs for high quality parts than bigger ones. The laser power has no effect on costs, because of low beam powers being used for high feature resolution. These results can be described as cost values for performance.

6.4.2 Taguchi L-18 orthogonal array

The Taguchi systematology for a L-18 orthogonal array (A15) is applied for five exemplary parts (figure 6.14), the same ones used in the random test in chapter 6.4.1. The chosen L-18 array fits for 5 different parameters and 3 levels for each parameter in order to study the sensitivity of the model to a variability of input parameters.

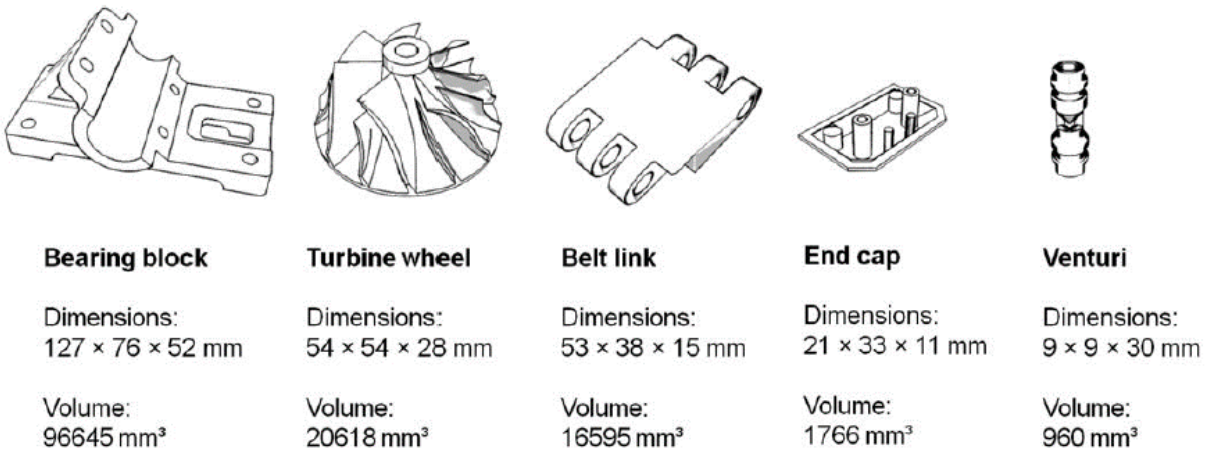

Figure 6.14: Exemplary parts (Baumers et al., 2012, p.935)

Input parameters

Number of parameters (5): Machine, Material, Accuracy, Part, Production volume

Number of levels: 3, 3, 3, 3, 3

- *Material:*
  AlSi10Mg, MS 1.2709, Ti6Al4V
- *Machine:*
  EOSINT M 280 (EOS), Concept Laser X line 1000 R (CL), SLM Solutions 500 HL (SLM)
- *Accuracy:*
  high, low, skin-core
- *Part:*
  Bearing block (BB), turbine wheel (TW), venture (V)
  Surface calculated by taking the rectangular solid:
  $S_{Bearing\ block}$ = 40416 mm^2, $S_{Turbine\ wheel}$ = 11880 mm^2, $S_{Venturi}$ = 1242 mm^2
- *Production volume:*
  1, 15, 100

Output parameters

Cost per part, total cost, total time

Table 6.5 outlines tested combinations based on Taguchi. All possible levels are included for each parameter, except for the material. The systematology leads to a non-consideration of Ti6Al4V, because it only regards two levels for the parameter “material”.

Table 6.5: Implemented parameters and levels

Expt. No	Material	Machine	Accuracy	Part	Production volume
1	AlSi10Mg	EOS	high	BB	1
2	AlSi10Mg	EOS	low	TW	15
3	AlSi10Mg	EOS	skin-core	V	100
4	AlSi10Mg	CL	high	BB	15
5	AlSi10Mg	CL	low	TW	100
6	AlSi10Mg	CL	skin-core	V	1
7	AlSi10Mg	SLM	high	TW	1
8	AlSi10Mg	SLM	low	V	15
9	AlSi10Mg	SLM	skin-core	BB	100
10	MS 1.2709	EOS	high	V	100
11	MS 1.2709	EOS	low	BB	1
12	MS 1.2709	EOS	skin-core	TW	15
13	MS 1.2709	CL	high	TW	100
14	MS 1.2709	CL	low	V	1
15	MS 1.2709	CL	skin-core	BB	15
16	MS 1.2709	SLM	high	V	15
17	MS 1.2709	SLM	low	BB	100
18	MS 1.2709	SLM	skin-core	TW	1

Table 6.6 shows the final results of the Taguchi method leading to varying cost per part, time per part, total cost and total time values.

Table 6.6: Results of Taguchi Method

Expt. No	Cost per part [€]	Time per part [h]	Total cost [€]	Total time [h]
1	310	14,90	310	14,9
2	36	1,27	420	19
3	3,3	0,14	330	14
4	420	10,47	6100	157
5	27	0,49	2700	49
6	115	2,20	115	2,2
7	150	5,30	150	5,3
8	9	0,15	85	2,3
9	245	10,20	24500	1020
10	4,6	0,19	460	18,7
11	320	12,20	320	12,2
12	74	3,33	1100	50
13	135	3,20	13500	320
14	113	2,10	113	2,1
15	635	15,00	9500	225
16	9	9,00	4,25	135
17	122	2,05	12200	205
18	176	6,30	176	6,3
Average	161,33	5,47	4004,63	125,44

The numbers from table 6.6 are presented in an effect diagram in figure 6.15 and 6.16.

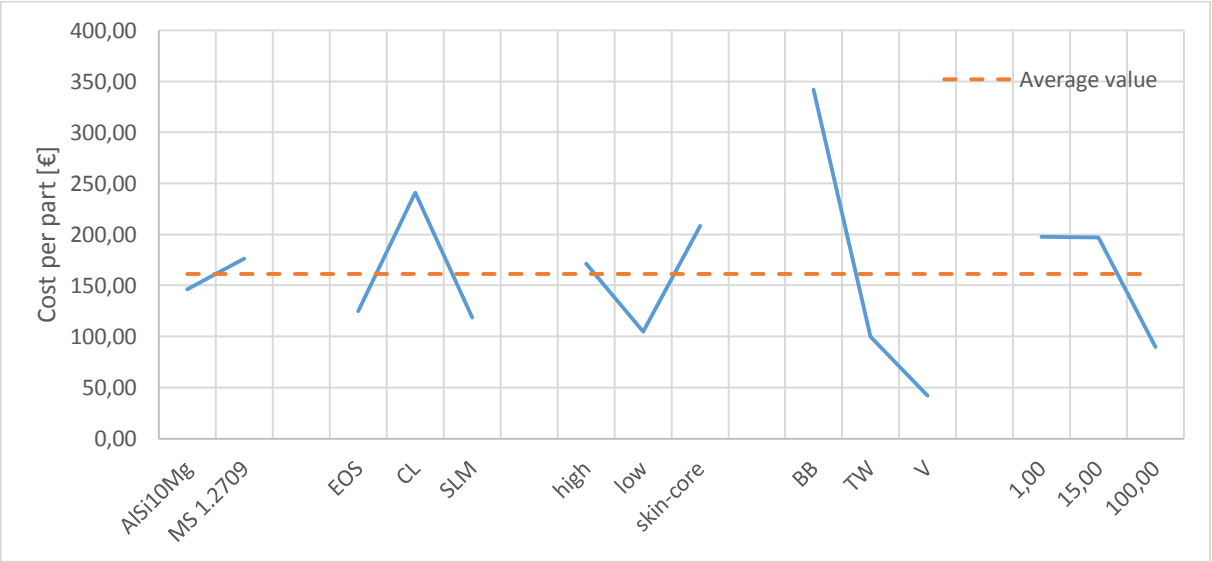

Figure 6.15: Effects on cost per part

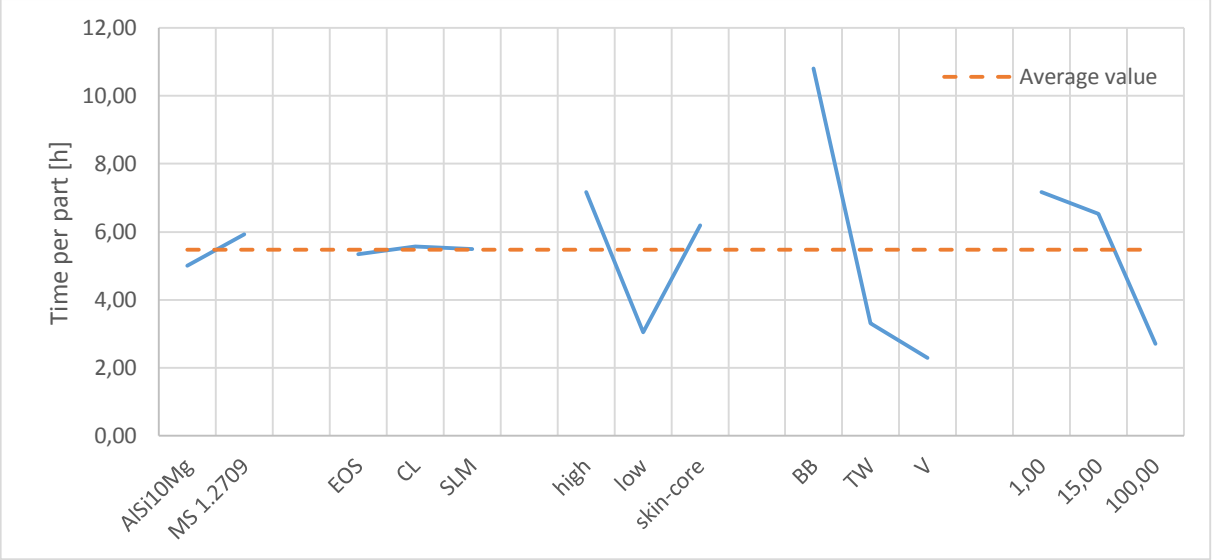

Figure 6.16: Effects on time per part

As a result, the effect of the part size is the most influential parameter in terms of cost per part and time per part. Moreover, the accuracy and the production volume indicate strong effects, while the machine type has only an effect on cost per part but not on the time per part, which arises from different machine costs. In addition, the material type does not influence costs and time significantly. However, titanium was not implemented into this test due to the limitations in the Taguchi methodology.

6.5 Result validation

The sensitivity analysis shows suitable results, because the cost model reacts on varying mass and changing building height. It could be expected that mass has a greater impact than the building height in metal-based AM. Additionally, the build time is more dependent on mass than on building height. This represents a major difference to AM processes based on plastics, where a strong correlation of the build time on the building height is existing (A12).

A comparison between skin-core and high quality process methods outlines the great advantage of dividing parts in areas with different feature resolution. The average build volume rate increases, while surface quality respectively feature resolution stays the same. Nevertheless, this technology is only useful for bigger parts, e.g. for the exemplary cube with (100x100x100) mm^3. The thickness of the area with high feature resolution and overlapping mechanisms affect the skin-core method and result in different build times.

The comparison between a DMLM and an EBM system is mainly dependent on the machine selection. In the exemplary case, the EBM system produces cheaper titanium parts than the DMLM system. Nevertheless, comparing the Arcam Q10 with the SLM 500 HL, the DMLM manufactures cheaper parts because of the bigger build volume, which reduces additional production times. Even though the EBM system enables highest build volume rates, the build volume effect has a greater impact on cost per part values.

The random test confirms the estimations of a positive effect on costs by implementing higher beam power levels. However, the same effect on machine volume and the number of inserted parts into one batch cannot be proved. On the one hand this result is based on the implementation of relatively low beam power levels for big machine volumes and therefore non-optimal positionings of parts in the powder bed. This failure results from the batch size estimator, if a user chooses the wrong positioning of the part. As a consequence, a low amount of parts fits into the powder bed.

The cost per part machine comparison for several components in Figure 6.10 giving a good overview of all implemented machines into the Matlab Works tool for exemplary parts. The results are understandable in terms of productivity, which means that higher beam powers increase the build volume rate and lower costs. Looking at high accuracy, which means that the feature resolution is excellent and all high beam power machines are downgraded to 200 W to fulfill required quality parameters, results look completely different. In this case, some smaller machines have cost advantages compared to machines with high productivity. Lower machine costs for smaller power machines are indicators to underline this argument.

The Taguchi testing confirms basic estimations like the importance of part volume and part size on costs and significant cost decrease for higher part numbers. Surprisingly, selecting skin-core as the accuracy level for the exemplary parts leads to highest cost values. This arises from the small part volume and part size of the parts and the weaknesses of the Taguchi method itself. A not suitable amount of tests is done with accuracy parameters. Looking at the influence of accuracy levels on time, more logical results were achieved, because build time is lower for the skin-core technology than for high quality accurate parts.

Another weakness of the used Taguchi L-18 orthogonal array is the low amount of tested levels in terms of material. Titanium is not tested, which has definitely an impact on costs. It can be assumed that the effect of material on costs is one of the most significant ones. Regarding different cost types, titanium as the input material usually displays a major ratio of total costs for manufactured parts.

7 Discussion

In chapter 2, the basics of metal- and powder bed based AM were presented to the reader and main characteristics of laser-beam based and electron-beam based systems explained. Consequently, chapter 3 already provides existing classification schemes to support the evaluation of manufacturing processes by describing the state of the art and AM decision support systems based on "MathWorks Matlab". This structure provides a quick entry into the topic by explaining basics as well as showing the goal of the thesis, a decision support system for current metal-based AM machines.

The purpose of these two chapters lies in the understanding of the goal and the reasons for establishing a metal-based AM decision support tool, which is described in chapter 3.3 under "resulting research gaps". In the end of chapter 3, a research design methodology process diagram is outlined to show the proceeding of the following chapters. The research design is clearly separated into three steps: input data and context, simulation and DoE. This structure should help the reader to understand the simulation tool better.

Before a set-up of the simulation tool can be started, input data like machine prices and material costs are mandatory, but also the context of DMLM and EBM systems. Therefore, a comparison between laser-beam based and electron-beam based technologies is presented. Regarding the output of the simulation tool, cost and time of the product, the user should always have in mind that Arcam's EBM systems are producing niche products. Typically, titanium alloys and pure titanium parts for medical and aerospace industries are manufactured with these machines.

7.1 Research questions

RQ1: How can several current metal-based Additive Manufacturing machines up to 3000 W be compared and evaluated with each other in terms of cost and feasibility?

Therefore, a decision-support tool based on "MathWorks Matlab" was established consisting of an adjusted cost model and build volume rates for beam power levels between 50 and 3000 W. In total, 9 metal-based AM systems can be compared with each other including a selection of three different materials and accuracy levels. As a result, cost per part, total cost, cost type and process time values can be evaluated. For more detailed information, see Chapter 5.

RQ2: What are the main differences between laser-beam (DMLM) and electron-beam based systems (EBM)?

Current machine parameters evidence that the balance of power is shifting to DMLM systems. Improvements were basically transacted in build envelope sizes, residual stresses as well as surface finish parameters. As a conclusion, the DMLM technology is more sufficient for a wide variety of applications, whereas EBM supplies niche markets. The previous main advantage of EBM systems, its faster build rates, cannot be observed in current metal based AM systems.

DMLM systems produce bigger build sizes, perform with less beam power and show higher surface finish parameters. Additionally, further differences like in the scanning process, the atmosphere and the applicable materials occur. More precise information can be found in Chapter 4.3.

RQ3: What are the most influential input variables to evaluate the performance of AM systems?

Based on the Taguchi method, the most influential parameter regarding costs is determined by the part volume and part size of evaluated parts. Additionally, the machine type, the production volume, the accuracy level as well as the used material contain significant impacts on costs. A sensitivity analysis has shown that the mass of manufactured parts induces much higher influence on costs than the building height. To receive an overview of exact results, go to Chapter 6.4.

7.2 Contribution, findings and practical implications

The simulation tool provides cost and time evaluation for several machines and is also able to compare them at the same time. Furthermore, accuracy plays a major role in this cost tool and a selection of materials is possible. An existing cost model is being adjusted for metal-based AM purposes, including characteristics like powder recycling, waste and monitoring time. Moreover, the user has the big advantage to choose skin-core as the accuracy level, which is providing a technology with a future potential.

Additionally, the Design of Experiments consists of a sensitivity analysis, a skin-core analysis, a DMLM and EBM comparison, a random test and a Taguchi L-18 orthogonal array. The big variety of testing should cover a wide range of user input possibilities.

The sensitivity analysis shows that costs are more dependent on mass than on the building height, which was expected and could be proved with this analysis. This analysis was executed for parts out of AlSi10Mg with low accuracy. Furthermore, it would be interesting, how results would change if you switch to low or skin-core quality. Probably, the building height will play a bigger role concerning costs, because build time and consequently costs increase.

The adjusted cost model includes recycling by implementing a waste factor, is based on several build volume rates for each material and allows a distinction of low, high and skin-core accuracy levels. Additionally, it is not exclusively focusing on one machine, but enables a comparison of two machines simultaneously. Another advantage can be seen in an easy adaption of machines being evaluated. New machine systems can be added quickly to model by changing the Matlab code.

Potential users of the decision-support tool can be seen in companies which are considering to buy metal-based AM systems, looking for the most suitable machine system. Further, it can be used for already bought machines in order to figure out costs of future production volumes.

7.3 Limitations of this research

A general problem to define which machines are being included into the model occurred. Due to a lack of data in trustable machine prices or specific machine characteristics, only a limited amount of machines could be used for the evaluation model. For example, it would have been interesting to implement the EOS M 270, but a reliable and present machine price was not available. Moreover, the EBM system Arcam Q20 could not be inserted, even though a machine price was available.

For the issue with the Arcam Q20, a different shape of the building platform displays the main reason, which is round and not rectangular like in all other regarded systems. The build size estimator exclusively works correctly with rectangular building platforms, because it operates with the distances of the parts length, width and height. Especially the orientation of parts in the powder bed has a significant effect on costs. The orientation problem is not fully covered in this study, the user should be able to decide by himself, if parts should be produced horizontally or vertically by adjusting length, width and height. Also, spacings between parts and the edge of the powder bed can differ. Nevertheless, the implemented build size estimator is a simple and effective tool to display a suitable build size approximation.

Another main problem can be seen in the evaluation of volume build rates. In this study, scan speed parameters with high density parameters were taken from literature and build volume rates were calculated. Additionally, build volume rates from DMLM machine manufacturers like EOS were added and general build volume rates for DMLM and three different materials were established. Despite the exactness of build volume curves for AlSi10Mg and Maraging Steel, which are based on many data points and show predicted results, build volume rates of titanium alloys show major disadvantages. Due to a not sufficient amount of data points the slope of this graph could deviate under real conditions massively. Moreover, thermodynamic parameters like melting points and heat conductions do not confirm the reason for those high build volume rates.

Presenting an evaluation on comparable DMLM and EBM machines outlines that EBM machines are cheaper in terms of low quality parts out of titanium. This experiment leads to a clear result, but more machines, materials and accuracy levels should be tested.

Random and Taguchi testing basically underlines general assumptions, e.g. that high beam power machines provide lower costs in terms of low quality or that a production volume of 100 parts causes lower cost per part values than a production volume of only one part.

7.4 Future research

Metal-based AM technologies have a big potential if build volume rates improve and the industry widely accepts and adapts its main advantages. Especially for low production volumes and complex parts a market for DMLM and EBM machines is already existing and growing steadily. If the manufacturing processes can be understood better and costs are decreased, it

becomes more competitive compared to conventional manufacturing and will have a strong impact on future manufacturing.

Regarding the AM cost tool in this study, more tests dealing with the "Matlab" simulation tool would be useful. Also, a comparison of cost and time respectively simulation and produced parts under real conditions is necessary.

Further, testings under real conditions and comparisons with the presented model are desirable. Investigations on support structure as well as a sensitivity analysis on machine costs, material costs and costs on employees could lead to improved results.

Moreover, interesting future topics are for example an investigation on disruptive factors. How do costs develop if maintenance will be required and takes 1, 3 or 9 hours? What if the powder recycling fails and the recycling rate goes back to 25, 50 or 100 %. Which effect has a decreased beam power of 5, 10 or 15 %?

Another interesting analysis is the investigation in skin-core quality parts. The potential of the skin-core method seems to be enormous. It is impressive how big the impact on costs by using this method can be, major cost and time reduction can be achieved without leading to quality disadvantages. However, only one exemplary part on two specific machines regarding one material is tested. Hence, main differences of this method were presented, but a more detailed investigation would be preferable. For which parts is it useful to implement this novel method? How does complexity influence the skin-core technology in terms of cost and time?

8 Summary and conclusions

This master thesis with the title "economic validation of metal- and powder bed based AM processes in the early stage of product development" initially illustrates main principles in AM and PBF processes and compares laser beam and electron beam based systems. Subsequently, existing AM classification schemes are presented and an own cost model specified for metal-based AM is established. The outlined cost model is determined by parameters such as build volume rates, machine and material costs.

A cost and time decision support system based on "Math Works Matlab" is developed providing a comparison of two metal-based AM machines at the same time. In total, 9 different machines, 3 different accuracy levels and 3 different material types can be chosen as input parameters. As an output, the user receives a cost per part figure, a total cost type comparison and a build time evaluation. Based on this knowledge, decisions can be made, which machine fits best for specific requirements.

Several experiments were executed including a sensitivity analysis for mass and building height, followed by a skin-core analysis, an exemplary comparison of DMLM and EBM machines and a random test on all implemented machines and five exemplary parts showing differences in volume and size. Moreover, the Design of Experiments is finished with a Taguchi L-18 orthogonal array test, leading to main effects and influences on several parameters on costs and build time.

Comparing DMLM and EBM machines, DMLM systems produce bigger build sizes, perform with less beam power and show higher surface finish parameters. Additionally, they provide a broader field for applications than EBM systems. Due to fastest build volume rates, electron beam-based systems show advantages in the production of low quality parts out of titanium for medical and aerospace industries.

Executed experiments show that both mass and building height of parts have an effect on cost and time per part. However, the effect of mass on costs and time is significantly bigger. Moreover, the skin-core method enables enormous cost savings by separating parts into high quality and low quality areas with different feature resolution characteristics. A random test leads to the result that average costs decrease with higher beam powers for low accuracy, while high accuracy causes an average cost increase for machines with higher build volumes.

Finally, each input parameter was tested respectively its influence. As a consequence, the part size is described as the most influential parameter in terms of cost per part and time per part. Moreover, the accuracy and the production volume indicate strong effects, while the machine type has only an effect on cost per part but not on the time per part.

References

3D Systems (2015) '3D printers overview'. http://www.3dsystems.com/3d-printers/production/overview (Accessed 20 January 2015).

A. Lifton, V., Lifton, G. and Simon, S. (2014) 'Options for additive rapid prototyping methods (3D printing) in MEMS technology', *Rapid Prototyping Journal*, Vol. 20, No. 5, pp.403–412.

Aboulkhair, N.T., Everitt, N.M., Ashcroft, I. and Tuck, C. (2014) 'Reducing porosity in AlSi10Mg parts processed by selective laser melting', *Additive Manufacturing*, 1-4, pp.77–86.

Arcam AB (2013) 'Arcam-Q20'.

ASTM (2012) *Terminology for Additive Manufacturing Technologies*, ASTM International, West Conshohocken, PA.

Attar, E. (2011) 'Simulation of Selective Electron Beam Melting Processes', *Doctoral Thesis*.

Atzeni, E. and Salmi, A. (2012) 'Economics of additive manufacturing for end-usable metal parts', *The International Journal of Advanced Manufacturing Technology*, Vol. 62, 9-12, pp.1147–1155.

Baumers, M., Truck, C., Wildman, R., Ashcroft, I., Rosamond, E. and Hague, R. (2012) 'COMBINED BUILD–TIME, ENERGY CONSUMPTION AND COST ESTIMATION FOR DIRECT METAL LASER SINTERING'.

Berman, B. (2012) '3-D printing: The new industrial revolution', *Business Horizons*, Vol. 55, No. 2, pp.155–162.

Brecher, C. (2015) *Advances in Production Technology* [online] https://books.google.de/books?id=k3J3BQAAQBAJ.

Bremen S., Meiners, W. and Diatlov A. (2012) 'Selective Laser Melting: A manufacturing technology for the future?'.

Buchbinder, D., Schleifenbaum, H., Heidrich, S., Meiners, W. and Bültmann, J. (2011) 'High Power Selective Laser Melting (HP SLM) of Aluminum Parts', *Physics Procedia*, Vol. 12, pp.271–278.

Byun, H.S. and Lee, K.H. (2005) 'A decision support system for the selection of a rapid prototyping process using the modified TOPSIS method', *The International Journal of Advanced Manufacturing Technology*, Vol. 26, 11-12, pp.1338–1347.

Concept Laser (2015) 'Biggest direct metal printing machine'. http://www.concept-laser.de/branchen/automotive/maschinen.html.

Concept Laser (2012) 'X line 1000R_EN_112012.indd'.

Deutsches Patent- und Markenamt 'Markenregistereintrag SLM'. https://register.dpma.de/DPMAregister/marke/register/300943229/DE (Accessed 19 January 2015).

Dewidar, M., Dalgarno, K. and Wright, C. (2003) 'Processing conditions and mechanical properties of high-speed steel parts fabricated using direct selective laser sintering'.

Encyclopedia of Tribology (2013) *Encyclopedia of Tribology E,* Springer US, Boston, MA.

EOS, e.-M.S. (2014a) 'EOS Aluminium AlSi10 Mg 2'.

EOS, e.-M.S. (2014b) 'Technical Data EOS M 290'.

EOS, e.-M.S. (2011a) 'EOS MaragingSteel MS1 material data sheet'.

EOS, e.-M.S. (2011b) 'EOS Material data sheet M 270 and M 280'.

EOS, e.-M.S. (2009) 'EOS Aluminium AlSi10Mg'.

EOS, e.-M.S. (2008) 'EOS material data sheet titianium'.

EOS, e.-M.S. (2007) 'MaragingSteel Material Data Sheet M270'.

EOS, e.-M.S. (2005) 'EOSINT M 270 / EOSINT M270 / EOS'.

Fraunhofer ILT (2007) 'Abschlussbericht Generative Fertigung von Aluminiumbauteilen für die Serienproduktion'.

Frick (2011) 'Marktübersicht Generative Fertigungsanlagen'.

Garrett (2013) 'Economic analysis of additive manufacturing for final products an industrial approach'.

Ge, W., Guo, C. and Lin, F. (2014) 'Effect of Process Parameters on Microstructure of TiAl Alloy Produced by Electron Beam Selective Melting', *Procedia Engineering*, Vol. 81, pp.1192–1197.

General Electric (2014) 'World's First Plant to Print Jet Engine Nozzles in Mass Production'. http://www.gereports.com/post/91763815095/worlds-first-plant-to-print-jet-engine-nozzles-in (Accessed 14 January 2015).

Ghazy, M.M. (2012) 'Development of an Additive Manufacturing Decision Support System', *School of Mechanical and Systems Engineering Newcastle University*.

Gibson, I., Rosen, D.W. and Stucker, B. (2010) *Additive Manufacturing Technologies,* Springer US, Boston, MA.

Hinduja, S. and Li, L. (2013) *Proceedings of the 37th International MATADOR Conference,* Springer, London, New York.

Holmström, J., Partanen, J., Tuomi, J. and Walter, M. (2010) 'Rapid manufacturing in the spare parts supply chain', *Journal of Manufacturing Technology Management*, Vol. 21, No. 6, pp.687–697.

Kelbassa, I., Gasser A. and Meiners, W. (2014) '3D-Drucker/Generative Fertigung – Wie sich die Produktion verändert und die Logistik vor neue Herausforderungen stellt'.

Koike, M., Greer, P., Owen, K., Lilly, G., Murr, L.E., Gaytan, S.M., Martinez, E. and Okabe, T. (2011) 'Evaluation of Titanium Alloys Fabricated Using Rapid Prototyping Technologies—Electron Beam Melting and Laser Beam Melting', *Materials*, Vol. 4, No. 12, pp.1776–1792.

Krishnan, M., Atzeni, E., Canali, R., Calignano, F., Manfredi, D., Ambrosio, E.P. and Iuliano, L. (2014) 'On the effect of process parameters on properties of AlSi10Mg parts produced by DMLS', *Rapid Prototyping Journal*, Vol. 20, No. 6, pp.449–458.

Kruth, J.-P., Levy, G., Klocke, F. and Childs, T. (2007) 'Consolidation phenomena in laser and powder-bed based layered manufacturing', *CIRP Annals - Manufacturing Technology*, Vol. 56, No. 2, pp.730–759.

Madeley, D. and Chaphalkar, N. (2013) 'Additive and Hybrid Manufacturing'.

Manfredi, D., Calignano, F., Krishnan, M., Canali, R., Ambrosio, E. and Atzeni, E. (2013) 'From Powders to Dense Metal Parts: Characterization of a Commercial AlSiMg Alloy Processed through Direct Metal Laser Sintering', *Materials*, Vol. 6, No. 3, pp.856–869.

Manfredi, D., Calignano, F., Krishnan, M., Canali, R., Paola, E., Biamino, S., Ugues, D., Pavese, M. and Fino, P. (2014) 'Additive Manufacturing of Al Alloys and Aluminium Matrix Composites (AMCs)', in Monteiro, W.A. (Ed.), *Light Metal Alloys Applications*, InTech.

Maschinenbautechniker.eu 'Salaries for technicians in mechanical engineering'. http://www.maschinenbautechniker.eu/maschinenbautechniker-gehalt.php (Accessed 10 March 2015).

Morris Technologies (2012) 'Comparison of DMLS and EBM'. http://www.3ders.org/articles/20120808-morris-technologies-setting-up-an-instrumentation-lab.html (Accessed 8 April 2015).

Munguía, J., Ciurana, J. and Riba, C. (2009) 'Neural-network-based model for build-time estimation in selective laser sintering', *Proceedings of the Institution of Mechanical Engineers, Part B: Journal of Engineering Manufacture*, Vol. 223, No. 8, pp.995–1003.

National Academy of Engineering of the National Academies (2012) *Frontiers of engineering 2011. Reports on leading-edge engineering from the 2011 symposium*, National Academies Press, Washington, D.C.

Read, N., Wang, W., Essa, K. and Attallah, M.M. (2015) 'Selective laser melting of AlSi10Mg alloy: Process optimisation and mechanical properties development', *Materials & Design*, Vol. 65, pp.417–424.

Rickenbacher, L., Spierings, A. and Wegener, K. (2013) 'An integrated cost-model for selective laser melting (SLM)', *Rapid Prototyping Journal*, Vol. 19, No. 3, pp.208–214.

Roland Berger Strategy Consultants (2013) 'Additive Manufacturing: A game changer for the manufacturing industry?'.

Rosenthal, I., Stern, A. and Frage, N. (2014) 'Microstructure and Mechanical Properties of AlSi10Mg Parts Produced by the Laser Beam Additive Manufacturing (AM) Technology', *Metallography, Microstructure, and Analysis*, Vol. 3, No. 6, pp.448–453.

Ruffo, M. and Hague, R. (2007) 'Cost estimation for rapid manufacturing simultaneous production of mixed components using laser sintering', *Proceedings of the Institution of Mechanical Engineers, Part B: Journal of Engineering Manufacture*, Vol. 221, No. 11, pp.1585–1591.

Ruffo, M., Tuck, C. and Hague, R. (2006) 'Cost estimation for rapid manufacturing laser sintering production for low to medium volumes', *Proceedings of the Institution of Mechanical Engineers, Part B: Journal of Engineering Manufacture*, Vol. 220, No. 9, pp.1417–1427.

Sanz, C. and García Navas, V. (2013) 'Structural integrity of direct metal laser sintered parts subjected to thermal and finishing treatments', *Journal of Materials Processing Technology*, Vol. 213, No. 12, pp.2126–2136.

Schleifenbaum, H., Meiners, W., Wissenbach, K. and Hinke, C. (2010) 'Individualized production by means of high power Selective Laser Melting', *CIRP Journal of Manufacturing Science and Technology*, Vol. 2, No. 3, pp.161–169.

Schuh, G., Behr, M., Brecher, C., Bührig-Polaczek, A., Michaeli, W., Schmitt, R., Arnoscht, J., Bohl, A., Buchbinder, D., Bültmann, J., Diatlov, A., Elgeti, S., Herfs, W., Hinke, C., Karlberger, A., Kupke, D., Lenders, M., Nußbaum, C., Probst, M., Queudeville, Y., Quick, J., Schleifenbaum, H., Vorspel-Rüter, M. and Windeck, C. (2012) 'Individualised Production', in Brecher, C. (Ed.), *Integrative Production Technology for High-Wage Countries*, Springer Berlin Heidelberg, Berlin, Heidelberg, pp.77–239.

SLM Solutions (2014) 'SLM 500 HL'.

SLM Solutions (2012) 'Laserstrahlschmelzanlage SLM 500 HL'.

Spierings, A., Wegener, K. and Levy, G. (2012) 'Designing Material Properties Locally with Additive Manufacturing technology SLM', *ETH Zürich*.

The Economist (2012) 'The third industrial revolution'. http://www.economist.com/node/21553017 (Accessed 14 January 2015).

Wohlers, T.T. (2014) *Wohlers report 2014. 3D printing and additive manufacturing state of the industry annual worldwide progress report*, Wohlers Associates, Fort Collins, Col.

Wohlers, T.T. (2013) *Wohlers report 2013. Additive manufacturing and 3D printing state of the industry : annual worldwide progress report*.

Yasa, E. and Kruth, J.P. (2009) 'Rapid Manufacturing Research at the Catholic University of Leuven', *RapidTech 2009: US-Turkey Workshop on Rapid Technologies*.

Appendix

A1 Technical Data EOSINT M 270

Technical Data

Effective building volume (including building platform)	*250 mm x 250 mm x 215 mm (9.85 x 9.85 x 8.5 in.)*
Building speed (material-dependent)	*2 – 20 mm³/s (0.0001 – 0.001 in³/sec.)*
Layer thickness (material-dependent)	*20 – 100 µm (0.001 – 0.004 in.)*
Laser type	*Yb-fibre laser, 200 W*
Precision optics	*F-theta-lens, high-speed scanner*
Scan speed	*up to 7.0 m/s (23 ft./sec.)*
Variable focus diameter	*100 – 500 µm (0.004 – 0.02 in.)*
Power supply	*32 A*
Power consumption	*maximum 5.5 kW*
Nitrogen generator	*standard*
Compressed air supply	*7,000 hPa; 20 m³/h (102 psi; 26.2 yd³/h.)*
Dimensions (B x D x H)	
System	*2,000 mm x 1,050 mm x 1,940 mm (78.8 x 41.4 x 76.4 in.)*
Recommended installation space	*approx. 3.5 m x 3.6 m x 2.5 m (137.9 x 141.8 x 100 in.)*
Weight	*approx. 1,130 kg (2,491 lb.)*
Data preparation	
PC	*current Windows operating system*
Software	*EOS RP Tools; Magics RP (Materialise)*
CAD interface	*STL. Optional: converter for all standard formats*
Network	*Ethernet*
Certification	*CE, NFPA*

Status 12/05. Technical data subject to change without notice. EOS®, EOSINT®, DMLS®, DirectTool®, DirectPart® and e-Manufacturing™ are registered trademarks of EOS GmbH. Windows is a registered trademark of Microsoft Corporation. EOS is certified according to ISO 9001.

Figure A1: Technical Data EOSINT M270 (EOS, 2005, p.2)

A2 Technical Data SLM 500HL

Anlagenparameter

Build Envelope Volume in mm (x/y/z)	500 x 280 x 320
Lenth, z-axis in mm	320
Laser Power	4x 400 W or 2x (400 W and 1000 W) Yb-Faser-Laser
Build Speed	105 ccm/h
Pract. Layer Thickness	20 µm - 200 µm
Min. Scale Line / Wall Thickness	160 - 180 µm
Operational Beam Focus	80 - 120 µm / 700 µm
Scan Speed	10 m/s
Inert Gas Consumption in Operation	Ar/N_2 , 5 l/min
Inert Gas Consumption Venting	Ar/N_2 , 2500 l @ 100 l/min.
Compressed Air Requirement	ISO 8573-1, 30 l/min. @ 1.5 bar
Dimensions in mm (B x H x T)	4000 x 2200 (2500) x 1100
Weight	approx. 2600 kg
E-Connection / Consumption	400 Volt 3NPE, 64 A, 50/60 Hz, 8 KW/h - 10 KW/h

Subject to technical changes

Figure A2: Technical Data SLM 500HL (SLM Solutions, 2012, p.3)

A3 Technical Data Arcam Machines

Table A3: Technical data Arcam

name	S12	A2	A1/A2X	A2XX	Q10/Q12
year	2002	2007	2009	2012	2013
max. build size [ccm]	7200	14000	7200	9139,80	7200
	7200	14000	7200	9139,80	9139,80
max. beam power [W]	3500	3500	3000	3000	3000
			3000		3000
min. beam spot size [µm]	300	200	200	200	100
	300	200	200	200	180

A4 Technical Data EOS Machines

Table A4: Technical data EOS (*build size includes building platform)

name	M250	M250 Xt	M270	M280	M400	M290
year	1995	2001	2004	2010	2013	2014
max. build size [ccm]	12500	12500	13437,5	20312,5	64000	20312,5
max. beam power [W]	100	200	200	400	1000	400
min. beam spot size [µm]	100	100	100	100	90	100

A5 Technical Data ConceptLaser Machines

Table A5: Technical data Concept Laser

name	M3 linear	M1 cusing	M2 cusing	M lab cusing	X line 1000R
year	2002	2008	2009	2010	2012
max. build size [ccm]	31500	648	17500	648	126000
max. beam power [W]	200	100	200	100	1000
min. beam spot size [µm]	70	20	70	20	100

A6 Comparison of DMLS and EBM Machines

Table A6: Comparison DMLS and EBM (Morris Technologies, 2012)

DMLS vs. EBM

Feature/Characteristic	DMLS M270	EBM	Advantage
Heat source	Laser	Electron beam	Draw
Maximum power to bed	200 watt	3,500 watt	EBM
Effective number of beams	1	Up to 50	EBM
Layer thickness	20-40 µm	50-70 µm	DMLS
Atmosphere	Inert gas (argon, nitrogen)	Vacuum	Draw
Build envelope	250 x 250 x 200 mm	200 x 200 x 350 mm -or- 300 diameter x 200 mm	Draw
Recoater dispenser	Dispenser below build area	Hopper above build area	EBM
Recoater material	Rigid (ceramic or steel)	Flexible	Draw
Approved materials	Ti64, Ti64ELI, CoCr, Inconel 625 and 718, AlSi10Mg, Aluminum 6061, MS-1, Stainless 17-4PH, Stainless 316L	Ti64, Ti64ELI, CoCr	DMLS
Residual stresses	Significant	Minimal	EBM
Surface finish/ detail resolution	Good	Fair	DMLS
Typical Ti64 dimensional accuracy	± .005	± .010	DMLS
Typical Ti64 ultimate tensile strength and elongation (as built)	1,215 MPa, 10%	970 MPa, 16%	Draw

MORRIS TECHNOLOGIES

A7 Technical Data Arcam Q20

Arcam Q20 Technical Data

Process type	Hot powder bed / high vacuum (temperature material-dependent)
Max. build size	350 x 380 mm (Ø/H)
Max. beam power	3000 W
Cathode type	Single crystalline
Min. beam diameter	180 µm
Arcam MultiBeam™ technology	Multiple melt pool process
Repositioning time	10 ms
Translation speed, melting	Continuously variable
Active cooling	Water-cooled heat sink
Vacuum base pressure	$1x10^{-4}$ mbar
Build atmosphere	$4x10^{-3}$ mbar, partial pressure of He
He consumption, build process	4 l/h
He consumption, build cool down	100-150 l/build
Process control	Layer verification camera system
Power supply	3 x 400 V, 32 A, 7 kW
Size	Approx. 2300 x 1300 x 2600 mm (W x D x H)
Weight	2900 kg
Process computer	PC
CAD interface	Standard: STL
Network	Ethernet 10/100/1000

Figure A7: Technical Data Arcam Q20 (Arcam AB, 2013)

A8 Technical Data EOS M 290

Technical Data EOS M 290	
Building volume	250 mm x 250 mm x 325 mm (9.85 x 9.85 x 12.8 in)
Laser type	Yb-fibre laser; 400 W
Precision optics	F-theta-lens; high-speed scanner
Scan speed	up to 7.0 m/s (23 ft./sec)
Focus diameter	100 µm (0.004 in)
Power supply	32 A
Power consumption	max. 8.5 kW / typical 3.2 kW
Nitrogen generator	integrated
Compressed air supply	7,000 hPa; 20 m³/h (102 psi; 706 ft³/h)
Dimensions (W x D x H)	
System	2,500 mm x 1,300 mm x 2,190 mm (98.4 x 51.2 x 86.2 in)
Recommended installation space	min. 4,800 mm x 3,600 mm x 2,900 mm (189 x 142 x 114 in)
Weight	approx. 1,250 kg (2,756 lb)
Data preparation	
Software	EOS RP Tools; EOSTATE; EOSPRINT; Materialise Magics RP with SG+ and further modules
CAD interface	STL. Optional: converter for all standard formats
Network	Ethernet

Figure A8: Technical Data EOS M 290 (EOS, 2014b, p.3)

A9 EOS Build volume rates

Table A9: EOS Build volume rates for several materials

M280 / 400W	Layer thickness [µm]	Volume rate [mm³/s] (Material Data Sheet)	Higher productivity with 400W [%]
MS1 Performance 2.0 (200W)	40µm	3,0	100%
MS1 Speed 1.0 (400W)	40µm	5,7	190%
MS1 TopSpeed 1.0 (400W)	80µm	7,7	257%
MP1 Performance 1.0 (200W)	40µm	2,6	100%
MP1 Speed 1.0 (400W)	40µm	5,5	212%
IN718 Surface 1.0 (200W)	20µm	2,1	100%
IN718 Speed 1.0 (400W)	40µm	6,0	286%
Ti64 Performance 2.0 (200W)	30µm	3,8	100%
Ti64 Speed 1.0 (400W)	60µm	8,2	216%
AlSi10Mg Performance 2.0	30µm	4,8	100%
AlSi10Mg Speed 1.0 (400W)	30µm	7,4	154%

A10 Logarithmic interpolation of build volume rates

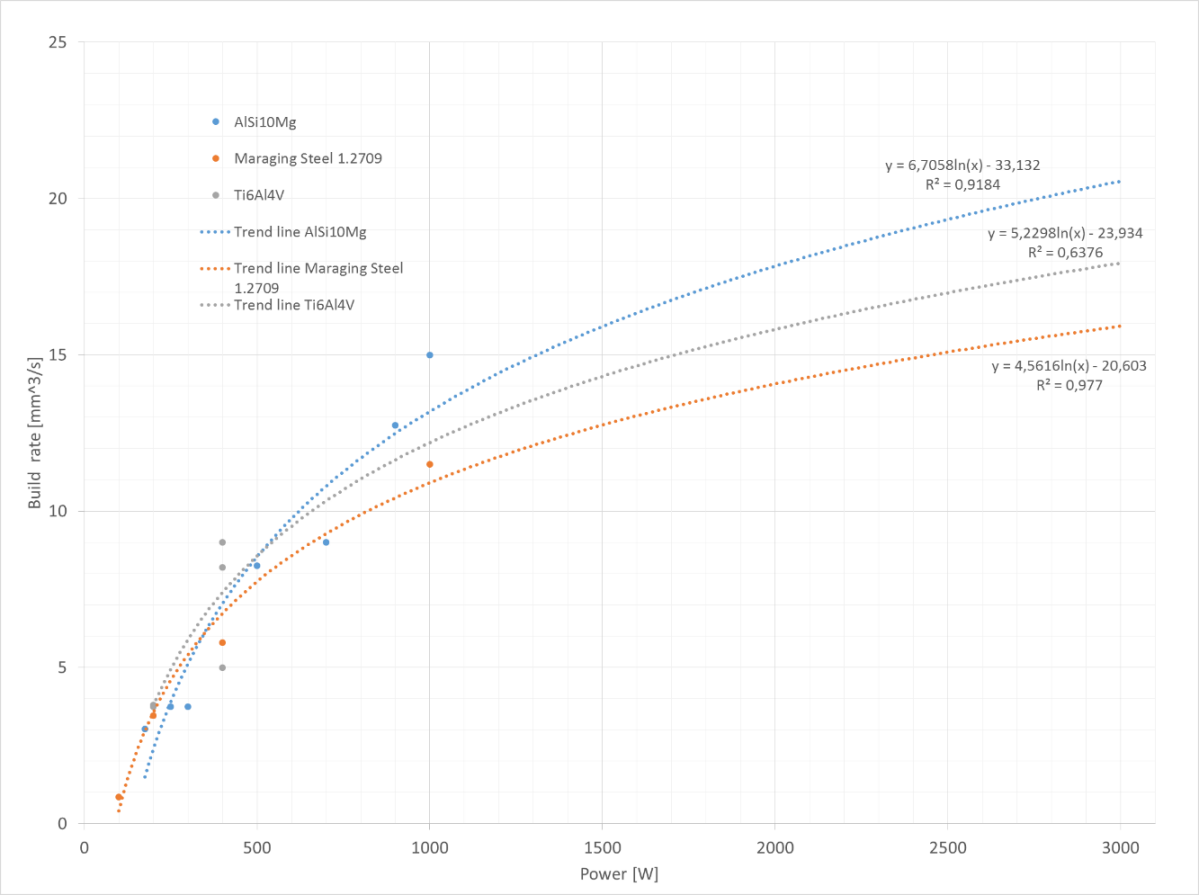

Figure A10: Logarithmic interpolation of build volume rates up to 3000 W

A11 Maraging steel 1.2709 build volume rates

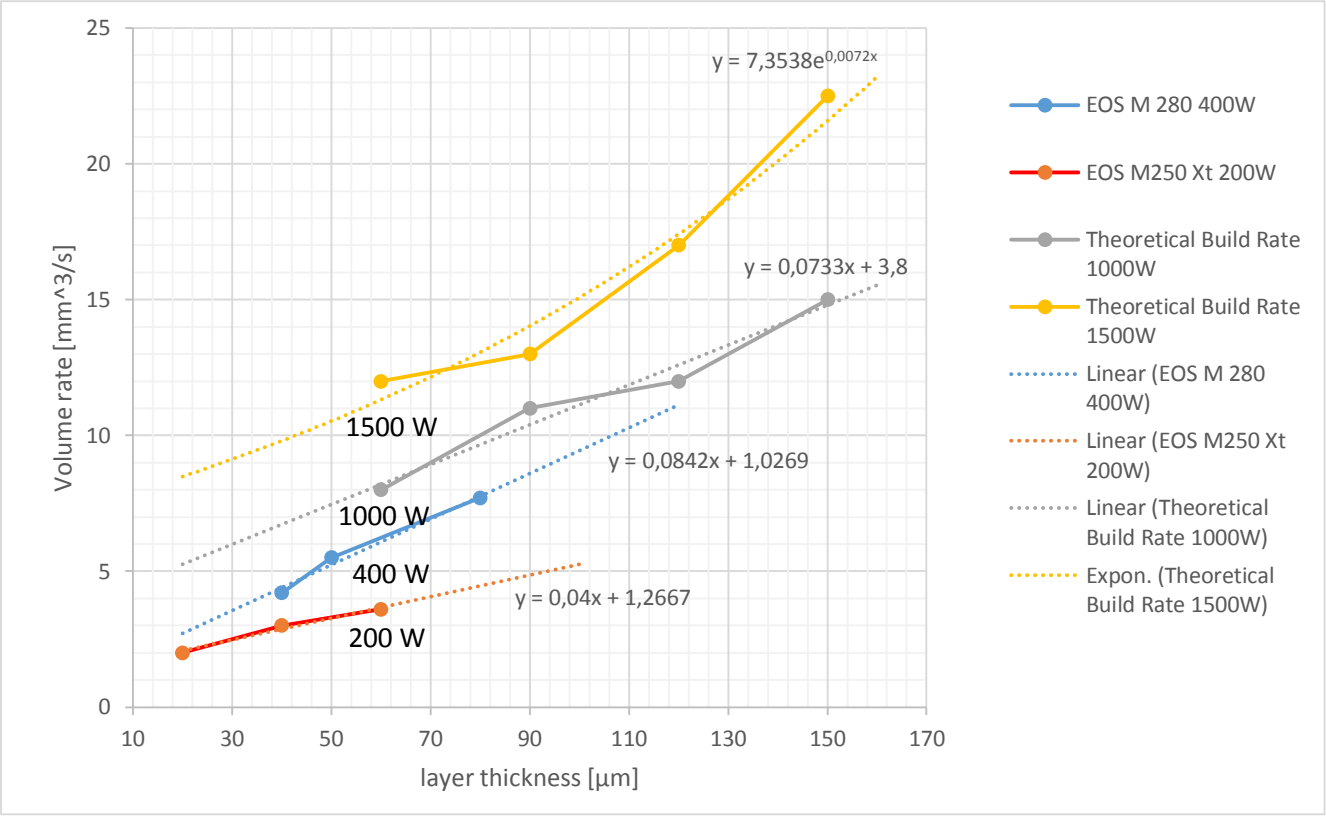

Figure A11: Volume rates of maraging tool-steel 1.2709 dependent on layer thickness

A12 Correlation analysis for plastic-based AM

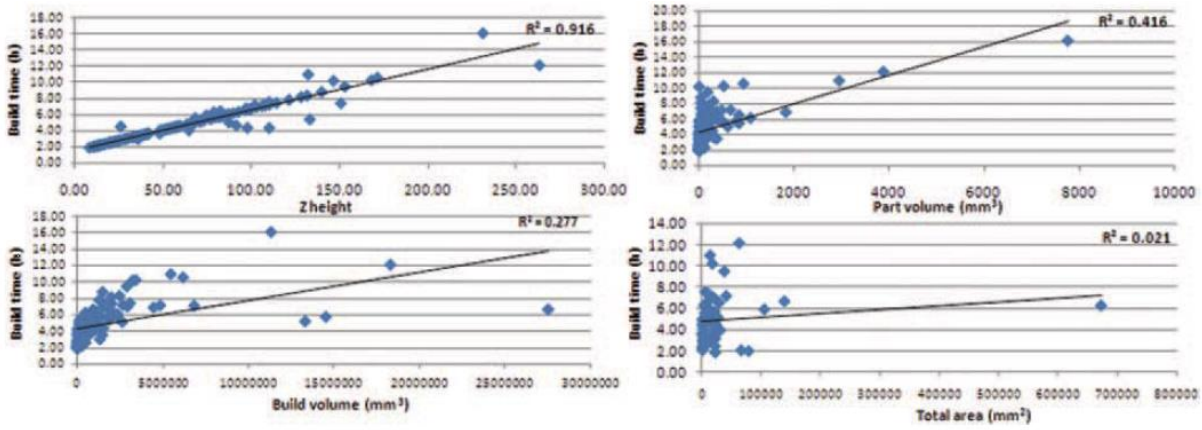

Fig. 3 Correlation analysis for potential input parameters against final build time

Figure A12: Correlation analysis for plastic-based AM (Munguía et al., 2009, p.998)

A13 Volume build rates for MS 1.2709

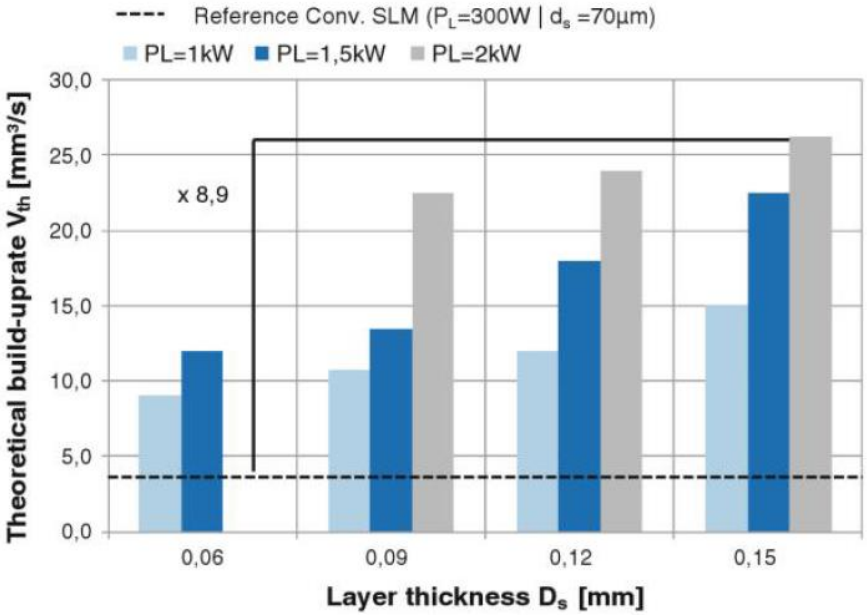

Figure A13: Volume rates of maraging tool-steel 1.2709 (Brecher, 2015, p.57)

A14 Volume build rates for MS 1.2709

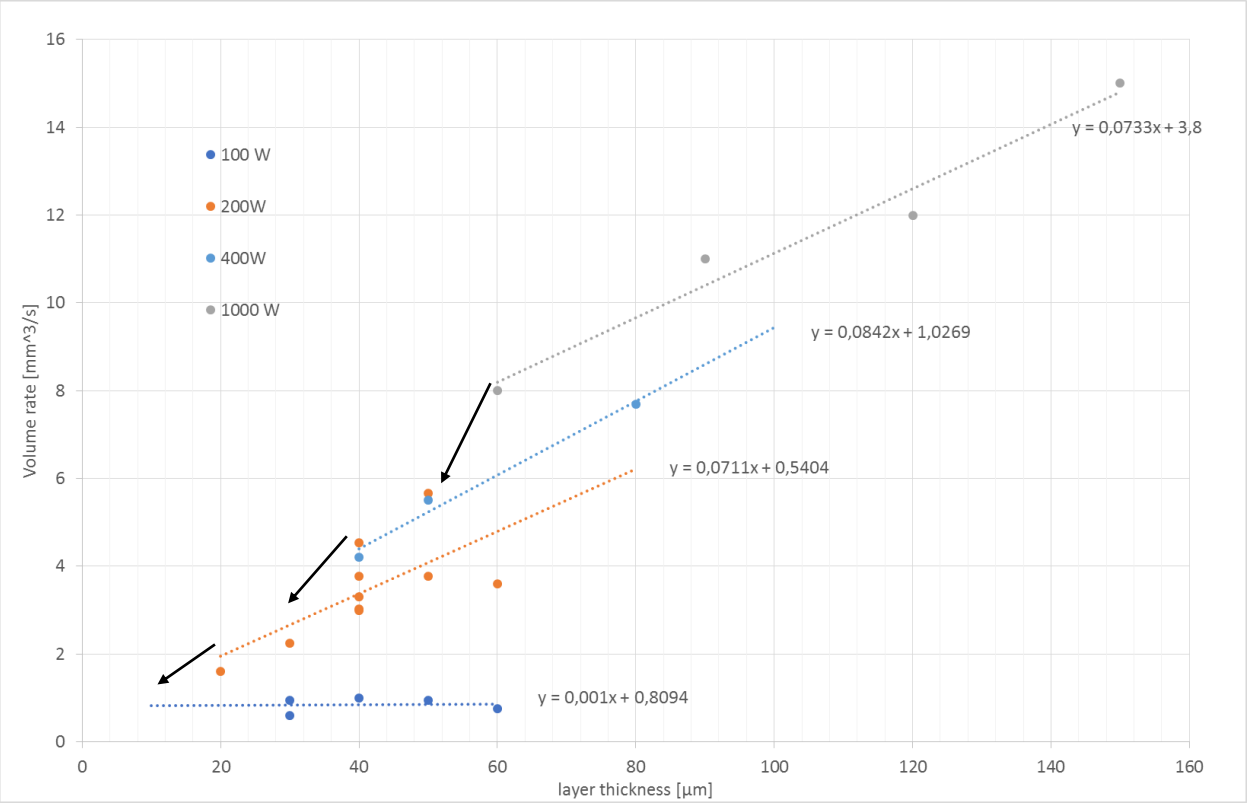

Figure A14: Volume rate dependencies on layer thickness with increasing laser power systems for maraging steel 1.2709

A15 Systematology for a L-18 orthogonal array

Expt. No.	Col. 1	Col.2	Col.3	Col.4	Col.5
1	1	1	1	1	1
2	1	1	2	2	2
3	1	1	3	3	3
4	1	2	1	1	2
5	1	2	2	2	3
6	1	2	3	3	1
7	1	3	1	2	1
8	1	3	2	3	2
9	1	3	3	1	3
10	2	1	1	3	3
11	2	1	2	1	1
12	2	1	3	2	2
13	2	2	1	2	3
14	2	2	2	3	1
15	2	2	3	1	2
16	2	3	1	3	2
17	2	3	2	1	3
18	2	3	3	2	1

Figure A15: Systematology for a L-18 orthogonal array

A16 Technical Data Arcam Q10

Arcam Q10 Technical Data

Process type	Hot powder bed/high vacuum
	(temperature material dependent)
Max. build size	200x200x180 mm (W x D x H)
Max. Beam power	3000 W
Cathode type	Single crystalline
Min. Beam diameter	100 µm
EBM MultiBeam™ technology	Multiple melt pool process
Max. EB translation speed	8000 m/s
Active cooling	Water-cooled heat sink
Vacuum base pressure	$1x10^{-5}$ mbar
Build atmosphere	$1x10^{-3}$ mbar partial pressure of He
He consumption, build process	1 liter / hour
He consumption, build cool down	50-75 liters / build
Process control	Layer verification camera system
Power supply	3 x 400 V, 32 A, 7kW
Size	1850 x 900 x 2200 mm (W x D x H)
Weight	1420 kg
Process computer	PC
CAD interface	Standard: STL
Network	Ethernet 10/100/1000
Certification	CE

Figure A16: Technical Data Arcam Q20 (Arcam AB, 2013)